DEVELOPMENT AND CHARACTERIZATION OF PORCINE MODELS OF GLIOMA

A Dissertation
Presented to
The Academic Faculty

by

Muhibullah Sayed Tora

In Partial Fulfillment
of the Requirements for the Degree
Doctor of Philosophy in the
Department of Biomedical Engineering

Georgia Institute of Technology
Emory University
May 2021

DEVELOPMENT AND CHARACTERIZATION OF PORCINE MODELS OF GLIOMA

Approved by:

Dr. Nicholas M. Boulis, Advisor
School of Biomedical Engineering
Georgia Institute of Technology

Dr. Steven Sloan
Department of Human Genetics
Emory University School of Medicine

Dr. John N. Oshinski
School of Biomedical Engineering
Georgia Institute of Technology

Dr. Peter D. Canoll
Department of Pathology
Columbia University Medical Center

Dr. Robert E. Gross
School of Biomedical Engineering
Georgia Institute of Technology

Date Approved: [March, 26, 2021]

لحبيبتي نورة

ACKNOWLEDGEMENTS

I am incredibly grateful to my advisor, Dr. Nicholas Boulis, for his advice and guidance throughout my training. This thesis began with an attempt at achieving something that had not been done before, with incredible inherent risk but with a high potential for reward. Whenever I was able to deliver productive results, he would ask more of me whether it was in relation to thesis research, grantsmanship, or clinical studies. This taught me to continue aspiring to do more in all facets of my life and encouraged me to persevere when the going got tough. Under his tutelage, I now better understand what it takes to be a successful researcher and hope to follow in his footsteps as a clinician scientist.

I would also like to offer special thanks to Thais Federici, Pavlos Texaklidis, Purva Nagarajan, and Nathan Hardcastle for their countless hours of technical assistance, experimental support, and participation in the day-to-day conduct of this research. I spent hours upon hours with these folks, feeding pigs, doing surgery, and performing analyses. This research and many other projects not included would not have been possible without such an exceptional and supportive team.

I would also like to thank my committee members for their support over these years. John Oshinski kept me centered in my research and taught me the ins and outs of MRI. Thanks to his support I was able to incorporate clinical MRI into the conduct of this thesis research. Even though he did not need to, he made time to come to nearly every single MRI scan despite the onset of the lockdown and his own packed schedule. He made the CSI available to me and helped me navigate the complexities of that administrative environment, and taught me firsthand how to operate the MR scanner. He went above and

beyond to put me in touch with experts in specific areas of interest to provide further validity to our imaging approaches in the present thesis research and in our grant proposals. I am grateful to Peter Canoll who, while he was based in New York, always had helpful feedback and suggestions and provided his expertise in glioma modeling as if he was present in the day-to-day. It was only due to his insight, counsel, and productive collaboration that we were able to devise a strategy to scale into what has become the completion of this dissertation research. I envision this program continuing due to, in no small part, his valuable and unique contributions. I would like to offer my gratitude to Steven Sloan, who taught me the fundamental concepts of RNA-seq and encouraged me to explore this area to a point where I could conduct my own analysis. His advice was instrumental to bringing this project to a fruitful conclusion. I would also like to thank Dr. Robert Gross for his thoughtful advice, suggestions, and project insights throughout these five years. He kept me focused on my long-term training goals and foreseeable eleven years of medical, neurosurgical, and scientific training. Our talks have stuck with me and I will carry his advice throughout my career.

I want to thank my mother, father, and siblings for their unconditional support throughout my upbringing and education. I could not have achieved what little I have, or come to where I am, without their help. My mother, tutored me daily after school and instilled in me a desire to question, learn, and study without refrain. My father humbles me still and has kept me focused on the path in front of me. He is my spiritual bedrock, greatest supporter, and most loving critic. My younger sister Ayesha, who has yet to define her bright future, reminds me of what it is to be hopeful, optimistic, and work toward goals

others may decide are unattainable. My elder brothers, Amin, Hamid, Habib, and Masoud provided a village in which I could grow and role models for me to aspire toward.

Lastly, and most importantly to me, I would like to acknowledge my wife, Norah, to whom the dedication is devoted. The dedication is the transliteration of “Le Habibti Norah”, meaning “to my love Norah” in her native tongue. You truly have been my guiding light in these past five years in countless ways. Your love and support were the only way I could push forward at times, and you always were there for me as a source of peace and tranquility whenever I needed you. You’re the smartest person I know and I can’t wait to see your amazing dissertation this year. I look forward to graduating together and sharing the next amazing chapter of our lives.

TABLE OF CONTENTS

LIST OF TABLES

LIST OF FIGURES

LIST OF SYMBOLS AND ABBREVIATIONS

5-ALA	5-Aminolevulinic Acid
CNS	Central Nervous System
CSF	Cerebrospinal Fluid
CL	Classical
CTRL	Control
CED	Convection Enhanced Delivery
DE	Differential Expression
DEA	Differential Expression Analysis
EGFR	Epidermal Growth Factor Receptor
FLAIR	Fluid Attenuated Inversion Recovery
FUS	Focused Ultrasound
fMRI	Funcctional Magnetic Resonance Imaging
GSEA	Gene Set Enrichment Analysis
GEM	Genetically Engineered Model

GBM	Glioblastoma
GTR	Gross Total Resection
H&E	Hematoxylin and Eosin
IHC	Immunohistochemistry
IDH	Isocitrate Dehydrogenase
KPS	Karnofsky Performance Status
LITT	Laser Interstitial Thermal Therapy
MRI	Magnetic Resonance Imaging
MES	Mesenchymal
NL	Neural
ONC	Oncogenic Transgene Group
PDX	Patient Derived Xenograft
PDGFB	Platelet Derive Growth Factor Beta
PDGFR	Platelet Derive Growth Factor Receptor
PNS	Porcine Neurobehavioral Scoring
PN	Proneural

SCG	Spinal Cord Glioma
STR	Subtotal Resection
TMZ	Temozolamide
TTF	Tumor Treating Fields
WNL	Within Normal Limits
WHO	World Health Organization

SUMMARY

Glioblastoma (GBM) is a debilitating disease process with poor overall outcomes in humans. Given this clinical need, the U.S. National Library of Medicine has over 350 completed phase II-III clinical trials registered as of this writing. Unfortunately, there have been limited changes to the outcomes. In part, this represents the aggressive nature of this disease process. On the other hand, this highlights the need for advanced pre-clinical models of the disease, especially for evaluation of surgical therapies. The present work outlines the development and characterization of a novel porcine models of high-grade glioma in both the brain and spinal cord using lentiviral gene transfer.

CHAPTER 1. INTRODUCTION

The objective of this research is to develop large mammalian models of glioblastoma (GBM). Although there have been numerous rodent models of GBM, at the time of this research there were no reports in the literature regarding reproducible large animal models. This is a concern for research programs aiming to investigate therapeutic strategies, especially those that require evaluation in a model system that is more anatomically relevant to the human. Thus, this research attempted to employ well-vetted vector-driven methodologies to drive gliomagenesis in a porcine system for the first time. In this chapter, the clinical characteristics of supratentorial and spinal cord GBM are discussed to provide a contextual understanding of the disease process in humans, including epidemiology, neuropathologic features, major pathways, and the current standard of care. Next, we briefly overview issues in the pre-clinical translational pipeline as it relates to animal modeling and the case for development of a large animal model of GBM. Lastly, the motivation, aims, and structure of this thesis is outlined.

1.1 Clinical Features of Glioblastoma

1.1.1 Epidemiology

From an epidemiologic standpoint, GBM represents the most common and most lethal primary brain tumor in adults, with an incidence of 5 per 100,000 in North America, and comprising up to 20% of all primary intracranial neoplasms and 54% of all gliomas [2-4]. The most common location of occurrence is supratentorial, including the frontal, temporal, parietal, and occipital lobes. GBM does also occur in occur in the posterior fossa

(cerebellum, brainstem) comprising up to 0.9-3.4% of all cases [5]. GBM occurrence in the spinal cord represents an orphan disease process, with reports at well below 1% of all cases [4, 6]. A recent single-center retrospective study examined the demographic characteristics and distribution of GBM by primary site and reported similar findings with the vast majority of primary sites in the supratentorial brain and approximately 2% found in the spinal cord [1].

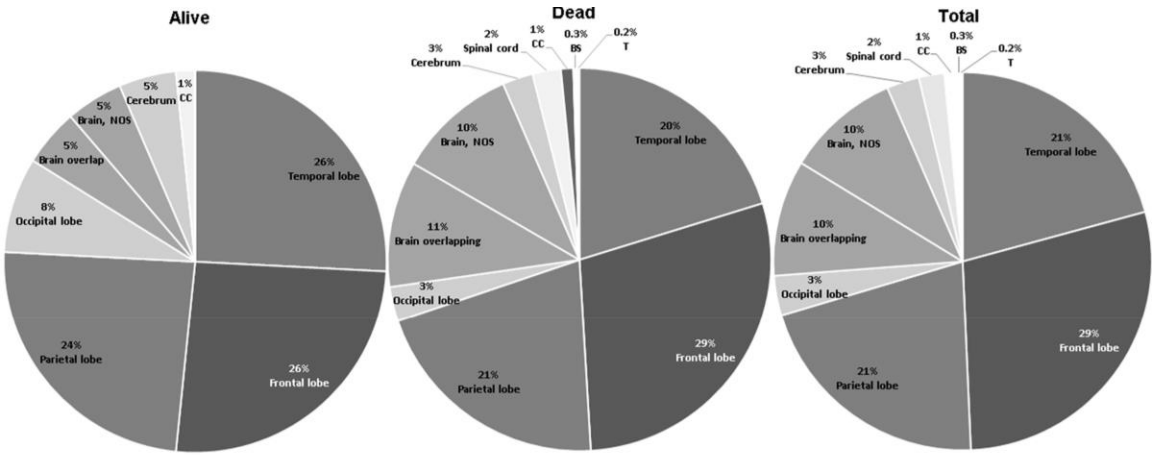

Figure 1-1. Incidence of GBM by primary site [1].

In order to maximize the impact of generating a large mammalian model of GBM, we decided to model both the most common location of GBM occurrence (supratentorial) and the rarest location (spinal cord) as it represents an orphan disease for which there is a paucity of literature in the field in comparison to its supratentorial counterpart.

1.1.2 World Health Organization Diagnostic Criteria

In 2016, the most recent world health organization (WHO) guidelines for the neuropathologic diagnosis of gliomas were updated to include both phenotypic and genotypic features [7]. Despite considering genotypic information as one of the main points

of division in diagnosis, histopathologic grading is still utilized to assign a WHO grade of I – IV. Histologic grading proceeds according to the presence or absence of four histologic features including: nuclear atypia, mitoses, microvascular proliferation, and necrosis.

To briefly define these features, nuclear atypia takes into account the morphological differences in nuclei in a neuropathologic specimen, examining differences in nuclear shape and staining as compared to phenotypically "normal" cells. Mitoses account for the presence of actively dividing cells, which can be visualized as the presence of a mitotic body or quantified and assisted by using proliferative immunohistochemical markers such as MIB-1 or Ki-67. Microvascular proliferation can include proliferation of endothelial cells, increased vascularity within the specimen, or the presence of glomeruloid bodies. Necrosis can include coagulative and pseudopalisading necrosis. The WHO grading for diffuse astrocytic and oligodendriglial tumors proceeds as follows, beginning at grade II: only nuclear atypia, III: including nuclear atypia, focal or dispersed anaplasia, significant proliferative activity and mitoses, and IV: showing nuclear atypia, mitoses, microvascular proliferation, or necrosis. For the purposes of this research, we will focus primarily on gliomas that are categorized as "Diffuse astrocytic and oligodendroglial tumors" which group tumors of astrocytic and oligodendroglial components under a larger overarching category, which include GBM assigned, WHO grade of IV, and subdivided based on their IDH mutational status. A simplified algorithm for classification of diffuse gliomas is presented in **Figure 2** summarizing the most recent WHO classification algorithm put forth in 2016 [7].

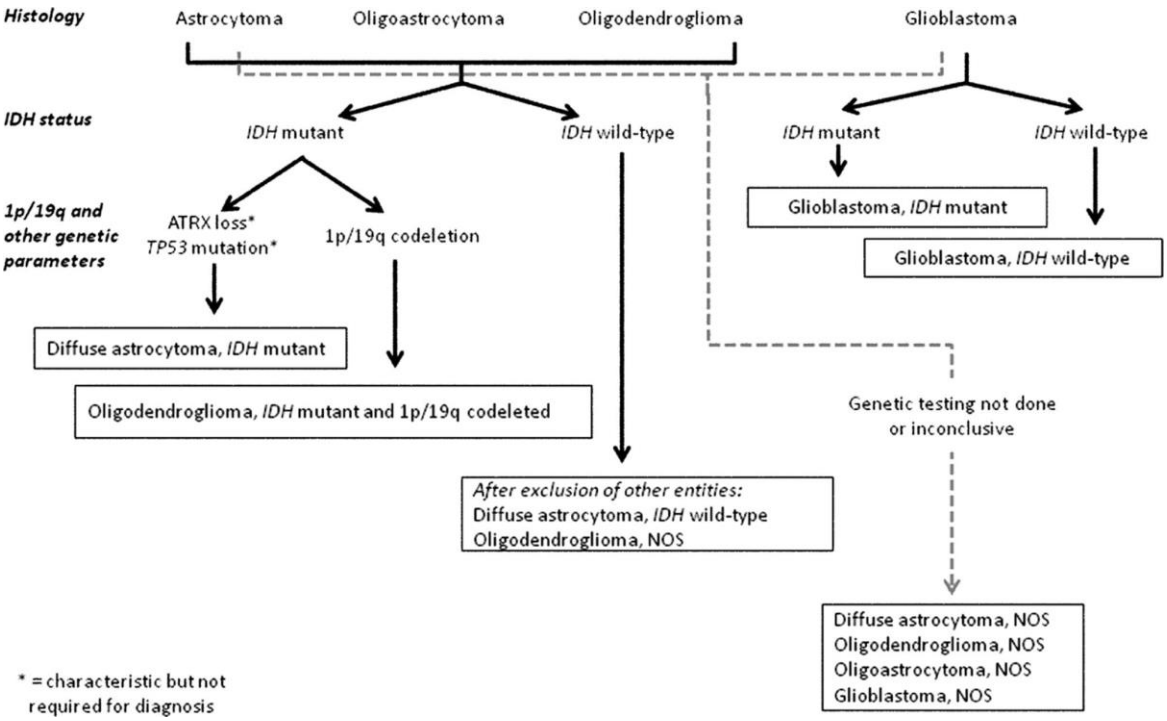

Figure 1-2. WHO Classification algorithm for diffuse gliomas based on hisopathologic and genetic features [7].

The fundamental point of distinction in the simplified diagnostic algorithm for GBM clinical diagnosis is isocitrate dehydrogenase (IDH) mutational status. WHO diagnostic criterion divides GBM into either IDH-wildtype, comprising approximately 90% of cases, and IDH-mutant, comprising approximately 10% of all cases. This was driven by a seminal paper by Yan et al [8] where the authors identified IDH1 (R132) and IDH2 (R172G/K/M) mutations, predominantly in secondary GBM and the vast majority of grade II/III gliomas. They further found a statistically significant difference in median survival (IDH-mutant: 31 months, IDH-wildtype: 15 months), suggesting a more aggressive course in IDH-wildtype GBM [8]. The authors proposed that this mutational status could be useful in distinguishing grade I and grade II gliomas, as well as its apparent stratification in the course of the disease in GBM (primary vs secondary). For the purposes

of the present research, we elected to focus on driving gliomagenesis to model primary de-novo lesions, without the introduction of IDH mutations, which may be pursued as a future strategy to better model secondary GBM lesions.

1.1.3 Presentation, Treatment and Outcomes

Patients with GBM present with progressive neurologic signs and symptoms that vary according to the localization of the mass forming lesion. The most common presenting symptoms include headache (50-60%), seizures (20-50%), and focal neurologic deficits including memory impairment, motor weakness, vision changes, and cognitive or personality changes (10-40%) [9, 10]. Large mass forming lesions can incur significant associated edema, mass effect, and increased intracranial pressure. Focal neurologic deficits are broadly considered more common with GBM compared to lower grade lesions. Rarely, GBM can present with meningeal gliomatosis, or meningeal dissemination, and when observed is typically later in the natural history of the disease process or on post-mortem examination [11, 12]. In 1-5% of patients, an existing germline mutations may be identified such as Li-Fraumeni syndrome (TP53 mutation) or other genetic polymorphisms (e.g. TET, CCDC26, CDKN2A/CDKN2B, TEL1, PHLDB1, EGFR) associated with increased rates of GBM [13-16]. In most patients presenting with GBM, there are no identifiable risk factors or associated family history. Following neuropathologic analysis and IDH mutational status based on WHO criterion, evaluation of O6-methylguanine-DNA (MGMT) promoter methylation status is of use in these patients, as this can be crucial for prognostication and prediction of response to alkylating agents such as temozolomide (TMZ).

Since 2005, the STUPP protocol has been widely adapted as the standard of care for GBM. Following maximal safe resection, concurrent and adjuvant TMZ in combination with radiotherapy is employed in patients with GBM. Systemic chemotherapy and radiotherapy is well reviewed elsewhere [3, 17]. Here we will overview neurosurgical considerations given the frank benefit that may be achieved in generation of an animal model that better recapitulates the anatomic conditions in humans, in reference to the main objectives of the present research project of generating a large mammalian model of GBM. The first step involves surgical debulking of the tumor in an actionable area. Maximal resection of the tumor must be balanced with preservation of neurologic function, which is augmented by using neuronavigation, intraoperative mapping, and preoperative imaging modalities such as functional magnetic resonance imaging (fMRI) and diffusion tensor imaging (DTI) well reviewed elsewhere [18-20]. Similarly, the use of awake craniotomy, frameless stereotaxis, intraoperative MRI, and the use of optical imaging agents such as 5-aminolevulinic acid (5-ALA) are all used to help achieve maximal resection while attempting to minimize surgical morbidity. However, despite the variety of advanced techniques already employed, local recurrence is almost certainly due to proximity to eloquent brain and the fact that GBM is characterized by poorly defined tumor margins that proceed along white matter tracts, perivascular spaces, and the potential for leptomeningeal dissemination.

Despite seemingly inevitable recurrence in GBM, initial surgical debulking with gross total resection (GTR), where possible, continues to be the mainstay of initial treatment as part of the STUPP protocol unless otherwise contraindicated due to the location of the tumor or the patient's other underlying condition [10, 21-23]. In cases where

GTR is not possible due to location and extent of tumor involvement, subtotal resection or biopsy may be alternatively employed. While randomized trials cannot be conducted due to the underlying ethics associated with such a study design, there is a preponderance of evidence in observational studies suggesting that the extent of resection is a strong prognostic factor impacting disease progression and duration of survival in patients with GBM even after adjustment for age, functional status, tumor size, and location [24-28].

Given these data, further intraoperative and perioperative modalities may certainly enhance the surgical aspects of treatment in the future. One example of attempting to address residual tumor in the resection cavity is the use of solid chemotherapeutic wafers (carmustine polymers) which have been employed and approved by the Food and Drug Administration (FDA) and used in several clinical trials, some of which have shown a survival benefit with continued dispute in the field whether there is a role for its employment in the surgical management of GBM. Certainly, some patients experience marked peritumoral edema, the safety of concurrent radiotherapy has not been fully established, and some clinical trials have not found a survival benefit [29-31]. A recent systematic review and meta-analysis of twenty-two RCTs and cohort studies involving 5,821 glioma patients made a commendable effort at attempting to address this question [32]. The authors reported that patients with GBM receiving intraoperative carmustine wafers with standard of care had a statistically significant overall survival benefit, as compared to standard of care alone [32]. However, this study utilized a fixed-effects model in several of their subgroup analysis, which may not be entirely appropriate given the underlying nature of heterogeneity of the included studies and may be better suited by utilization of a random-effects model, which likely would not have yielded statistical

significance in their analysis. In addition, the magnitude of survival benefit and a robust analysis of associated risks was lacking. Of note, patients with carmustine wafers had nearly twice the odds of complications, the most common of which was post-operative infection. Other adverse events included post-operative edema leading to elevated intracranial pressure, wound dehiscence, seizure, and neurologic decline.

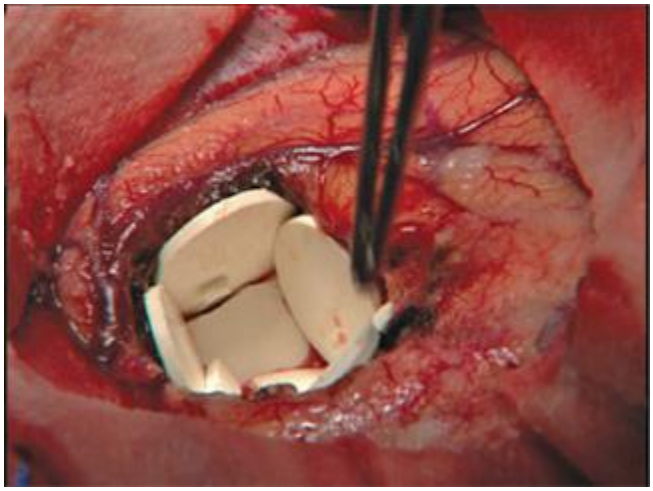

Figure 1-3. Carmustine wafers implanted in GBM resection cavity [33].

The use of carmustine wafers is currently not recommended save for employment in clinical trials and its role in the surgical management of intracranial GBM continues to be elucidated. The ambiguous utility of carmustine wafers, in part, represents the recalcitrance of GBM. On the other hand, its development and employment offers a case study by which creative methodologies may be developed to add to the armamentarium of neurosurgical strategies for GBM. Indeed, the development of numerous approaches including intratumoral convection enhanced delivery (CED), oncolytic vectors, laser interstitial thermal therapy (LITT), focused ultrasound (FUS), improved intraoperative

surgical guidance, local intra-arterial delivery, tumor treating fields (TTFs) and robotic resection continue as of this writing in the pre-clinical and clinical setting [17, 34-44].

The prognosis of GBM is poor despite aggressive intervention. From population based studies, the median overall survival of patients with GBM is estimated at 10 to 12 months from initial diagnosis. The most critical prognostic factors impacting the duration of survival in patients with GBM are baseline Karnofsky Performance Status (KPS), MGMT methylation, and IDH mutational status, and other genetic mutations [8, 45, 46]. KPS as a readout of a patient's functional capacity (e.g. activities of daily living, disability) has been used in combination with patient age and mutational status to determine a nomogram that can be used in an individual patient to predict individual prognosis, albeit with limitations due to lack of available mutational information in the validation cohort. In general, a lower KPS and increased patient age is correlated with a worse prognosis. Methylation of MGMT, involved in DNA repair, is indicative of improved overall survival and progression-free survival independent of other clinical factors as a marker of susceptibility to TMZ [45]. IDH1/2 mutations are enriched in long-term survivors of GBM, and are associated with up to a three-fold increase in survival compared with IDH wildtype GBM [47-49]. Despite the identification of prognostic factors that are associated with survival benefit, the overall clinical outcomes in patients is abysmal. A recent systematic review and meta-analysis of 63 population based studies highlighted that despite improvements in 2- and 3- survival of patients with GBM in patients after the adoption of the STUPP protocol, the 5-year overall survival remains unchanged at approximately 4 percent [50] as presented in Figure 1-5.

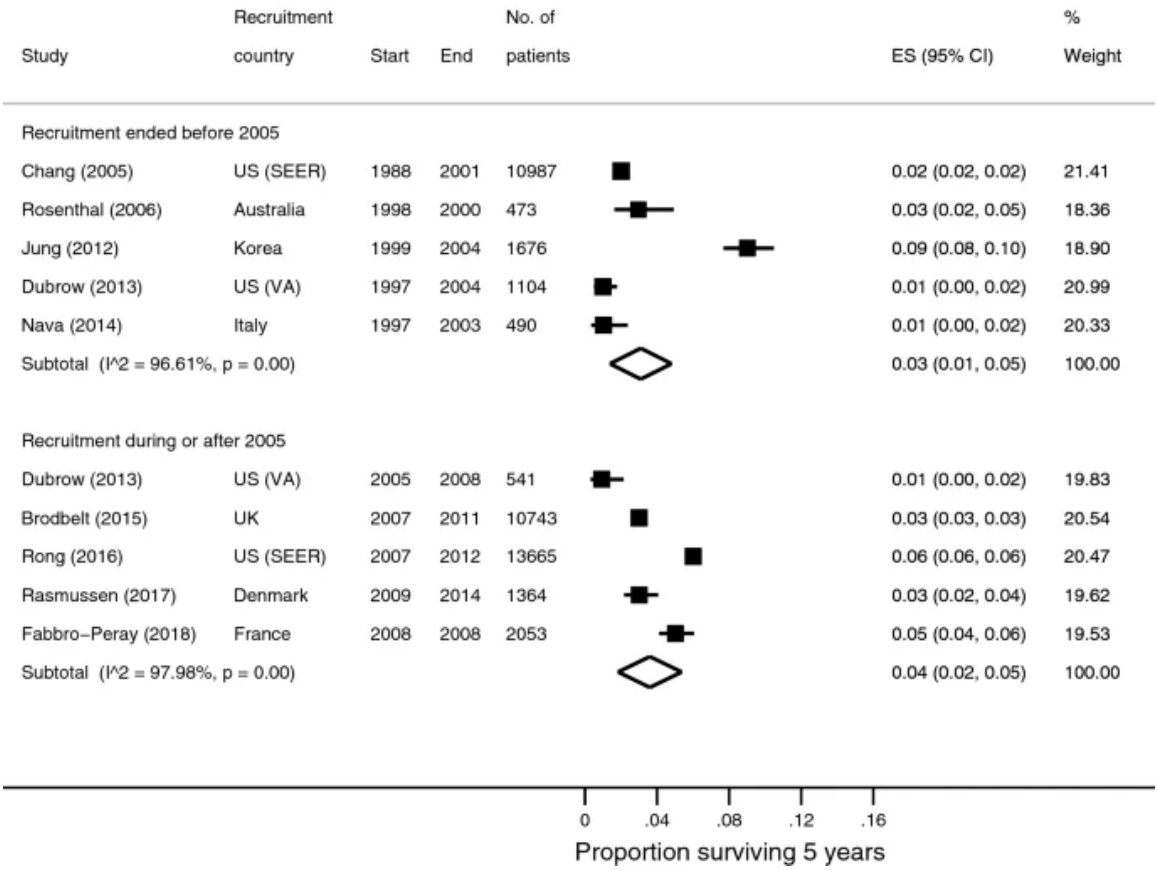

Figure 1-4. Forest plot of 5-year overall survival recruited before or after STUPP protocol adoption [50].

1.1.4 Clinical Context of Glioma in the Spinal Cord

The majority of the aforementioned discussion is drawn from literature focused on the more common entity of supratentorial GBM. There is, by comparison, a paucity of literature on intramedullary diffuse astrocytic and oligodendroglial tumors of the spinal cord, including GBM, given its orphan disease status. Nonetheless, prevailing trends can be drawn from what evidence is available from mostly retrospective chart reviews and small cohort studies. From a clinical presentation standpoint, glioma in the spinal cord presents with neuropathic pain or other neurologic deficits depending on the vertebral level

of involvement. Spinal cord gliomas (SCG) of all grades comprise 8-10% of all primary spinal cord tumors, with up to 10,000 cases occurring annually and 5-year survival rates of 11-23% in high grade lesions [51, 52]. While survival appears greater in this group of patients compared to the supratentorial counterpart, these patients almost always have permanent disability and morbidity either from the lesion itself or attempts at intervention.

Despite significant morbidity and mortality, there is no consensus treatment strategy, especially for high-grade lesions. Currently, there is a weak level of evidence in the literature (Class IIb, level of evidence C) which largely relies on expert opinion and case series. While surgical debulking is the initial mainstay of treatment in supratentorial GBM, this proves incredibly difficult in the spinal cord where the entire bulk of the parenchyma is eloquent tissue. The compact architecture of the spinal cord and its associated tracts and nerves, and the infiltrative growth pattern of these tumors lead to the decision by most neurosurgeons to avoid aggressive resection of these tumors. There are approaches such as the "inside out" technique with intraoperative monitoring to debulk the tumor as much as possible. However, even with such approaches there are most often poorly actionable surgical margins in high grade SCG [52, 53]. A review by Abd-el-barr et al outlined treatment outcomes specifically for astrocytomas of varying grade and, of note, reported greater than 67% perioperative morbidity and mortality with less than 25% incidence of actionable surgical margins at the time of surgery [51]. Consequently, maximal surgical debulking while balancing operative morbidity is often not feasible and even surgical biopsy can lead to permanent deficits.

Characteristics and treatment of different grades of SCA

WHO Grade	1	2	3	4
Percentage of all SCA	27–51%	23–29%	14–18%	6–12%
Imaging characteristics	Enhancing mural nodule, rim-enhancement	Expansile, T2 hyperintensity	Expansile, T2 hyperintensity and contrast enhancement	Expansile, T2 hyperintensity and contrast enhancement
Treatment considerations	Surgical resection in well-selected patients	Biopsy with expansile duraplasty, XRT, resection can be considered if clear planes identified	Biopsy for tissue diagnosis, XRT, gross total resection often difficult, high risk of neurologic deficit with resection	Biopsy for tissue diagnosis, XRT, gross total resection often difficult, high risk of neurologic deficit with resection
Incidence of good resection planes at surgery	29–38%	<57%	<25%	<25%
Perioperative neurologic morbidity and mortality rate	13–33%	40–73%	>67%	>67%
5 year survival rate	67–91%	50–63%	<23%	<11%

Figure 1-5. Overview of treatment and outcomes in Spinal Cord Astrocytoma [51].

Typically, patients with SCG will undergo a laminectomy to remove the overlying bone to gain access to the spinal cord and will then undergo biopsy for neuropathologic evaluation. At this time, resection is considered, but most often not pursued due to lack of actionable margins. Instead, an expansile duraplasty is performed to alleviate cord compression, effectively permitting more space for inevitable cord expansion [52].

Beyond surgery, other treatment options are also problematic for SCG. The utility of chemotherapy is undefined, and practice varies from physician to physician. Partial response with intravenous chemotherapy is noted in up to 40% of patients, but its use is primarily palliative in the clinical setting and SCGs are notoriously chemoresistant [51]. One retrospective chart review evaluated the use of TMZ in spinal cord GBM and appeared to identify a survival benefit (16 months vs 10 months) but did not reach statistical significance [54]. The authors highlighted the need for multi-institutional, prospective, controlled studies in spinal cord GBM. Given the rarity of these tumors, no randomized trials have been conducted and only handful of observational studies in pediatric patients have evaluated chemotherapy [55, 56]. Radiotherapy is similarly controversial with some studies showing no benefit, while others show some benefit in progression-free but not

overall survival [52]. Patients with SCG, especially high-grade lesions, are in a vulnerable patient population with no well-defined effective treatment options available.

1.1.5 Major pathways implicated in GBM

A discussion of the major pathways implicated in GBM pathogenesis is critical to understanding the rationale used for driving glioma formation in the pig model. In humans, one of most commonly affected pathways in GBM involves receptor tyrosine kinases (RTK). Following the binding of a respective growth factor, dimerization of an RTK occurs leading to down-stream signal transduction. For example, epidermal growth factor receptor (EGFR) is the most commonly implicated RTK in the pathogenesis of GBM. Aberrant hyperactive signaling can occur through either overexpression of its ligand, receptor amplification, or receptor mutation leading to constitutive activation. One example of constitutive activation in primary GBM lesions is the case of EGFRvIII where the loss of exons 2-7 leads to the absence of the extracellular domain of EGFR, leading to ligand-independent signaling [57]. Other RTKs such as c-MET, PDGFRA, and PDGFRB [58-60] have also been widely implicated in GBM pathogenesis. Gene expression data from 156 patients in the cancer genome atlas (TCGA) database demonstrates a range of expression values for EGFR, PDGFRB, PDGFRA, and c-MET (**Figure 1-6**) [61].

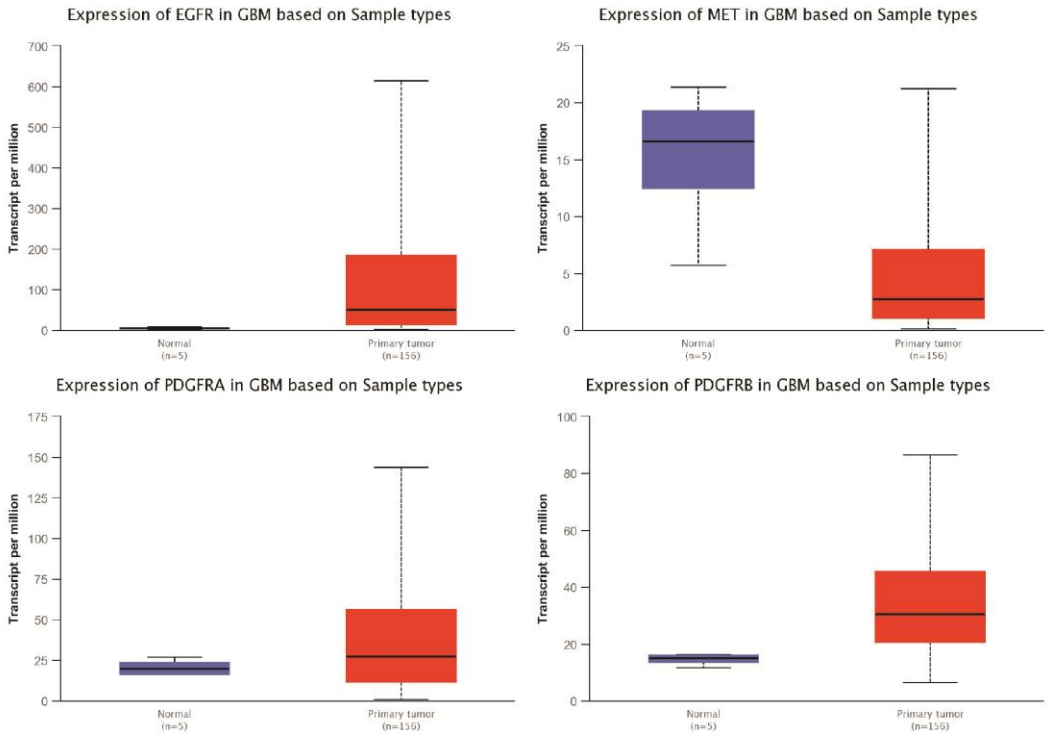

Figure 1-6. Receptor Tyrosine Kinase Expression Profiles in 156 TCGA-GBM samples.

Up to 30% of human gliomas have shown gene expression patterns that are correlated with increased PDGFR signaling. While point mutations in PDGFR may occur, they are rare events. Instead, PDGF ligands are upregulated in approximately 30% of glioma biopsies and cell lines and may serve as a mechanism by which this PDGFR signaling is hyperactivated in GBM pathogenesis [62]. c-MET is reported to be amplified in approximately 5% of human glioblastomas. Downstream of these RTKs, the overarching signaling cascade proceeds, leading to activation of rat sarcoma oncogene (RAS) and phosphatidylinositol 3'-kinase (PI3K) leading to modulation of cellular proliferation, invasion, survival, and angiogenesis, summarized in **Figure 1-7** [57].

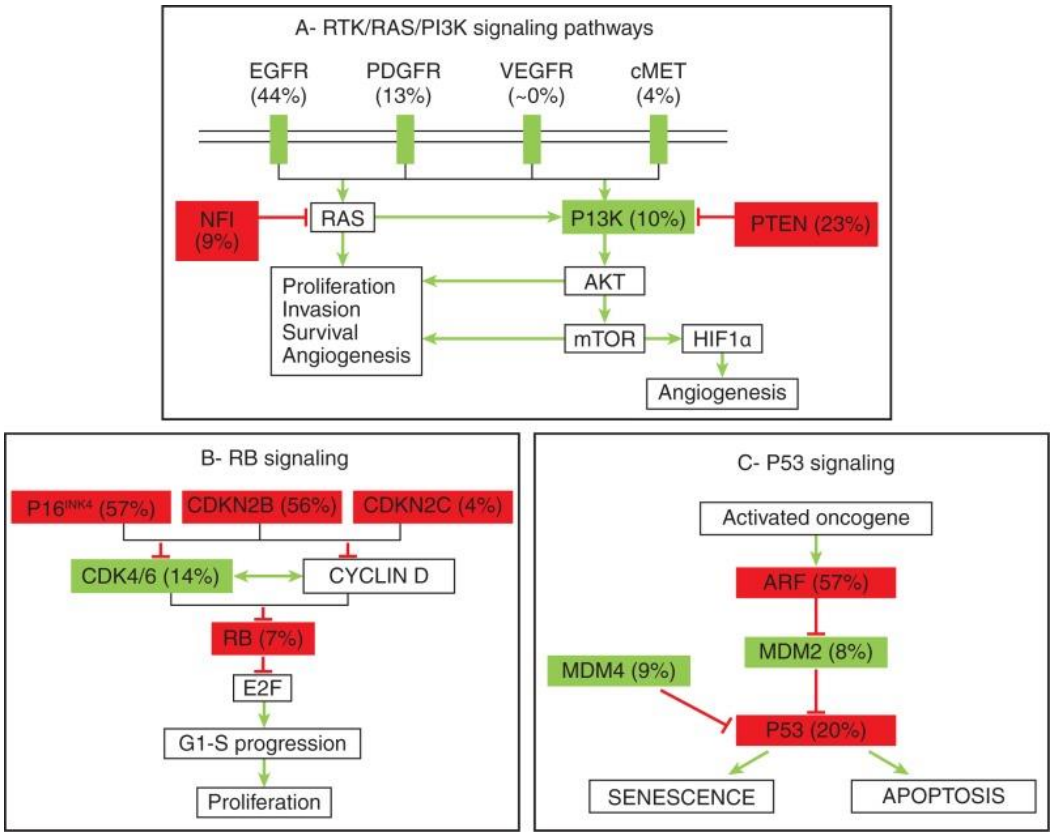

Figure 1-7. Major pathways and genetic changes in glioblastoma. Red: inactivating alterations (mutations/deletions), Green: activating mutations and amplifications. [57]

The RTK/RAS/PI3K and RAS/RAF/MEK signaling pathways is implicated in up to 88% of human gliomas. Two other major signaling axes implicated in human GBM include the P14ARF/CDKN2A & TP53 implicated in up to 87% of cases, and the RB/INK4A signaling pathway implicated in up to 78% of cases [62, 63]. The major implicated genomic changes are well reviewed elsewhere by Dunn et al [62] and Lombardi et al [57]. Mutations in RAS are exceptionally rare in GBM with only a few reported cases in smaller cohort studies [64, 65] and approximately 2% mutation rate in a larger TCGA study[66]. Nonetheless, from a broader perspective increases in the RAS signaling pathways are present in nearly all GBMs [57], and the involvement of upstream RTKs (e.g.

PDGFR, EGFR) and downstream effectors (BRAF, PI3K, AKT) are well known as previously discussed.

The genetic underpinnings of SCG are less well defined, but with some notable advancements in recent years. Grade III and IV astrocytomas are associated with various histone 3 variant H3.3 (H3F3A) mutations, and most commonly the H3F3A-K27M. This mutation has been predominantly found in high-grade astrocytomas in midline structures including the thalamus, brainstem, and spinal cord and is listed as a separate entity in the WHO 2016 classification [53]. Many grade III and grade IV astrocytomas in the spinal cord harbor K27M mutations. In addition, TP53 mutations have been identified in patients with spinal cord astrocytoma, but not IDH1, in contrast to patients with intracranial GBM [52]. The largest study examining whole genome sequencing of spinal cord glioma found a greater degree of mutational burden in GBM and anaplastic astrocytoma (N = 4 patients), as compared to lower grade lesions (N = 12) but did not identify recurrent mutations, albeit limited by its sample size [67]. The authors conducted a pathway analysis observing enrichment of cell death and survival, cellular growth and proliferation, cellular development, cellular function and maintenance, and cell cycle functions. Two of four patient samples were immunopositive for H3K27M mutations (1 GBM, 1 anaplastic astrocytoma).

A more recent study by Zhang et al examined the transcriptomic profile and differentially expressed genes in spinal cord gliomas [67]. This was the largest study of its kind with 5 spinal cord GBMs included. 5/5 (100%) of patient samples harbored H3K27M mutation, and 2/5 (40%) had ATRX mutations. Of note, they conducted a pathway analysis based on copy number variation and identified upregulation of prothrombin activation

pathway, MAPK signaling, and enrichment of epithelial to mesenchymal transition. The authors identified differentially expressed genes (DEGs) by comparing GBM and grade II spinal cord astrocytomas, and identified four genes of interest including GRM5, GALR1, NPYR, and AGTR1 as potential candidates for future study. Unfortunately, no comparisons were made to "normal" spinal cord parenchyma for differential expression (DE) analysis. The authors further identified fusion genes in the included samples and identified PDGFR and BRAF mutants in GBM samples. Overall, while inclusion of some select genetic lesions (e.g. H3K27M) appear to be associated with high grade SCG, the disease process appears to be comprised of a large degree of heterogeneity between patients.

1.1.6 Challenges to Treatment Development and the Case for Large Animal Models

As of this writing, clinical trials have yet to reveal an effective therapy for GBM. An editorial was put forth in 2019 by Aldape et al as part of an international panel to address the limited progress in therapeutic development. There are a variety of challenges including: i) a rising but incomplete understanding of disease pathogenesis, ii) lesion heterogeneity and microenvironmental complexity leading to difficulty in target optimization, iii) inherent sensitivity of eloquent surrounding parenchyma leading to patient morbidity, iv) tumor recurrence even with aggressive surgical intervention, and v) a translational research pipeline in need of improvement [68]. Bearing particular relevance to the present research is the need for improvement of the translational pipeline in the arena of animal modelling. Limited progress has been made, in large part, due to preclinical models that have failed to recapitulate both response to treatment and anatomic considerations critical for neurosurgical evaluation. This is in part due to historical reliance

on poorly characterized commercial *in-vitro* systems and respective subcutaneous/orthotopic xenografts. While these systems are important platforms for proof-of-concept studies and understanding aspects of disease pathogenesis, they have several disadvantages. Briefly, the absence of recapitulation of tumor microenvironmental features, the use of monoclonal cell lines for expansion, and immunocompromised hosts lead to several limitations. At minimum, the authors assert that a catalogue of all pre-clinical models should be generated, maintained, and that all such pre-clinical models should be subject to a minimum set of histopathologic, genomic, and imaging evaluations [68]. In the pediatric setting, initiatives such as the ITCC paediatric preclinical proof of concept platform are already working toward creating such a central resource. The authors of this editorial further emphasized that a shift toward patient derived xenografts (PDXs) and genetically engineered models (GEMs) will serve as a putative strategy for more accurate pre-clinical modeling.

Patient GBM samples can be resected, dissociated, and cultured to form GBM neurospheres for a variety of assays [69]. This has several advantages, including the retention of tumor heterogeneity, mimicking tumor genetic, epigenetic, and transcriptional make-up. These can further be transplanted as PDXs into immunocompromised animals for the *in-vivo* study. Another more recent development is the exponential rise in the use of these biopsies for generation of Organoid-GBM models [69]. This type of GBM model was first reported by Hubert et al, with co-culturing of GBM with multiple cell types instead of homogenous 3D spheroids [70]. This has since advanced to include a variety of types of GBM organoid models as a major advancement for *in-vitro* study and potential high-throughput exams. One major limitation of this approach is however the reduced

dimensionality of in-vitro studies leading to the inability to study immunotherapy or immune response to therapy due to the need for immunocompromised animals when scaling findings into PDX models.

More central to the present research is the concept of GEMs. These can be developed by germline manipulation, exogenous vector driven gene transfer, or a combination of the two to incur gain/loss of function and induce tumor growth de-novo, well-reviewed elsewhere [71, 72]. The advantages of utilizing a GEM through vector driven gene transfer are numerous, including the capacity to target specific genetic lesions and induce glioma *in-vivo* in immunocompetent animals. Platelet-derived growth factor Beta (PDGF-B) driven glioma models have been demonstrated *in-silico*, *in-vitro*, and in *in-vivo* – using rodent models with retroviral expression of PDGF-B, HRAS-G12V, shRNA-P53, and other transgenes implicated in the disease pathogenesis [63, 73-77]. In mouse models, it is reported that additional genetic lesions may be required to model high-grade gliomagenesis with either constitutive RAS, or more importantly, knockdown of CDK2NA or p53 [78, 79]. While it remains to be seen if these approaches will offer more appropriate prediction of treatment response, as GEMs continue to advance they offer an appealing option to be able to use vector driven gene transfer to generate GBM lesions in otherwise immunocompetent and wild-type animal models. This is especially promising given the issue of anatomic considerations in the pre-clinical neurosurgical pipeline and the possibility of generating a large mammalian model.

Given that surgical therapy continues to be the mainstay of initial treatment for GBM, and several drug delivery and neurosurgical strategies in pre-clinical development, the development of a large animal model of glioma is warranted. Rodent models of glioma,

including GEMs, have proven to be a strong platform for pre-clinical study. However, they unfortunately present with anatomic limitations for translation of surgical and drug delivery study [80-82]. These include, but are not limited to, decreased connective tissue, decreased white matter volume, thin meninges, more intimate dura mater and lower CSF volume [83]. In terms of size alone, the murine spinal cord is approximately 3 mm in diameter, as compared to the human spinal cord at up to 13 mm [84].

Porcine model systems provide a promising alternative, given that the genetic profile, immune system, and the size and anatomy of the porcine CNS is recognized to better model the human [82, 85-87]. Indeed, the more similar degree of musculature, connective tissue, and bony structures in the swine provides a situation where surgical approaches, drug delivery, and subcutaneous implantation of devices and catheter bearing systems may be more appropriately evaluated in a translational study. Swine are already used for a variety of endoscopic and laparoscopic surgical studies as well as imaging studies [88, 89], as well as neurosurgical techniques in both the brain and spinal cord [36, 90-98].

Recognizing these issues, groups have utilized U87 xenografts for glioma modeling in pigs, but have continued to face the known limitations of the U87 cell line and the need for immunosuppression [80, 81]. However, porcine models have already been generated using genetic manipulation (transgenic pigs, vector driven gene transfer) for a variety of cancer models outside of the CNS including familial adenomatous polyposis, bladder cancer, osteosarcoma, and others through genetic manipulation [82, 99-101]. It therefore stands to reason that employing techniques from highly advance mouse GEMs may be successful in modeling GBM in a higher order species such as the pig. These considerations bring into central focus the goal of the present study, whereby scaling well-vetted GEM

strategies from rodents to pigs, we aim to demonstrate the feasibility of inducing de-novo GBM in a space that may be more relevant for translational study.

1.2 Motivation and Objectives

1.2.1 Motivation

This work attempts to establish the feasibility of developing a novel porcine model of high-grade glioma using vector driven gene transfer. This will provide an initial model for surgical testing and to promote more advanced models in the future. The central motivation of this work draws from the current absence of topical large mammalian models of glioma, leading to reliance on phenotypically normal large animal models and stifling pre-clinical translational studies.

1.2.2 Aims

In order to successfully develop porcine GBM models and broaden the impact of this research, this thesis describes introduction of oncogenic vectors in both the most common location of GBM occurrence (supratentorial brain) and the most rare location (spinal cord). Induction of glioma growth is separated into specific aims:

- **AIM1**. Development and characterization of a porcine model of high-grade glioma in the spinal cord
- **AIM2**. Development and characterization of a porcine model of intracranial high-grade glioma

1.2.3 Structure of the Thesis

This dissertation is organized as follows.

Chapter 1 introduces the clinical context of GBM, describes challenges in the preclinical setting, and outlines the motivation and aims of the research.

Chapter 2 describes all experiments and analyses conducted for the development of spinal cord glioma in the Göttingen minipig. This chapter is focused on AIM1, and presents behavioral, histopathologic, immunohistochemical, and transcriptomic data used to characterize the model. This chapter has been adapted from the open-access publication of this research [102] with additional data included.

Chapter 3 describes all experiments and analyses conducted for the development of an intracranial glioma model in the Göttingen minipig. This chapter is focused on AIM2, and presents behavioral, radiologic, histopathologic and immunohistochemical data used to characterize the model.

Finally, Chapter 4 provides conclusions and discussion of recommended future work for improvement of modelling glioma in the minipig and potential applications that may provide more immediate translational impact.

CHAPTER 2. PORCINE MODEL OF HIGH-GRADE SPINAL CORD GLIOMA

2.1 Introduction

High-grade glioma has a clinical picture of untenable morbidity and mortality [4, 51]. Given this clinical need, the U.S. National Library of Medicine has over 350 completed phase II-III clinical trials registered as of this writing. Unfortunately, there have been limited changes to the clinical outcomes in patients with high-grade glioma over the past years. In part, this represents the malignant nature of a disease that is refractory to a variety of treatment approaches. On the other hand, this raises the question of the translational value of existing pre-clinical animal models as a pathway to the clinic [71, 72]. Given numerous strategies with measured preclinical optimism including immunotherapy, oncolytic vectors, and targeted drug delivery, more appropriate large animal model systems are necessary to bridge the translational gap [34-39].

When examining the issue of glioma modeling from an engineering perspective, an ideal animal model should recapitulate the features of human glioma in several parameter spaces including but not limited to histopathology, gene expression, heterogeneity, immunocompetence, radiologic features, and anatomy. In patients, high-grade gliomas present with marked invasion along white matter tracts and surrounding parenchyma, an immunosuppressive microenvironment, and significant inter and intra-tumoral heterogeneity [103]. Existing models of high-grade gliomas are variable in recapitulation

of these features. The most common are xenograft and syngeneic models which have drawbacks including non-invasive growth (9L, U87, U251), immunogenicity (U251, U87, C6, 9L), and restriction to murine (CT-2A, GL261) and rat models (C6, CNS-1)[104]. One of the most extensively used models for immunotherapeutic studies is the GL261 line. Originally developed in 1939 through administration of methylcholanthrene pellets into the murine brain, it has served as a critical resource given its diffuse infiltration, histopathologic characteristics, and capacity to be employed in wildtype C57BL/6 mice. Unfortunately, since this is a syngeneic mouse model, transplantation of these cannot be scaled into large animals for use a more surgically translatable anatomic space [105].

Vector-driven glioma models represent an immunocompetent option that could feasibly be scaled up to a large animal model, well reviewed elsewhere[71]. In particular, platelet-derived growth factor Beta (PDGF-B) driven glioma models have been demonstrated *in-silico*, *in-vitro*, and in *in-vivo* – using rodent models with retroviral expression of PDGF-B, HRAS-G12V, shRNA-P53, and other transgenes implicated in the disease pathogenesis[63, 73-77]. In 2011, Lei et al first reported that PDGF-B-driven models recapitulate the proneural glioblastoma subtype [106]. This was further investigated by Sonabend et al in 2014 with robust characterization of the master regulator transcriptional network that drives glial progenitor transformation [107]. As recently as 2018, transcriptomic characterization of mouse models using lentiviral PDGF-B and shRNA-CDK2NA have also been shown to produce pro-neural subtype glioblastoma [78]. In mouse models, it is reported that additional genetic lesions may be required to model high-grade gliomagenesis with either constitutive RAS, or more importantly, knockdown of CDK2NA or p53 [78, 79].

In optimizing a model system for high-grade glioma, the use of a large animal system would provide improved utility for translation of neurosurgical strategies, device development, drug delivery, and radiologic study [82, 98, 108]. From an anatomic standpoint, the rodent brain is lissencephalic creating a minimization of drug leakage and improvement of local drug delivery [80, 109]. Furthermore, the murine brain and spinal cord have significant developmental differences in comparison to large animal systems [80, 86, 109]. In addition to these anatomic considerations, the aforementioned concerns with immunocompromised models using xenograft cell lines have generated a translational space that may explain some of the limited success with preclinical strategies [72, 82, 110]. Moreover, the use of viral vector-driven approaches in targeting distinct genetic lesions implicated in the human disease have been widely reported as reliable, highly penetrant, and with striking histopathologic and molecular validity [63, 73, 75, 78].

The genetic profile, immune system, and the size and anatomy of the porcine brain and spinal cord is recognized to better model the human [82, 85, 86]. For these reasons, device implantation, stereotactic radiosurgery, and intrathecal and intraparenchymal drug delivery have all been performed in pigs [36, 80, 111-115]. Furthermore, while the Food and Drug Administration (FDA) has recognized proof-of-principle data on therapeutic efficacy in highly characterized rodent models, the use of large animals is considered critical for clinical relevance. Groups have utilized the U87 xenografts in pigs, but required Cyclosporine-based immunosuppression and continued to face the known limitations of the U87 cell line [80, 81]. Overall, existing animal models have limited translational utility due to a confluence of factors including immunogenicity, immunocompromised systems, variable recapitulation of histopathologic features, and limited anatomic translatability,

highlighting the significance of generation and validation of an immunocompetent large-animal model.

Thus, the goal of the present study is to scale previous strategies from murine models into a large animal model. Here we describe the use of lentiviral gene transfer to generate an immunocompetent large animal model of high-grade glioma in the porcine spinal cord with subsequent histopathologic, radiologic, and behavioral analysis.

2.2 Materials and Methods

2.2.1 Vector Design

It is well known that HGGs involve a mixed mutational profile with marked heterogeneity between patients. However, the RTK/RAS/PI3K and p14(ARF)/CDKN2A and TP53 pathways are involved in up to 88% and 50% of high-grade gliomas respectively[63]. Therefore, we decided to target these pathways, as has been performed in rodent models, to establish the feasibility of scaling this strategy into a pig model. Three individual lentiviral vectors were designed to target the RTK/RAS/PI3K and TP53 pathways. These vectors were designed separately to avoid the risk of decreased transduction efficiency from larger insert sizes, biosafety requirements, and to provide

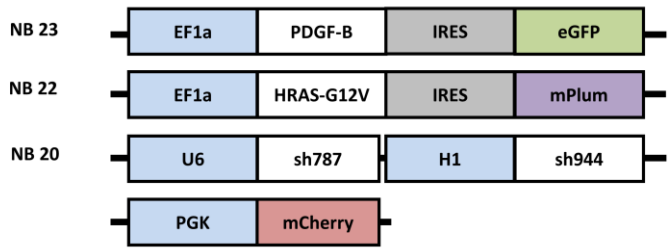

flexibility to adjust included vectors for future study[116]. Transfer plasmid schematics are presented in **Figure 2-1**.

Figure 2-1. Schematic of Lentiviral Transfer Plasmid Design

All lentiviral vectors were VSV-G pseudotyped, third-generation, replication deficient systems titered at >10^9 infectious units (IU)/ml. Vector 1: PDGF-B-IRES-eGFP and Vector 2: HRASG12V-IRES-mPlum were designed using a pCDH transfer plasmid backbone with an Ef1α promoter and reporters following an internal ribosomal entry site (IRES) sequence. Vector 3 was designed using a pLKO1 backbone and expressed two sequences of shRNA targeting porcine p53 including sequences 787 and 944 under the H1 and U6 promoters, respectively as reported by Merkl et al [117]. These shRNA sequences have 100% homology to two regions of porcine TP53 mRNA and have been used for efficient knockdown in porcine cell culture models [117]. Controls for vectors 1-3 only included reporters and shRNA scramble, referred to as **CTRL**. The oncogenic cocktail will be referred to as **ONC**. All vectors (ONC or CTRL) were thawed and combined in equal parts immediately prior to inoculation.

2.2.2 Surgical Approach

The development of an intraparenchymal mass forming lesion, as with a glioma in the spinal cord, would progress in human patients to yield an anatomically localizable neurologic deficit. As such, we selected the thoracolumbar spinal cord of the Göttingen minipigs to inject the oncogenic lentiviral vectors. This location of injection provides a distinct advantage, where tumor progression will incur clinically appreciable and quantifiable motor deficits affecting the hind-limb ipsilateral to the site of injection. The surgical procedure was performed as in prior studies and as depicted in **Figure 2-2 A-B**. [118]

Briefly, the animals underwent a two-level laminectomy and dural exposure. The spinal derrick stereotactic platform was mounted onto the dorsum of the animal for targeting the lateral white matter (2.5 mm lateral to midline, at rostral or caudal positions for each injection, spaced by 2 vertebral levels).[118] This spacing is necessary to allow for exclusive analysis of the injection sites, space for tumor growth, and delineation of laterality of motor deficits. This intraparenchymal injection strategy has been reported to be safe in pigs and has been implemented in human clinical trials [118, 119].

All injections were performed at a rate of 2.5 ul / minute, maximal volume of 25 ul, and a 3 mm depth with a 30-gauge stainless-steel needle and MINJ-PD microINJECTOR pump (Tritech Research, Inc., Los Angeles, CA). CTRL and ONC injections were randomized to either rostral or caudal site of injections on contralateral sides, as depicted in **Figure 2-2A**. A 1-minute dwell time was applied before removal of the needle to minimize reflux of the injection. The investigators performing post-operative evaluations were blinded to CTRL and ONC assignments.

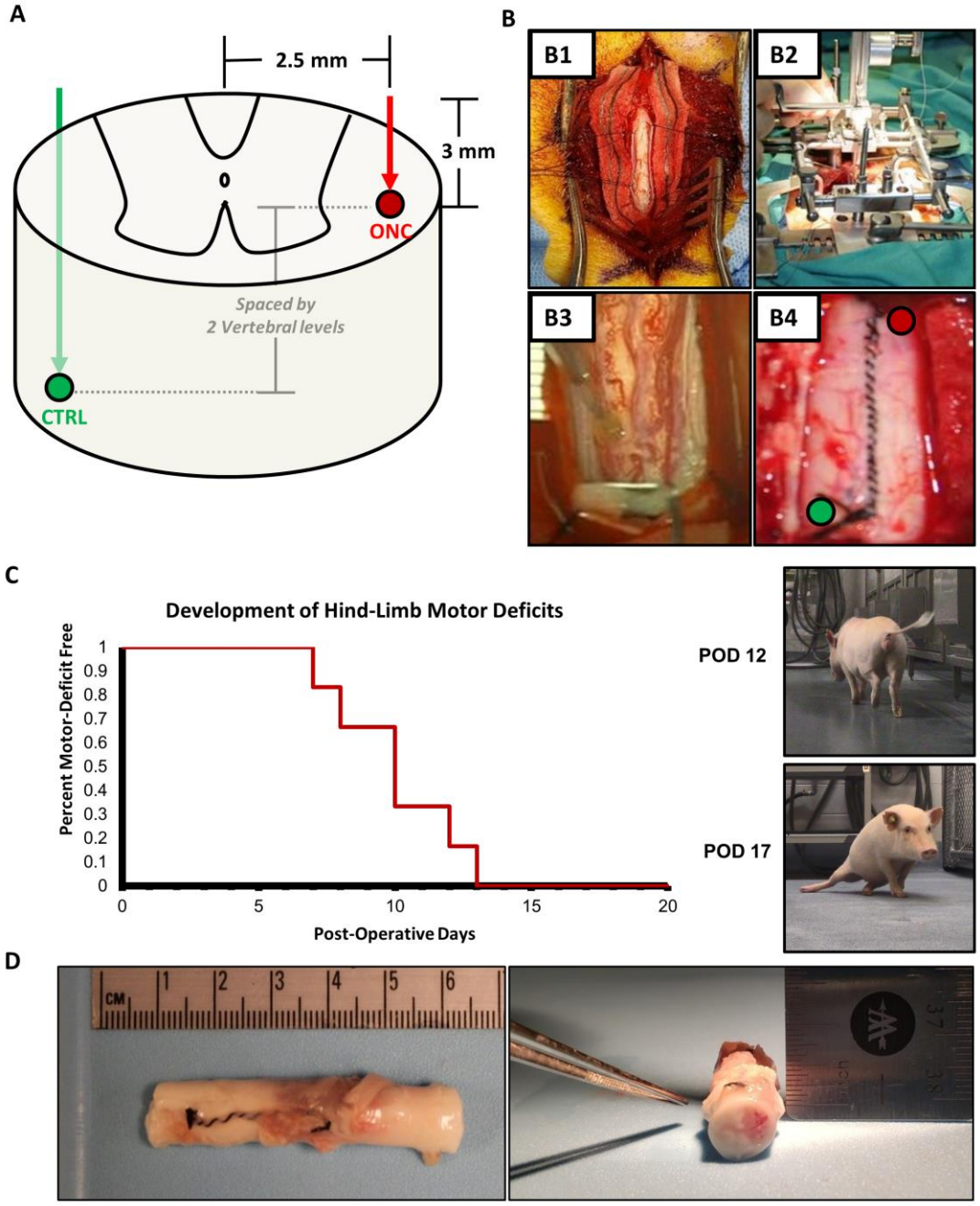

Figure 2-2. Surgery, Motor Deficits, and Gross Pathology.

2.2.3 Animals, Physical Examination, and Behavior

Our laboratory has previously used the Göttingen minipig as optimal systems for scaling vector-driven studies into large animals, given that the genetic profile, immune system, and the size and anatomy of the porcine spinal cord is recognized to better model the human [82]. Göttingen minipigs >15 kg (n = 6, 3 males and 3 females) were used in the present study. All animals underwent daily modified Tarlov-motor scoring to provide an ordinal scale of behavioral motor deficits for quantitative analysis (scored 0-9, **Table 2-1**) [120].

All scoring was performed by investigators blinded to the side of injection and study design. Other clinical deficits may manifest due to a mass forming lesion in the thoracolumbar spinal cord. As such, physical examinations were performed by laboratory staff in consultation with veterinary staff daily, with both baseline and post-operative assessments until endpoint. All surgical procedures, animal care, endpoints, and the respective experiments on pigs were approved by the Emory University Institutional Animal Care and Use Committee (IACUC). All experiments were conducted with adherence to approved protocols set forth by the IACUC in coordination with the division of animal resources (DAR) and veterinary staff.

Table 2-1. Criterion for modified Tarlov Scoring (mTS) used in Gait Assessments

mTS	Description of Criteria
9	normal HL motor function
8	ability to walk > 1 minute
7	ability to walk < 1 minute
6	ability to get up and stand unassisted more than 1 minute
5	ability to get up with assistance and stand unassisted more than 1 minute
4	ability to get up with assistance and stand unassisted less than 1 minute
3	ability to get up and stand with assistance less than 1 minute
2	good movements at joints but inability to stand
1	perceptible movements at joints
0	no voluntary movements

2.2.4 Baseline and Endpoint Magnetic Resonance Imaging

The gold-standard for non-invasive tracking of tumor progression and recurrence of glioma in human patients is magnetic resonance imaging (MRI) [121]. To evaluate tumor growth, all animals underwent baseline and endpoint MRI scans. All scans were performed on a clinical Siemens 3T Trio MRI scanner with an integrated spine coil (Siemens Medical Solutions, Malvern, PA). Pre-contrast sequences included sagittal T1-weighted, T2-weighted, T1-fluid attenuated inversion recover (FLAIR) and T2-FLAIR sequences. Following intravenous gadolinium administration (0.1 mmol/kg, MultiHance-gadobenate dimeglumine, Bracco Diagnostics Inc.), post-contrast sequences were performed (sagittal and axial T1-FLAIR). Spatial saturation pulses were used for elimination of respiratory artifacts, and appropriate adjustments of field of view, flip angle, echo time, TR, and TI-interval were made. Radiologic features of interest included iso/hyper/hypo intensity, necrosis, contrast enhancement, rostro-caudal expansion, transverse cord involvement, tumor volume, spinal cord expansion, edema, and CSF obstruction. All scans were processed and representative images were acquired using ONIS-Dicom Viewer (DigitalCore, Co.Ltd, Tokyo, Japan).

2.2.5 Tissue processing, H&E, and Immunohistochemistry

At 3-week endpoint, all animals underwent euthanasia through intravascular administration of pentobarbital sodium and intracardiac perfusion with heparinized 0.9% saline solution. Tumor core biopsies were taken and frozen for RNA-sequencing analysis. The remaining spinal cords were harvested, post-fixed in 4% paraformaldehyde overnight, and cut into blocks at 5mm intervals for paraffin embedding. Serial transverse spinal cord

sections were cut on a microtome at 8um thickness for hematoxylin and eosin (H&E) and immunohistochemistry. H&E staining was performed with deparaffinization by serial xylene incubations and ethanol gradients in a standard fashion (Hematoxylin Gill No. 3, Sigma Aldrich, Cat: GHS332; Eosin Y, Sigma Aldrich, Cat: HT110132).

Qualitatively, H&E sections were evaluated by a board-certified clinical neuropathologist (S.N. and P.C.) under wide-field microscopy blinded to the study design. Immunohistochemical stains were performed with primary antibodies for GFAP (Dako, Z0034), Olig2 (abcam, ab109186), Ki67 (abcam, ab15580) with appropriate secondaries for subsequent diaminobenzidine (DAB) and hematoxylin counterstaining (Thermo Scientific, Autostainer 480S). Immunohistochemical stains for glial markers (Olig2, GFAP) were qualitatively evaluated. Ki-67 index was quantified with manual counting of at least 1000 cells, scored as positive or negative. Representative images were acquired at 2x, 10x, 20x, and 40x magnifications (DS-Qi1 high sensitivity Cooled CCD camera, Nikon E400 microscope, NIS-Elements imaging software, Nikon Instruments, Inc) with calibrated scale bars prepared in ImageJ[122]. Whole slides were scanned in a raster pattern at 40x (Leica Aperio AT2 Slide Scanner).

2.2.6 RNA Sequencing

We employed bulk RNA-sequencing using serial biopsies from the tumor core compared to contralateral white matter biopsies in each animal. Expression data was evaluated through differential expression (DE) analysis, gene set enrichment analysis (GSEA). RNA-sequencing will be conducted in a standard fashion. Quality control was performed with FastQC with subsequent STAR alignments to the *Sus Scrofa 11.1* reference

genome [123]. Raw counts were be generated with HTseq-Count [124]. Porcine orthologues from the *Sus Scrofa 11.1* were mapped to human gene symbols using ENSEMBL. DE analysis was be conducted using DESeq2, with a fold change >1.5 and FDR <0.1 considered statistically significant [125]. GSEA will be performed using the Broad Institute platform [126] using the most recent Verhaak, Wang, and Neftel gene sets [127-129]. Other relevant gene sets will be explored through curated and hallmark published gene sets vis the Broad Institute database.

2.2.7 Data Analysis and Statistics

Behavioral and radiographic features are presented with descriptive statistics summarized with absolute and relative frequencies. Continuous and ordinal variables were summarized as appropriate using mean, standard deviation (SD), median and range. Statistical comparisons between tumor core and leading edge were conducted using two-way ANOVA, where $P < 0.05$ considered statistically significant (Prism Graphpad 9, San Diego, CA).

2.3 Results

2.3.1 Animals develop motor deficits ipsilateral to ONC injections by post-operative week 3.

Post-operative behavioral analysis and physical examination was performed daily by blinded investigators until a 3-week endpoint. All animals developed clinically appreciable progressive motor deficits ipsilateral to the ONC injection, with 100% of animals (n = 6/6) developing hindlimb motor deficits by the 13^{th} post-operative day

(**Figure 2-1 C**). 33% of animals (n=2/6) progressed to develop bilateral hindlimb paralysis by the 3-week endpoint.

At endpoint, Tarlov scores among animals ranged from 0-8, including either complete paralysis or impaired ambulation with the ability to walk greater than 1 minute respectively. Following tissue harvesting, appreciable mass-forming lesions were observable through the dura mater on gross pathology (**Figure 2-1C**). No animals exhibited clinical signs of cachexia and the mean difference between baseline and endpoint body weight was 0.61 kg (SD: ± 0.94, Range: -0.5 to 2.1, Median: 0.55). A summary of hindlimb motor deficits, laterality, and clinical symptoms are outlined in **Table 2-2**. On gross examination, (**Figure 2-1D**), a mass forming lesion was appreciated in 6/6 animals with appreciable expansion of the spinal cord. No tumoral or peritumoral cysts were appreciated.

Table 2-2. Overview of Clinical Findings at Baseline and Endpoint All Animals.

	Baseline			Endpoint					
Animal	**Injection Site**	**Weight (kg)**	**mTS**	**Hindlimb Motor Deficits**	**Superficial Pain Response**	**Conscious Proprioception**	**GI/GU**	**Weight (kg)**	**mTS**
1	R: ONC L: CTRL	20.2	9	Right	R: Delayed	R: Delayed	WNL	20.4	8
2	R: CTRL L: ONC	19.7	9	Bilat	R: Absent L: Absent	R: Absent L: Absent	Urine Retention	21.8	0
3	R: ONC L: CTRL	15.3	9	Bilat	WNL	R: Absent L: Absent	WNL	16.4	3

4	R: CTRL L: ONC	15.5	9	Left	WNL	L: Delayed	WNL	15.4	8
5	R: ONC L: CTRL	21.6	9	Right	R: Delayed	R: Absent	WNL	21.1	8
6	R: CTRL L: ONC	17.2	9	Left	WNL	WNL	WNL	18.1	8

Abbreviations: R – right, L – left, ONC – oncogenic vectors, CTRL – control vectors, Bilat – bilateral, GI/GU – Gastrointestinal or Genitourinary, WNL – within normal limits, mTS – modified Tarlov Score.

2.3.2 Endpoint MRI demonstrates mass forming lesions consistent with high grade glioma.

All 6 animals received baseline and endpoint MRI scans. Baseline imaging demonstrated normal spinal cord anatomy with unobstructed cerebrospinal fluid (CSF) pathways in the sub-arachnoid space that were visible on sagittal views. Representative images from two animals presented in **Figure 2-3 A, T2, Baseline**. 3-weeks post-operatively, T2 and T1-FLAIR scans demonstrated mass forming lesions at the location of ONC injections, but not CTRL injections, and appreciable cord expansion and obstruction of CSF **(Figure 2-3 A, Post-Operative)**. No cysts, hemorrhage, or syrinx formations were observed. The mass forming lesions (6/6) localized to clinical motor deficits and the locations of ONC injections. Intravenous Gadolinium contrast was administered (0.1 mmol/kg) for post-contrast scans. Sagittal T1-FLAIR post-contrast scans showed contrast enhancing, invasive, mass forming lesions with up to two vertebral levels of rostro-caudal involvement **(Figure 2-3 A, T1-FLAIR + Gadolinium, Post-Operative, Yellow Arrows).** All animals developed radiologically consistent masses on MRI with T1

weighted isointensity, T2 iso/hyperintensity, and T1-post contrast enhancement. Transverse T1-FLAIR post-contrast images demonstrated degree of cord involvement in a representative animal**(Figure 2-3 B, Yellow Arrow)**. Measurements on post-contrast axial and sagittal scans demonstrated a mean of 27.8 mm rostro-caudal invasion (SD ±4.8; Range: 22.7 to 36.2; Median: 26.88) and a mean of 7.7 mm axial invasion (SD ±1.2; Range: 6.1 to 9.0; Median: 8.1).

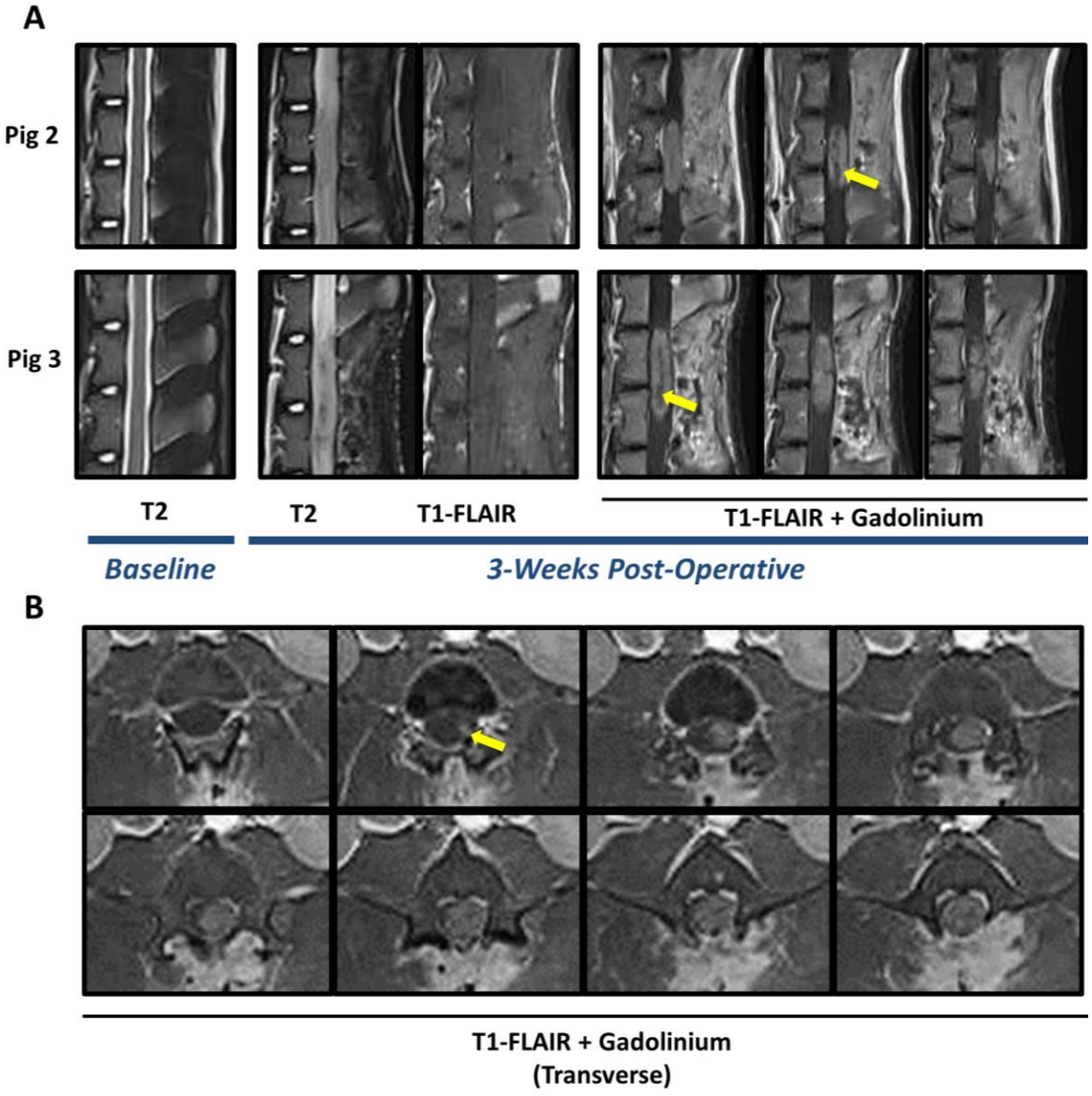

Figure 2-3. Endpoint MRI scans demonstrate mass forming lesions consistent with high-grade intramedullary spinal cord glioama.

2.3.3 Histopathologically confirmed High-Grade Glioma

On H&E staining at low magnification, the tumors diffusely infiltrate the spinal cord, spreading rostral and caudal with respect to the injection site, and invading both grey and white matter. There is noticeable mass effect on the central canal and contralateral structures (**Figure 2-4 A**) in all animals. In addition, there is marked invasion along the white matter tracks with cellular regions showing hyperchromasia visible in sections distal to the site of injection (**Figure 2-4 A**).

Histopathologic features identified at high magnification include: high cellularity with epithelioid, and fibrillary astrocytic morphology, microvascular proliferation**,** necrosis, thrombosed blood vessels, and invasion along the tumor border into surrounding normal parenchyma **(Figure 2-4 B)**. Subsequent evaluation by board-certified neuropathologists (S.N. and P.C.) resulted in confirmation of the mass forming lesions as high-grade gliomas with astrocytic morphology, with consistent features in all animals. Ki-67 staining was highly positive across animals, (**Figure 2-4 C**) with a mean proliferative index of 37.1% (SD: ±14.2). In addition, immunohistochemical staining was highly positive for glial markers GFAP and Olig2 (**Figure 2-4 C**). Comparison of tumor core and leading edge ROIs demonstrated statistically significant differences in percent immunopositivity of Ki-67, SOX2, Olig2, and NG2 immunopositivity ($P<0.001$) (**Figure 2-5)**.

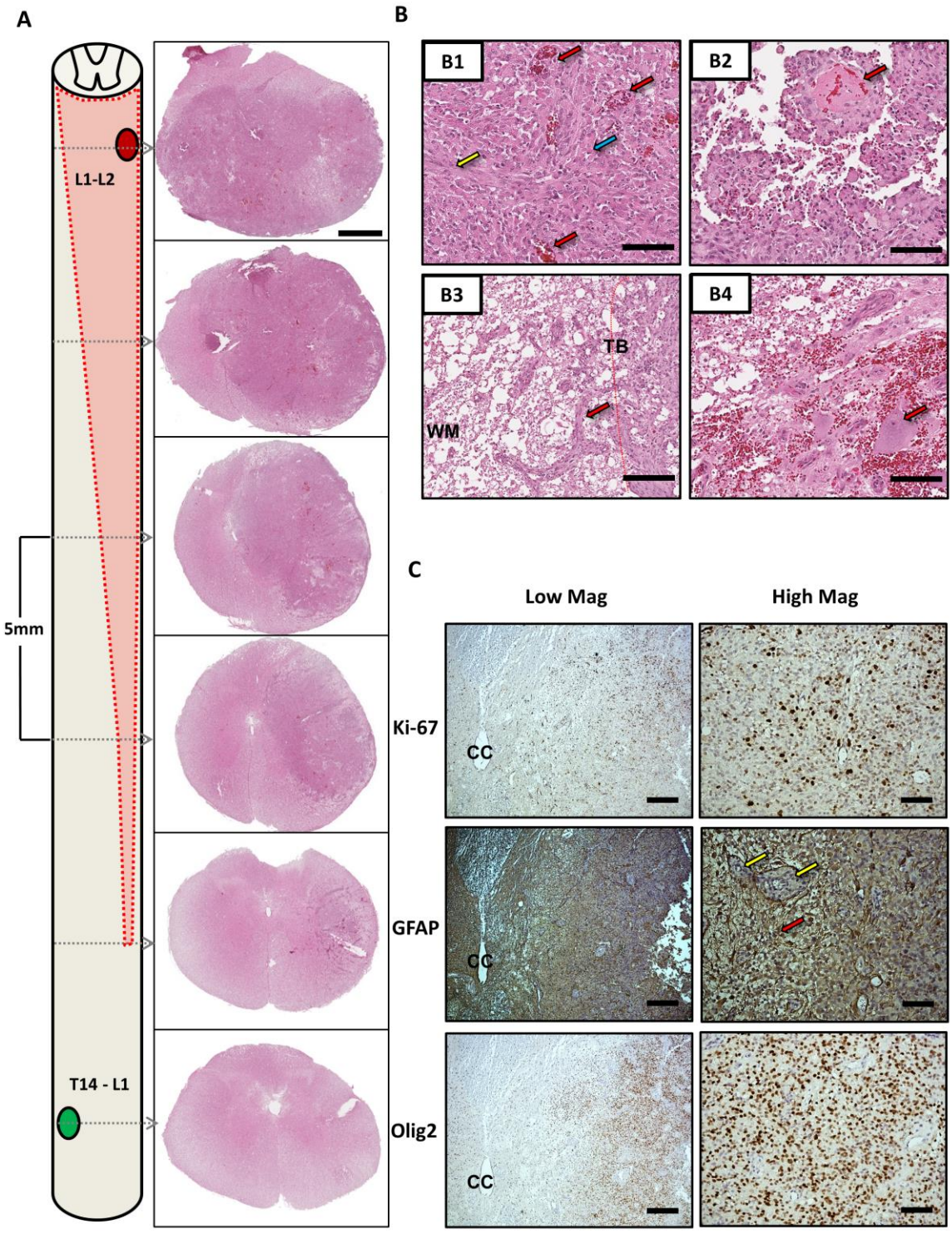

Figure 2-4. Histopathologic and Immunohistochemical Characterization.

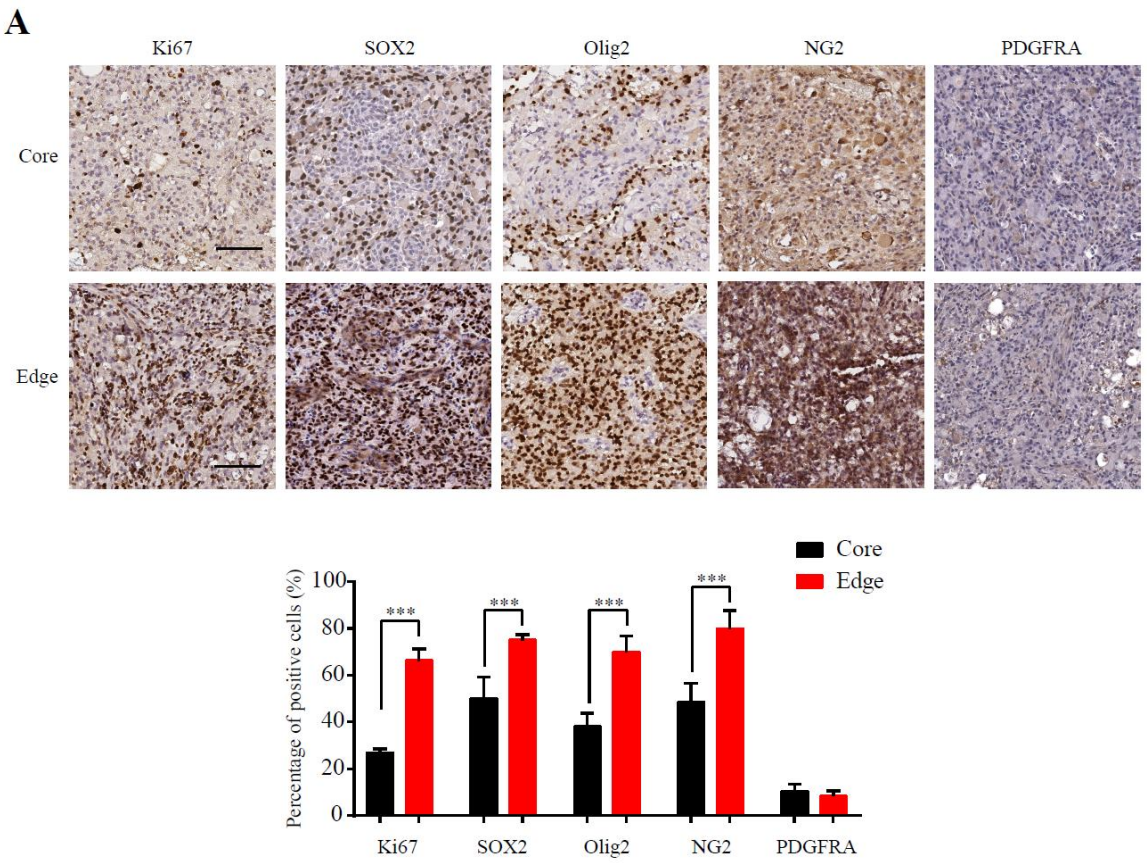

Figure 2-5. Comparison of tumor core and leading edge proliferative and glial progenitor markers.

2.3.4 Differential Expression and Gene set enrichment analysis

RNA sequencing was conducted on tumor core (N=6) and distal white matter biopsies (N=6). STAR alignment generated a mean of 94.5% alignment (Range: 93.8-95.1). DEA with DEseq2 identified a total of 10757 differentially expressed genes (FDR <0.1, FC >1.5) the pig spinal cord compared to distal white matter biopsies **(Figure 2-6 A)**, with 6019 downregulated genes and 4688 upregulated genes. PCA of normalized expression values of the top 5000 genes demonstrated 61% variance across PC1 and illustrate clustering of tumor and white matter samples (**Figure 2-6 B)**. In order to evaluate enrichment of classical (CL), mesenchymal (MES), and proneural (PN) subtypes, GSEA was conducted on previously identified respective gene sets. Verhaak-MES, -CL, and Wang-MES glioma gene sets were enriched (FDR <0.05) with the top 50 upregulated and downregulated genes in the Verhaak-CL and –MES presented in **Figure 2-6 C**. Verhaak-PN, and Wang-CL and -PN were not enriched. GSEA of the Neftel gene sets further identified enrichment of the mesenchymal signature MES1, and G2/M and G1/S (**Table 2-3 and Table 2-4**).

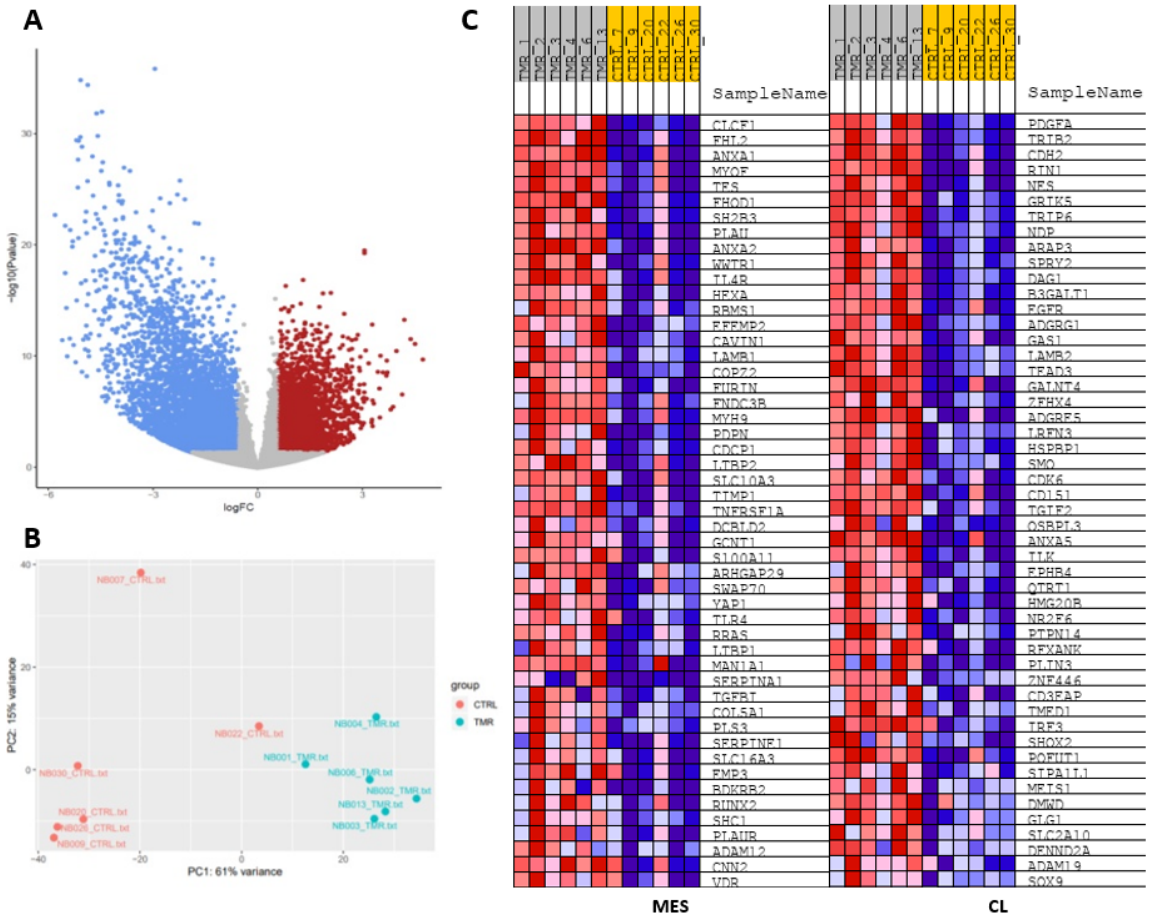

Figure 2-6. Gene set enrichment analysis demonstrates enrichment of Verhaak Mesenchymal and Classical subtypes in the minipig spinal cord glioma.

Table 2-3. GSEA of Verhaak and Wang Glioma Subtype Gene Sets.

Gene Set	SIZE	ES	NES	NOM p-val	FDR q-val
Upregulated					
VERHAAK-CL	148	0.24	3.38	0.000	**0.000**
VERHAAK-MES	202	0.10	1.66	0.031	**0.044**
WANG-MES	48	0.20	1.59	0.061	**0.049**
Downregulated					
VERHAAK-NL	121	-0.35	-4.45	0.000	**0.000**
WANG-CL	45	-0.29	-2.26	0.002	**0.003**
VERHAAK-PN	169	-0.13	-1.85	0.014	**0.019**
WANG-PN	46	-0.21	-1.71	0.029	**0.027**

Table 2-4. GSEA of Neftel Gene Sets.

Gene Set	SIZE	ES	NES	NOM p-val	FDR q-val
Upregulated					
G2/M	44	0.38	2.99	0.000	**0.000**
MES1	85	0.17	1.86	0.006	**0.024**
G1/S	26	0.26	1.57	0.063	**0.085**
NPC1	46	0.18	1.40	0.127	0.140
MES2	97	0.09	1.07	0.354	0.363
Downregulated					
AC	87	-0.42	-4.50	0.000	**0.000**
OPC	90	-0.26	-2.90	0.000	**0.000**
NPC2	39	-0.18	-1.34	0.000	0.135

2.4 Discussion

The data of the present study illustrates the first lentiviral vector induced large animal model of high-grade glioma with histopathologic, radiologic, and behavioral characterization. We found that high-grade gliomas formed in a highly penetrant fashion following the injection of ONC lentiviral vectors and exhibited histopathologically confirmed features of high-grade gliomas. Importantly, this has not been performed in large animal models prior to this study and we assert that this paradigm using intraparenchymal gene transfer may be adapted for use in spinal cord, brainstem, cerebellum, and brain modeling of glioma.

Molecular subtyping of glioma has provided general categories by which lesions can be further characterized with known genetic lesions and differences in clinical outcomes [127, 129, 130]. The Canoll laboratory and others have shown that PDGF-B driven rodent models of high grade glioma elicit a proneural subtype [66, 78, 106, 107]. A transplanted EGFRvIII rodent model also surprisingly reported convergence to a proneural subtype [131]. We found statistically significant enrichment in both historical and more recent MES gene sets [127, 129]. Using the most recent gene sets put forth by Neftel et al [128], we also found significant enrichment in G2/M, MES1, and G1/S gene sets. Though it should be noted that Neftel et al utilized single-cell RNA sequencing data to identify these new potential gene signatures.

However, one present issue is the lack of data in the realm of the spinal cord, forcing the use of transcriptomic signatures identified and validated in supratentorial glioma. Illustrative of this issue is that the largest study examining the transcriptomic profile of

high-grade SCG was conducted in 2019 by Zhang et al, studying only 5 patient samples. Furthermore, publicly available databases, such as the TCGA, do not provide curated data sets for high-grade SCG as in the supratentorial setting. Nonetheless, the results of our present study are promising and suggest that the transcriptomic profile of the present model may potentially resemble existing categories of glioma, especially the MES subtype. Further work should examine the feasibility of conducting a correlation analysis on SCG samples in humans to identify whether gene expression in this model is related to the human disease. MES subtype glioma is known to contain a larger proportion of tumor associated macrophages and immunologic involvement, making this a potential space to further study this particular subtype of glioma. Future work should examine the inflammatory microenvironmental features of the present model.

Our immunohistochemical examination was limited due to the nature of these preliminary experiments and study design, but was still able to identify statistically significant differences between tumor core and leading edge in Ki-67, and glial progenitor markers SOX2, OLIG2, NG2. This may suggest that the present model has a degree of intratumoral heterogeneity between these regions. Other studies have indeed shown differences in expression of these markers in the tumor core and leading edge [132{Bastola, 2020 #70{Bastola, 2020 #70]}. While this serves as a first step and further study is needed to investigate intratumoral heterogeneity in this model, as well as the tumor microenvironment of high grade SCG in the pig model.

2.4.1 Modeling Strategy

Current preclinical studies for therapeutic approaches including, but not limited to, oncolytic viral therapy, immunotherapy, convection-enhanced delivery, fluorescein dyes and laser interstitial thermal therapy in high-grade glioma rely on large animal models with no ability to evaluate therapeutic efficacy in disease models[36]. By using orthotopic intraparenchymal gene transfer in higher-order species, given the advantages of an immunocompetent porcine model, investigators can reasonably adjust transgenes and/or promoters to dissect the disease process and develop translationally relevant systems in a variety of glioma grades and subtypes.

Utilizing gene transfer in pigs as a system for modeling tumors in the CNS offers several advantages. For one, this approach has been previously employed in porcine CNS gene transfer for other neurologic disease modeling and can be widely scaled for implementation and adaptation in wildtype pigs for use in preclinical therapeutic development programs [133, 134]. . Importantly, this would circumvent the need for generation and maintenance of numerous transgenic breeds, providing a pathway for rapid induction in widely available pigs. In addition, when using lentiviral gene transfer – third or second generation replication deficient lentiviruses permit large insert size, minimal immunogenicity, and a broad tissue tropism with a VSV-G pseudotype [116]. Furthermore, lentiviral genomic integration into the transduced cell permits the continued expression in daughter cells of the proliferative environment of an induced glioma [75]. As such, examination of the most common patient-population and respective patterns of mutations may allow for targeted modeling with ease of inclusion or exclusion of specific genetic lesions (e.g. loss of ATRX, IDH1 mutations, EGFRvIII, PTEN, p53, H3K27M) with

multiple combined constructs. Consequently, this paradigm could provide a foundation for utilizing specific transgenes, promoters, and titer for a host of potential glioma grades, subtypes, and other CNS tumors in porcine models.

The aforementioned strategies can be reasonably implemented using non-viral systems (sleeping beauty transposon system) or other vector driven gene editing approaches (CRISPR) to develop an armamentarium of immunocompetent translational animal model systems for neoplasia of the central nervous system. By drawing from clinical insights, applying foundational research, and validating response to the clinical standard of care, we assert that such a modeling approach would provide a highly impactful space for both bench science and translational therapeutic initiatives.

2.4.2 Limitations and Future Directions

There are several areas that warrant investigation in future studies. One area of interest is whether these tumors progress as the result of clonal expansion of virally infected cells, or through the recruitment and transformation of resident glial progenitors[74, 75, 78]. In addition, it is necessary to evaluate tumor biopsies for accumulated mutations that occur in the environment of p53 knockdown, PDGF-B expression and HRAS-G12V expression, and an overall picture of proliferative stress[135]. As such, the importance of sequencing tumor biopsies for evaluation of copy-number variation, single-nucleotide polymorphisms and mutational insertions or deletions cannot be overstated. In addition, the present model induces glioma formation within weeks, which may prevent the evaluation of long-term therapeutic strategies and may limit the ecologic validity of the model. Future studies should examine, in part, whether more indolent course of de-novo

tumor induction is possible by using alternative transgenes or modifying viral titer, volume, or location of injection.

The rise of molecular subtyping have provided putative categories for glioblastoma and high-grade glioma[129, 130], which have marked inter-tumoral and intra-tumoral heterogeneity in patients[136, 137]. To validate such models with respect to these subtypes and evaluate the degree of inter- and intra-tumoral heterogeneity, the use of bulk and single-cell RNA sequencing for transcriptomic investigation is warranted. Furthermore, it is critical from a translational standpoint to study the use of surgical resection, associated strategies and challenges, and the characterization of tumor recurrence in the present model. Lastly, the characterization of host immunologic responses in the swine in response to these lentiviral injections will need to be understood for testing and understanding immunotherapeutic interventions. Limitations and future directions notwithstanding, the present study describes the first histologically, radiologically, and behaviorally characterized immunocompetent porcine spinal cord glioma model.

2.5 Conclusion

Lentiviral gene transfer of driver mutations represents a feasible pathway to modeling glioma in higher order species. Here we report the first lentiviral induced large animal model of high-grade spinal cord glioma. This can potentially be used in a variety of preclinical neurosurgical therapeutic development programs.

2.6 Figure Legends

Figure 2-1. Schematic of vector design. Lentiviral vectors targeting the RTK/RAS/Pi3K and p53 pathways were designed separately to avoid the risk of decreased transduction efficiency from larger insert sizes, safety considerations. All lentiviral vectors are third-generation, replication deficient systems. Two of the lentiviral vectors used a pCDH transfer plasmid backbone with a ubiquitous Ef1α promoter and fluorescent reporters following an internal ribosomal entry site (IRES) sequence. These included Vector 1: PDGF-B-IRES-eGFP and Vector 2: HRASG12V-IRES-mPlum. Vector 3 was designed using a pLKO1 backbone and expressed two sequences of shRNA targeting porcine p53 including sequences 787 and 944 under the H1 and U6 promoters, respectively. These sequences have 100% homology to two regions of porcine p53 mRNA and have been used for efficient knockdown in porcine cell-culture models [12]. For a fluorescent reporter in this vector, the PGK promoter was included with expression of mCherry. Controls for vectors 1-3 only included fluorescent probes and shRNA scramble, herein referred to as CTRL. The oncogenic cocktail will be referred to as ONC.

Figure 2-2. Surgery, Motor Deficits, and Gross Pathology. (A) Targeted injection of lateral white matter of the thoraco-lumbar spinal cord. **(B)** Surgical approach with exposure of the spinal cord (B1), mounting of the spinal derrick stereotactic platform (B2), injection (B3), and dural closure (B4). **(C)** All animals developed clinically appreciable hindlimb motor deficits by post-operative day 13 (n = 6/6). **(D)** Gross pathology of spinal cord demonstrates spinal cord expansion and a mass forming lesion at the site of ONC injection and not CTRL (Pig 3 necropsy shown).

Figure 2-3. Endpoint MRI scans demonstrate mass forming lesions consistent with high-grade intramedullary spinal cord glioma. (A) Baseline T2 weighted scans

demonstrate normal spinal cord anatomy. At 3-weeks post-operatively, T2 and T1-fluid attenuated inversion recovery (FLAIR) scans show mass forming lesions at the site of ONC injection in 6/6 animals (representative images of pig 2 and 3 shown). T2 weighted scans demonstrate cord expansion and obstruction of CSF, as compared to baseline scans. Sagittal T1-FLAIR post-contrast images show contrast enhancing mass with non-enhancing / heterogeneously enhancing core suggestive of necrotic foci (yellow-arrows). **(B)** Axial T1-FLAIR post-contrast images show complete cord involvement of contrast-enhancing mass forming lesion (yellow arrow demonstrates beginning of contrast enhancing lesion). Axial images spaced by 2.5 mm.

Figure 2-4. Histopathologic and Immunohistochemical Characterization. (A) Schematic of Tumor Growth and Low magnification H&E. Tumor growth occurred in 6/6 animals at the site of ONC injection (Red Oval) and not CTRL injections (Green Oval). Invasive growth was noted with frank rostro-caudal and transverse involvement (schematic, red dotted line and shaded region) and can be appreciated in serial sections with H&E staining demonstrating invasion along the lateral white matter (1x magnification, Scale Bar = 2mm). The CTRL injection site did not demonstrate any morphological changes as depicted in the lowest low magnification panel (T14-L1). **(B) High magnification tumor characteristics on H&E.** Histopathologic features were investigated at high magnification, noting high cellularity with gemistocytic (Blue Arrow) and fibrillary (Yellow Arrow) astrocytic morphology (Panel B1), microvascular proliferation (B1, Red Arrows), and regions of necrosis and thrombotic blood vessels (B2, Red Arrow). Invasion along the tumor border (TB) into surrounding white matter (WM) (B3, Red arrow). In addition, background parenchyma was visible in regions of the tumor,

here depicting motor neurons of the ventral horn (B4, Red Arrow). (40x magnification, Scale Bar = 100um). **(C) Immunohistochemical Staining for Glial Markers and Proliferative Index.** Standard fixed, paraffin embedded staining protocols with citrate mediated antigen retrieval were applied to 8um thick serial sections (n = 6-8 sections/animal/stain). GFAP staining demonstrated highly positive staining in the tumor mass (Red Arrow) with intervening negative staining of vasculature (Yellow Arrows). Olig2 demonstrated highly positive regions within the tumor mass. Ki-67 showed a high proliferative staining with a mean proliferative index of 37.1% (SD: ±14.2). (Left: 4x magnification, Scale Bar = 500 um, Right: 20x magnification, Scale Bar = 100 um. CC: Central Canal.)

Figure 2.5. Comparison of tumor core and leading edge proliferative and glial progenitor markers. High powered fields were quantified for each immunostain in each region, (N=8 per animal). The leading edge demonstrated a statistically significant greater percent immunopositivity for Ki67, SOX2, Olig2, and NG2 as compared to the tumor core. ***P< 0.001.

Figure 2.6. Minipig spinal cord GBM Preliminary Differential Expression and Gene Set Enrichment Analysis. (A) 10757 differentially expressed expressed genes (FDR <0.1, FC >1.5). Red: up, Blue: Down, Grey: Not sig. (B) Principle component analysis shows clustering of TMR and CTRL biopsies. **(C)** Heatmap of top 50 genes in rank-list in Verhaak MES and CL.

CHAPTER 3. MODELING SUPRATENTORIAL GLIOBLASTOMA IN GOTTINGEN MINIPIGS: A PILOT STUDY

3.1 Introduction

Glioblastoma (GBM) is the most common and most deadly primary brain tumor in adults. While there have been numerous surgical translational studies demonstrating anti-tumor activity in rodents, the anatomy of such models present limitations that are difficult to scale into humans [1-6]. Unfortunately, there have been limited improvements in outcomes. This represents the recalcitrance of a disease process that is refractory to the standard of care and highlights the importance of development of topical animal models that can serve as pre-clinical neurosurgical platforms.

While rodent models of glioma have proven to be an informative platform for pre-clinical study, they unfortunately present with anatomic limitations for clinical translation [80-82]. These include, but are not limited to, decreased connective tissue, decreased white matter volume, thin meninges, more intimate dura mater, lower CSF volume, and lissencephalic brain structure [83]. In terms of size alone, the murine brain is approximately 4 mm in diameter, as compared to the human brain at up to 140 mm [84]. As an alternative, the Göttingen minipig is a large mammalian system that overcomes many of these anatomic limitations and has been increasingly employed in neuropathologic disease modeling as a putative preclinical platform. Recognizing these considerations, groups have indeed utilized U87 xenografts in the pig brain, but have continued to face the known limitations of the U87 cell line, and the prohibitive cost of a longitudinal immunosuppressive regimen,

inability to evaluate immune response to therapy, and side effects of long-term cyclosporine administration [80, 81].

Vector-driven strategies represent a well-vetted non-xenograft option that could feasibly be scaled into large mammalian systems [71]. In human GBM, the RTK/RAS/PI3K pathway is widely implicated and affects up to 88% of cases [63, 66]. The second most commonly affected pathway is the p14Arf/CDKN2A and TP53 axis which is involved in at least 50% of cases. Targeting these pathways to drive gliomagenesis have been shown to induce GBM formation in rodent models through PDGF-B, HRAS-G12V, shRNA-P53, and others [63, 73-77, 138]. PDGF-B alone has been shown to induce GBM with compelling neuropathologic features [73-75, 78, 79, 139]. In mice, it is reported that additional genetic lesions may be required to model high-grade gliomagenesis with either constitutive RAS or knockdown of CDK2NA or p53 [63, 78, 79, 140, 141]. In addition, our prior work in the minipig spinal cord successfully utilized PDGF-B, shRNA-P53, and HRAS to induce high-grade spinal cord glioma [102]. These prior vector driven modeling studies and translational considerations form the foundation of our present exploratory study. Here we describe a series of minipigs treated with lentiviral vectors to induce supratentorial GBM with subsequent behavioral, radiologic, and histopathologic findings.

3.2 Materials and Methods

3.2.1 Vector Design

Lentiviral vectors were designed to target the RTK/RAS/PI3K and TP53 pathways (**Figure 3-1a**). Vectors were designed separately maintain transduction efficiency and in accordance with biosafety requirements [116]. All vectors were VSV-G pseudotyped,

third-generation, replication deficient lentiviral systems and tittered at >10^9 infectious units (IU)/ml. PDGF-B-IRES-eGFP and HRASG12V-IRES-mPlum vectors were produced on a pCDH transfer plasmid backbone under an Ef1α promoter. shRNA-P53 vectors utilized a pLKO1 backbone and expressed shRNA targeting porcine p53 including sh787 and sh944 under the H1 and U6 promoters, respectively as previously reported by Merkl et al [117]. All vectors were thawed and combined in equal parts immediately prior to inoculation.

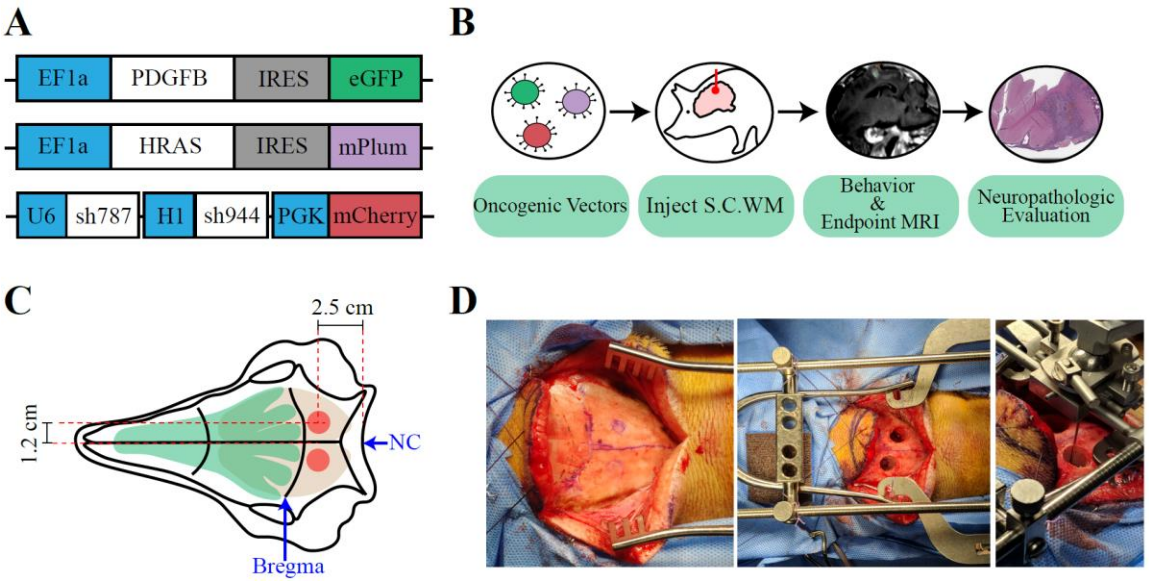

Figure 3-1. Vector and Experimental Design

3.2.2 Animals, Physical Examination, and Behavior

Four Göttingen minipigs (>15 kg, 8 months old) were used in the present study. All animals underwent modified Tarlov-motor scoring (mTS) and porcine neurobehavioral scoring (PNS) to provide an ordinal scale of neurologic deficits (Supplemental Table 1 and 2) [98, 120]. Physical examinations were performed in coordination with veterinary staff with both baseline and post-operative assessments until a pre-determined 4-week endpoint.

All experiments were conducted with adherence to approved protocols set forth by the Institutional Animal Care and Use Committee (IACUC) in coordination with the division of animal resources (DAR) and veterinary staff.

3.2.3 Surgical Approach

Under general anesthesia minipigs underwent bilateral craniotomy 1-2 cm in diameter over the injection site at pre-determined coordinates (**Figure 3-1 B-D**). The stereotactic injection platform was fixed to the cranium and cervical spine above and below the primary incision to permit four points of fixation. The dura mater was incised and a bolus of Methylprednisolone (125mg, Intravenous) was administered. The injection microdrive and ball-joint was then rigidly attached to the stereotactic platform for controlled advancement of the microinjection cannula. The injection cannula consists of a 30-gauge needle with sharp, beveled tip and polyethylene tubing to minimize viral adhesion. Intraparenchymal injections of the viral vector targeting the subcortical white matter were performed at a depth of 7-8 mm from contact at the pial surface as determined from minipig radiologic atlas. The overall target was the parieto-occipital subcortical white matter as this region contains high concentrations of glial progenitor cells, allowing for the most appropriate space for tumorigenesis, and is one of the most common sites of primary GBM growth in humans. 50 or 25 ul of viral vector was used per injection and infused set at a rate of 1.5ul/min using a microinfusion pump. A 1 minute dwell time was employed at the end of each injection to minimize vector reflux as described in our prior study [102].

3.2.4 Magnetic Resonance Imaging

Animals underwent endpoint scans using a clinical Siemens 3T Trio MRI scanner with a 64-channel head coil (Siemens Medical Solutions, Malvern, PA). Sequences included sagittal and axial T1, T2, T1-fluid attenuated inversion recovery (FLAIR), T2-FLAIR, and gradient echo sequences (GRE). After intravenous (IV) gadolinium injection (0.1 mmol/kg, MultiHance-gadobenate dimeglumine, Bracco Diagnostics Inc.), post-contrast T1w saggital and axial scans were obtained. Spatial saturation pulses were employed to eliminate respiratory artifact, with adjustment of field of view, flip angle, echo time, TR, and TI-interval as necessary. Radiologic features of interest included iso/hyper/hypo intensity, necrosis, contrast enhancement, mass effect, tumor volume, perilesional edema, and CSF obstruction. All scans were processed and representative images were acquired using RadiAnt Dicom Viewer (Medixant, Poznand, Poland).

3.2.5 Tissue processing, H&E, and Immunohistochemistry

Animals were euthanized through IV sodium pentobarbital and intracardiac perfusion with heparinized saline. Brains were post-fixed in 4% paraformaldehyde overnight, sliced at 5mm intervals for paraffin embedding through serial gradients of xylene and ethanol, and sectioned at 8um thickness. Hematoxylin and Eosin staining (H&E) was performed in a standard fashion (Hematoxylin Gill No. 3, Sigma Aldrich, Cat: GHS332; Eosin Y, Sigma Aldrich, Cat: HT110132). Immunohistochemistry (IHC) was performed with primary antibodies for GFAP (Dako, Z0034), Vimentin (ab45939), Ki-67 (abcam, ab15580), EMA (abcam, ab15481), Progesterone Receptor (PR) (abcam, ab16661), eGFP (ab6556), mCherry (ab125096), PDGFRA (ab203491), Olig2 (abcam, ab109186), NG2 (ab129051), SOX2 (abcam, ab92494), and Neurofilament (NF) (Dako, clone2F11) with subsequent diaminobenzidine (DAB) staining (Vector Laboratories,

PK8200). Whole slides were scanned in a raster pattern at 40x magnification (Leica Aperio AT2 Slide Scanner) with calibrated scale bars prepared in ImageJ [122]. Qualitatively, H&E sections were evaluated by a board-certified clinical neuropathologist. Immunohistochemical stains were qualitatively evaluated (neurofilament, GFP, mCherry, GFAP, Vimentin, EMA, PR) and quantitatively evaluated for immunopositivity. Proliferative index and glial progenitor markers (Ki67, SOX2, Olig2, NG2, PDGFRA) were quantitatively evaluated in at least eight high powered fields per animal comparing the tumor core and leading edge to investigate intratumoral heterogeneity.

Data Analysis and Statistics

Behavioral and radiographic features are presented with descriptive statistics summarized with absolute and relative frequencies. Continuous and ordinal variables were summarized as appropriate using mean, standard deviation (SD), median and range. Statistical comparisons between tumor core and leading edge were conducted using two-way ANOVA, where $P < 0.05$ considered statistically significant (Prism Graphpad 9, San Diego, CA).

3.3 Results

3.3.1 Animals are asymptomatic with decreased volume of oncogenic vector injection by a 4-week endpoint.

In order to elucidate a feasible volume of injection in our pilot study, we conducted two groups of animals at 50ul and 25ul injections. Two animals (N = 2/2) that received 50ul injections developed decreased appetite, neurologic decline, and weight loss

corresponding to a decline in PNS score at endpoint. One animal reached endpoint by the end of post-operative week 1 and exhibited a generalized tonic-clonic seizure. The second animal reached endpoint by the end of post-operative week 2, presenting with localized seizures as facial automatisms, inappetance, emesis, and neurologic decline. We then conducted two animals at the 25ul dose. These animals (N = 2/2) were asymptomatic until the pre-determined 4-week endpoint, with no signs of weight loss, cachexia, or neurologic symptoms. Summary behavioral findings are presented in **Figure 3-2**.

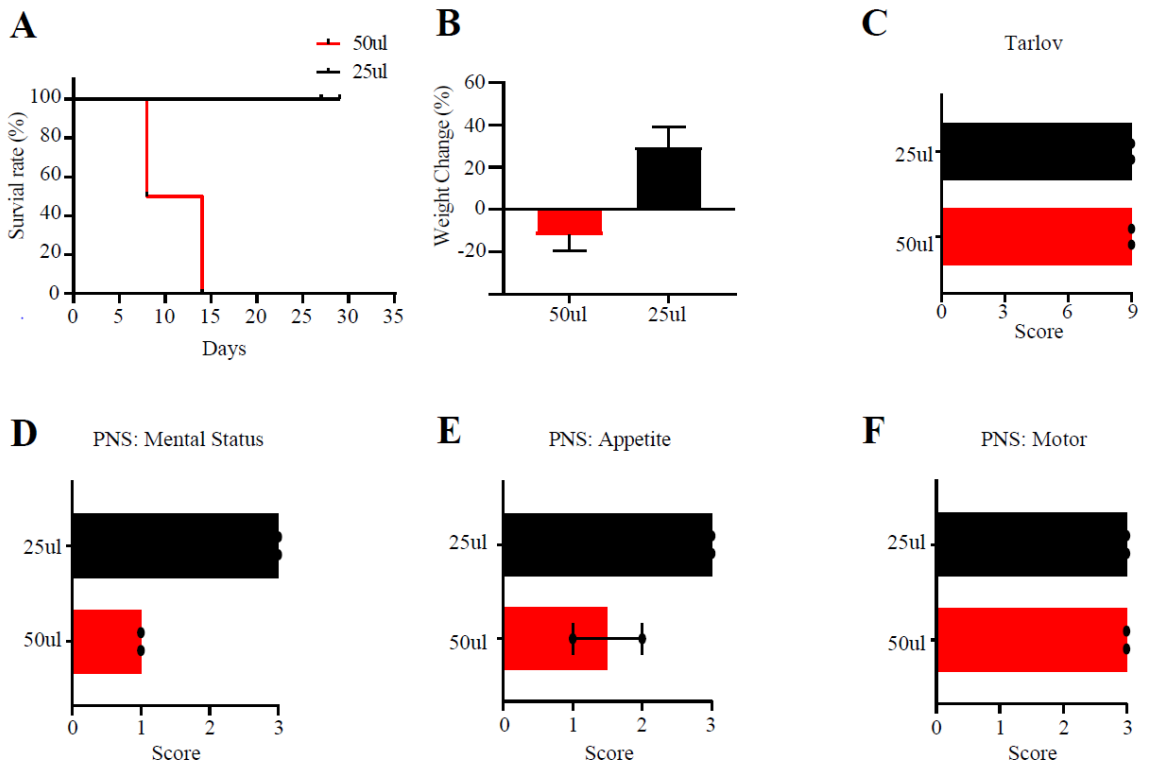

Figure 3-2. Clinical and Behavioral Findings.

3.3.2 Magnetic Resonance Imaging at Endpoint demonstrates lesions with radiologic features consistent with Glioblastoma

At endpoint, animals underwent MRI imaging prior to euthanasia and necropsy. In our pilot experiments, three animals (N=3/4) underwent MRI imaging due to the onset of seizure in the 50ul group and need for emergent euthanasia at veterinary direction. Endpoint scans demonstrated the presence of T1w contrast enhancing mass forming lesions with marked peri-lesional edema in both groups (**Figure 3-3 A,** T1w + Contrast, T2-FLAIR MIP). Tumor features across animals included T1w contrast enhancement (N=3/3), peri-tumoral edema on T2-FLAIR (N=3/3), and hemorrhage on GRE (N=2/3) (**Figure 3-3 B)**. Mass effect was noted in all animals (N=3/3) with compression of the posterior horn of the lateral ventricle at a mean 4.33mm (±1.06) measured on coronal multiplanar reconstruction. Endpoint tumor volumes were calculated using T1w gadolinium enhancing signal, with tumor volume in the first pig calculated using histopathologic volume, and summary findings presented in **Figure 3-3 C**. Tumor dimensions included a mean maximal diameter of 11.7 mm (± 2.93) and mean volume of 713.7 mm^3 (± 537.3).

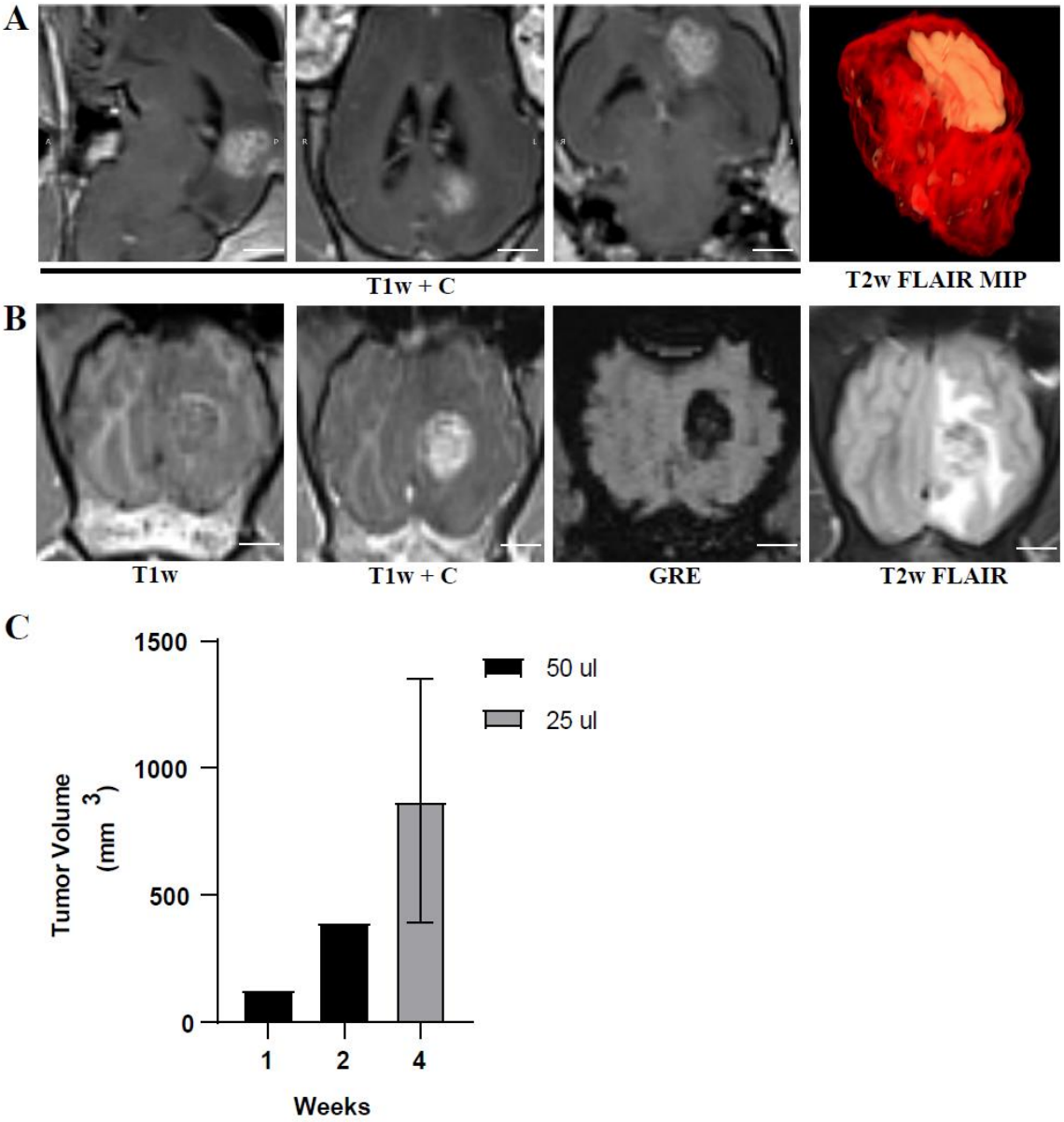

Figure 3-3. Endpoint MRI Scans.

3.3.3 Histopathologically confirmed high-grade glioma

On H&E staining at low magnification, the tumor demonstrates a cellular regions showing hyperchromasia with diffuse invasion of grey and white matter. Cortical spread of the lesion was observed confluent with the parenchymal lesion (**Figure 3-4A**). At high magnification at sites distal to the injection, tumor invasion was observed along white matter tracts. Histopathologic features at high magnification included: high cellularity with epithelioid and fibrillary astrocytic morphology, microvascular proliferation, necrosis, thrombosed blood vessels, and invasion along the tumor border into surrounding normal parenchyma, consistent with a high-grade glioma (**Figure 3-4 A**).

Evaluation of the IHC staining for vector reporters demonstrated sparse immunopositivity in the tumor bulk (**Figure 3-4 B**) with diffuse GFAP and Vimentin immunopositivity **(Figure 3-5 A-B)**. Neurofilament staining identified background parenchyma present in the infiltrative lesion (**Figure 3-5C).** To rule out the potential of a distinct meningioma-like tumor growth, EMA and PR staining were conducted and were found to be immunonegative (**Figure 5 D-E**). Ki-67 proliferative index was highly positive across animals, with a mean proliferative index of 44.1% (SD: 13.6). In order to evaluate the presence of glial progenitor markers, SOX2, Olig2, NG2, and PDGFRA staining was conducted. The tumors were grossly immunopositive for SOX2, Olig2, and NG2, and were immunonegative for PDGFRA. We observed an impression of heterogeneity in staining between the tumor core and leading edge. Consequently, we conducted quantifications of high-powered fields (N=8/animal) at the core and leading edge of the tumors. We observed statistically significant differences in Ki-67, SOX2, Olig2, ($P<0.001$) and NG2 ($P<0.05$)

immunopositivity in comparing the tumor core and leading edge, but not PDGFRA (**Figure 3-6**).

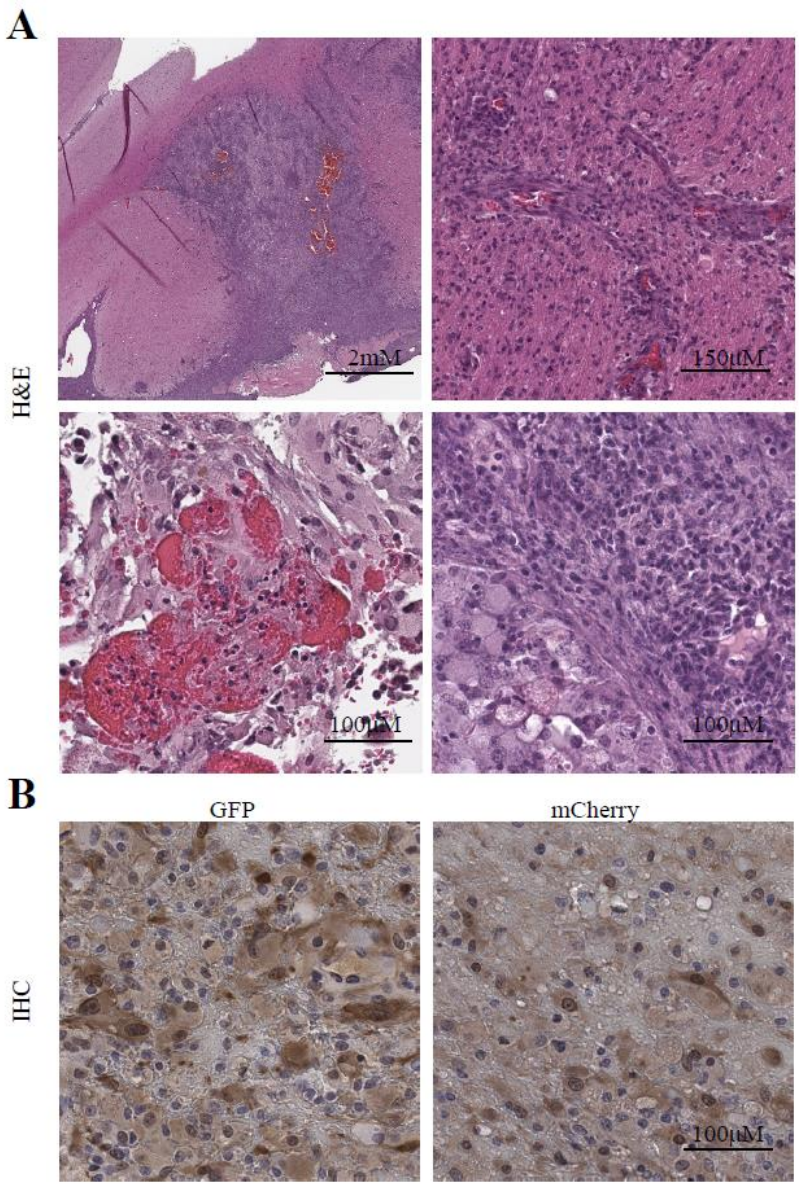

Figure 3-4. Histopathologic features and confirmation of vector reporter expression.

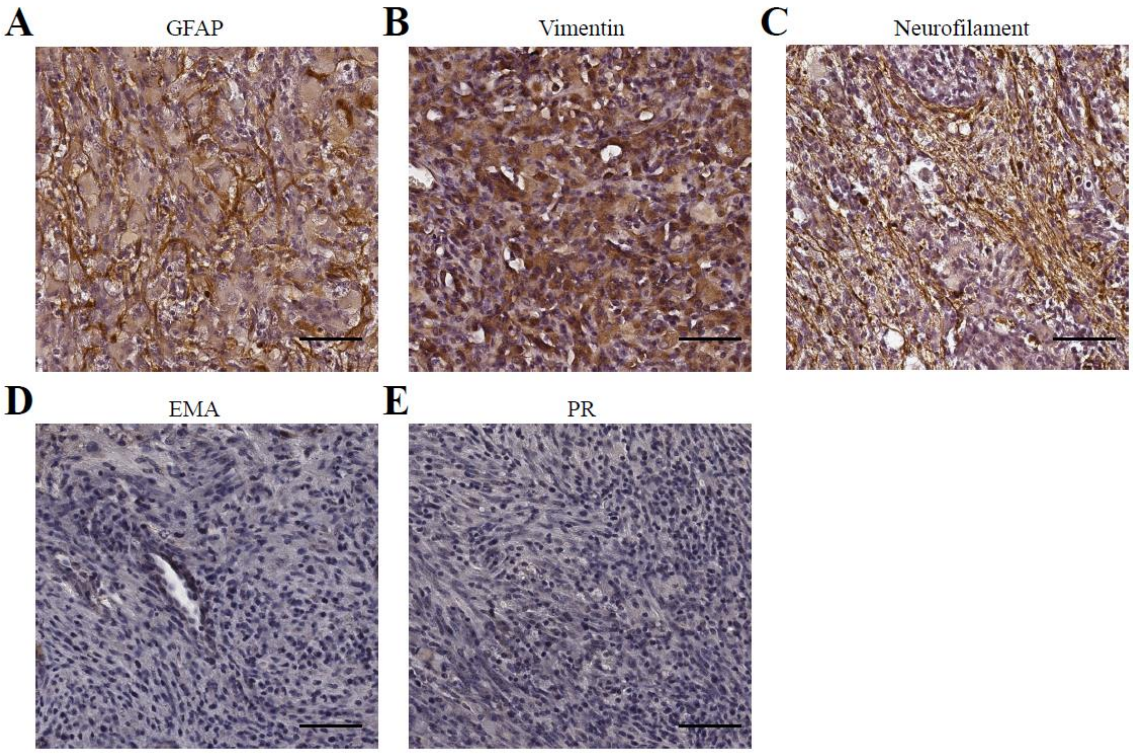

Figure 3-5. Immunohistochemical characterization of tumors.

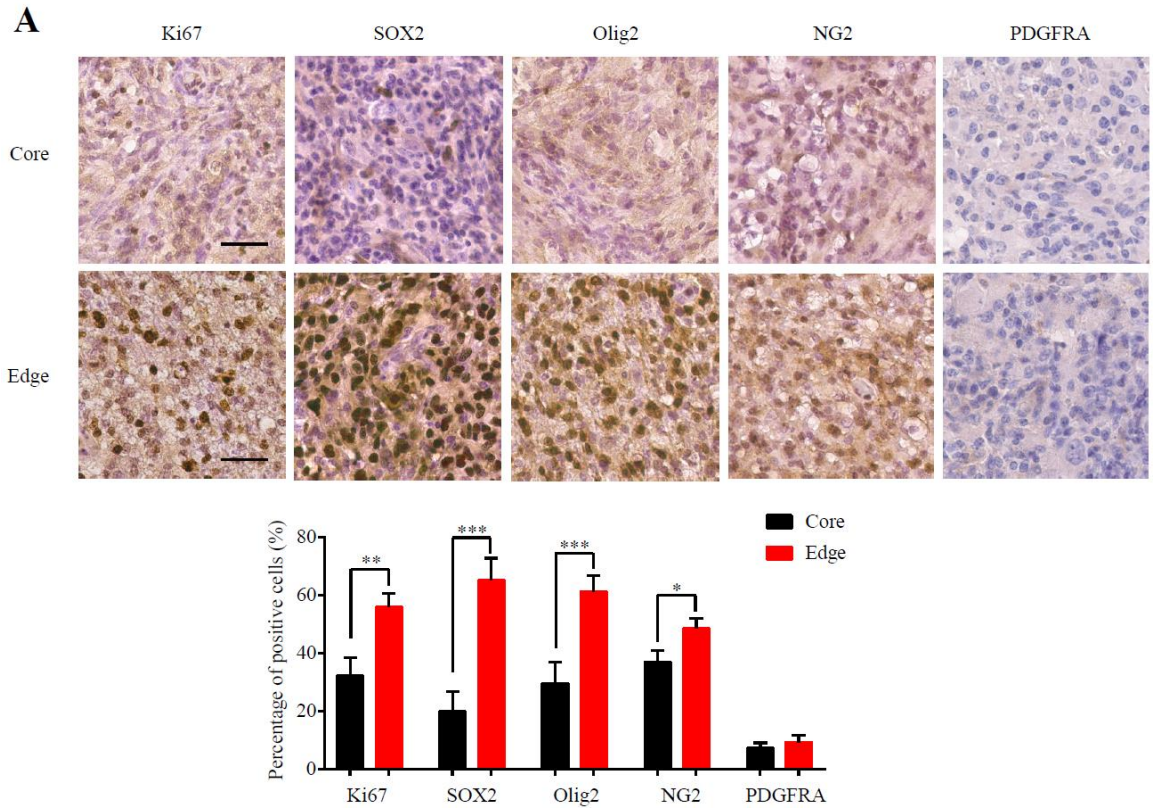

Figure 3-6. Proliferative index and glial progenitor staining comparison of tumor core and leading edge.

3.4 Discussion

The data of the present exploratory study illustrates the first lentiviral vector induced large mammalian model of supratentorial GBM. We found that high-grade gliomas formed in a highly penetrant fashion following the injection of vectors with histopathological and radiologic confirmation. We also observed that the lesions demonstrated evidence of intratumoral heterogeneity in the core and leading edge as highlighted in prior studies [142]. Importantly, intracranial vector driven GBM modeling has not been performed in large animal models prior to this study and we assert that this paradigm using intraparenchymal gene transfer may be adapted, optimized, and employed for preclinical neurosurgical study.

Despite significant advances in our knowledge of GBM, there have been limited improvements in outcomes. In part, this represents the recalcitrance of GBM. On the other hand, this highlights the limitations of surgical translation based on existing rodent models [71, 72, 102, 104], which has stifled the translation of neurosurgical strategies [41, 80, 82, 98, 108]. Our study challenges the notion of pre-clinical translational reliance on phenotypically normal large mammalian models used by investigators and regulatory bodies in the pathway for developing neurosurgical strategies. This is a major limitation. For example, in prior studies to bring novel drug delivery strategies to clinical trials, groups have been unable to rigorously study drug delivery variables or drug tracking in a large animal disease model [36, 98]. As such, we assert that the development of a highly characterized large mammalian model of GBM fills a translational gap in the field for the study of pre-clinical neurosurgical strategies. Indeed, the development of numerous technologies including convection enhanced delivery, oncolytic vectors, laser interstitial thermal therapy (LITT), focused ultrasound (FUS), intraoperative surgical guidance (e.g. 5-ALA), intra-arterial delivery, and robotic resection [34-44] would benefit from a readily available highly characterized immunocompetent large animal model of GBM.

Fundamentally, our pilot study has established the feasibility of modeling supratentorial GBM in a large mammalian model. Future work should focus on characterization of growth rate, advanced radiologic features (positron emission tomography, magnetic resonance spectroscopy), the selection of further neuropathologically relevant genetic lesions (e.g. CDKN2A, EGFR, PTEN, IDH) and the transcriptomic phenotype of these tumors. By doing so, these systems will provide not only

an advanced anatomic space for pre-clinical investigation of neurosurgical techniques, but also the potential for evaluation of response to therapy an in immunocompetent space.

3.4.1 Limitations

The main limitation of this study is the sample size. However, as a pilot study to evaluate the feasibility of modeling GBM, we are able to observe that it is indeed possible to achieve glioma growth in the minipig brain. Future work should evaluate whether these tumors progress as the result of clonal expansion of virally infected cells, or through the recruitment and transformation of resident glial progenitors [74, 75, 78]. In our present study, we found sparse immunopositivity for viral reporters suggesting the possibility of recruitment of surrounding parenchyma. However, due to the limitations in sample size this was not investigated further. Given that patients present with marked inter-tumoral and intra-tumoral heterogeneity [136, 137] future studies with appropriate power should evaluate whether vector driven models as in our study, or the use of other vector strategies reproduce this level of lesional heterogeneity. In addition, our study did not evaluate the trancriptomic profile or methylation status of these tumors which will be critical for future studies investigating the molecular phenotype and/or potential response to therapeutic agents.

3.5 Conclusion

Lentiviral gene transfer represents a feasible pathway for GBM modeling in the Gottingen minipig. The present model is the first vector induced pig model of supratentorial GBM and with further optimization may potentially be used in preclinical surgical development programs.

3.6 Acknowledgements

The authors acknowledge the numerous faculty and staff of the Division of Animal Resources (DAR) and the Emory Center for Systems Imaging (CSI) for their guidance and expertise in the conduct of this study. In addition, we acknowledge the support of the Emory Integrated Genomics Core (EIGC). Lastly, we acknowledge the support of the Emory Neuroscience Neuropathology Core.

3.7 Figure Legends

Figure 3.1. Vector and Experimental Design. (A) Lentiviral vectors expressing PDGFB, HRASG12V, and shRNA targeting P53 (sh787, sh944) were designed based on prior literature at a titer of $3x10^9$ IU/ml. **(B)** Vectors were combined in equal parts, and injected into the subcortical white matter of mature minipigs to induce glioma formation. Animals were followed with clinical and behavioral evaluation until a pre-determined 4-week endpoint as part of this pilot study. Post-mortem neuropathologic evaluation was conducted to evaluate GBM growth. **(C)** All animals were injected using pre-determined stereotactic coordinates (**Red Circle**) at 2.5 cm rostral to the nuchal crest (NC), and 1.2 cm lateral to midline. Bregma was used as an intraoperative indicator of the extent of frontal-sinus extent (**Green Shaded Region**) to avoid violation of the sinus. **(D)** Intraoperative surgical images depicting exposure of the skull surface, craniotomy, injection platform, and advancement of the injection cannula for vector infusion.

Figure 3.2 Clinical and Behavioral Findings. (A) Two animals with 50ul injections reached endpoint by post operative day 8 and 14, respectively. Two animals with 25ul injections survived until the pre-determined 4-week endpoint. **(B)** Baseline and endpoint

weights were compared, demonstrating weight loss in the 50ul group animals not the 25 ul animals. **(C)** modified Tarlov scoring was 9/9 in all animals with no signs of motor deficits or gait instability. **(D)** Mental status declined to a PNS score of 1/3 among animals with 50ul injections, but not 25ul injections. (**E)** Animals undergoing 50ul injections experienced inappetance by endpoint, refusing solids and liquids (PNS appetite score = 1), and refusing solids (PNS appetite score = 2). Animals with 25ul injections exhibited no changes in appetite. **(F)** No motor deficits were noted as per PNS scoring.

Figure 3.3 Endpoint MRI Scans. (A) T1 weighted axial scans demonstrate a heterogeneous contrast-enhancing lesion with mass effect and effacement of the lateral ventricle (T1w + C, Saggital, Axial, Coronal). T2 weighted FLAIR 3d maximal intensity projection demonstrates marked perilesional edema (T2w FLAIR MIP). Representative images from 25ul injected animal at post-operative week 4. **(B)** Comparative panels of axial scans at 1cm depth from cortical surface. T1 weighted pre-contrast (T1w) demonstrate a region of hypo/iso intensity. T1w post-gadolinium scan (T1w + C) shows heterogenous enhancement. Gradient echo (GRE) scans display signal void and blood products and T2 fluid attenuated inversion recovery (T2-FLAIR) show peri-tumoral edema. **(C)** Radiologic tumor volume calculated at 1, 2, and 4 weeks post-operatively.

Figure 3.4 Histopathologic features and confirmation of vector reporter expression. (A) Low magnification H&E demonstrates hypercellular region with hyperchromasia invading along white matter tracts, violation of grey and white matter borders, hemorrhage, and extension of the tumor to the cortical surface (Top-left panel). Examination of distal sites at 2.5cm from the tumor core show tumor invasion along white matter (top-right panel, 10x magnification). Numerous regions of necrosis and thrombosed

blood vessels are appreciated (bottom-left panel, 20x magnification). Anaplastic astrocytic morphology is present with spindled and epithelioid cells (bottom-right panel, 20x magnification). **(B)** Tumors show immunopositivity for reporters GFP and mCherry.

Figure 3.5. Immunohistochemical characterization of tumors. (A-B) GFAP and Vimentin staining demonstrates high immunopositivity at approximately 50% of cells per hpf. **(C)** Neurofilament staining is appreciated in the tumor illustrating presence of background tissue. **(D-E)** Cortical involvement of the tumor was stained for Epithelial membrane antigen (EMA) and Progesterone receptor (PR) and appear grossly immunonegative, with <1% cells immunopositive per hpf. 20x magnification, Bar: 100um.

Figure 3.6. Proliferative index and glial progenitor staining comparison of tumor core and leading edge. (A) Immunohistochemical stains were analyzed comparing the tumor core to leading edge. Grossly, Ki-67, SOX2, Olig2, and NG2 staining appeared higher in the leading edge as compared to the core. **(B)** N=8 high powered fields were quantified for each immunostain in each region, per animal. The leading edge demonstrated a statistically significant higher percent immunopositivity for Ki67, SOX2, Olig2, and NG2 as compared to the tumor core. ***P< 0.001. *P <0.05.

CHAPTER 4. CONCLUSIONS AND FUTURE WORK

4.1 Conclusion and Contributions

The present research demonstrated that using lentiviral mediated gene transfer of PDGFB, shRNA-P53, and HRAS-G12V was able to induce high-grade glioma in both the minipig brain and spinal cord. This was validated through histopathologic features in line with WHO criterion with subsequent evaluation by board certified neuropathologists. The characterization of the model was further supported by immunohistochemical data, showing a staining pattern that identified a tumor that was highly proliferative and rich in glial progenitor markers. In the spinal cord, transcriptomic analysis suggested enrichment in gene signatures in glioma subtypes. Overall, the aims given in Chapter 1 were achieved and demonstrated as presented in Chapters 2 and 3.

4.2 Significance and Impact

The present research describes the first reproducible model of high-grade glioma using lentiviral gene transfer. The significance of this work is inherent in the novelty of the model itself that is based upon prior well-vetted strategies for inducing glioma *de-novo* in rodent models. By demonstrating the feasibility of scaling this model into the porcine system, this research has presented the first step toward developing advanced animal models for therapeutic, diagnostic, and pathophysiologic study.

The immediate impact of these models is that they already provide a reproducible space for evaluation of surgical therapeutic strategies. Whether this model reflects therapeutic efficacy is currently unknown and further model characterization is still

needed. However, the present system can be used as a proof-of-concept space for investigation of neurosurgical techniques and drug delivery studies. For example, prior studies evaluating techniques such as CED have relied on murine models that bear limitations in translatability as discussed in Chapter 1. In addition, when attempting to evaluate these strategies in large animal models, groups have been forced to utilize otherwise wild-type models without lesions in the brain parenchyma, or use xenografts and immunosuppressive regimens that bear several limitations. Instead, the present model provides an immediate space to study the details of such neurosurgical techniques in the minipig which provides a wealth of anatomic advantages. This is in line with one of the current goals of the National Cancer Institute and the consensus statement put forth by Aldape et al in reformulating the translational pipeline in CNS cancers[68].

4.3 Recommendations for Future Work

The work presented in this dissertation introduced the first lentiviral vector induced porcine model of high-grade glioma. The main motivations of this research are to demonstrate the feasibility of this modeling strategy, provide a platform for initial translational studies, and to encourage further advanced minipig models of glioma. The work presented in this thesis was limited by funding availability and the novelty of this strategy in pigs. However, given these successful results, future work can now proceed in both porcine genetically engineered glioma modeling and in translational surgical therapies. Recommendations for future work are briefly outlined below.

4.3.1 Investigation of additional clinically relevant transgene combinations and PET reporters for enhanced clinical relevance.

The porcine system provides an anatomic, genetic, and immunologic space that is thought to be much closer to the human. The present models described in this demonstrates the induction of high-grade glioma using lentiviral gene transfer of PDGF-B, shRNA-P53, and HRAS-G12V. As discussed in Chapter 1-3, these transgenes were chosen given the broad involvement of their pathways in malignant glioma. However, a more advantageous approach to mirror human disease development may be achieved by utilizing combinations of genetic lesions more clinically relevant. By doing so, response to targeted therapy may potentially be more translatable. For example, while upregulation in the RAS pathway is a common occurrence, constitutive RAS activation due to a mutation is an exception in human glioma. Other relevant transgene combinations to be investigated may include the elimination of RAS, and combinatorial inclusion of PTEN, EGFR, H3K27M, or ATRX. It may be certainly be feasible to generate a panel of available vectors to induce glioma in the minipig, in the brain, brainstem, or spinal cord of varying grade and phenotype. Even if the lesions themselves resemble murine lesions, safety and toxicity studies would benefit from demonstrating putative tumoricidal potential, given that rodents have been shown to be poor predictors of safety and toxicity in humans. Lastly, the use of CRISPR pigs, or other vector strategies may prove advantages to provide a more targeted means of inducing glioma de-novo in a phenotypically wild-type pig.

A limitation of current rodent models is the inability to apply clinical MRI and positron emission tomography techniques. The pig models overcome this, by providing a larger anatomic space and the use of clinical scanners that more faithfully resemble

diagnostic techniques in humans. However, to take full advantage of this the capacity of imaging the pig model using these modalities is needed. Furthermore, the ability to identify tumor burden non-invasively as a pre-clinical tool using transgenic PET reporters may provide a critical tool for imaging and diagnostic studies. This is exemplified in the fact that while many intraparenchymal drug delivery studies utilize MRI based contrast agents (e.g. CED + gadolinium), they cannot monitor tumor size while drug delivery is performed.

Using lentiviral delivery, we have already proposed the first steps toward advanced modeling in these areas through NIH grant proposals, with abbreviated versions presented in **Appendix B and C**.

4.3.2 Employment of the model in Neurosurgical Translational Studies

While response to therapy has not yet been elucidated in the present pig high-grade glioma models, they can still be used to study aspects of surgical techniques. These include many techniques listed in Chapter 1 (e.g. CED, LITT, intraoperative fluorescent aids, intra-arterial drug delivery). At present, we have proposed demonstrating the translational utility of the model by characterizing key parameters of CED using implanted devices in both the brain and spinal cord as described in **Appendix B and C.**

APPENDIX A. HALLMARK AND ONCOGENIC GENE SET ENRICHMENT

Table A-1. Hallmark Gene Sets - UP

NAME	SIZE	ES	NES	p-value	FDR	FWER
HALLMARK_MYC_TARGETS_V1	193	0.415	6.767	0.000	0.000	0.000
HALLMARK_G2M_CHECKPOINT	189	0.298	4.886	0.000	0.000	0.000
HALLMARK_MYC_TARGETS_V2	58	0.488	4.306	0.000	0.000	0.000
HALLMARK_DNA_REPAIR	137	0.307	4.248	0.000	0.000	0.000
HALLMARK_E2F_TARGETS	192	0.251	4.019	0.000	0.000	0.000
HALLMARK_EPITHELIAL_MESENCHYMAL_TRANSITION	190	0.249	3.937	0.000	0.000	0.000
HALLMARK_UNFOLDED_PROTEIN_RESPONSE	108	0.297	3.567	0.000	0.000	0.000
HALLMARK_GLYCOLYSIS	191	0.200	3.197	0.000	0.000	0.000
HALLMARK_MTORC1_SIGNALING	194	0.171	2.728	0.000	0.000	0.001
HALLMARK_TNFA_SIGNALING_VIA_NFKB	191	0.156	2.475	0.000	0.000	0.003
HALLMARK_PI3K_AKT_MTOR_SIGNALING	102	0.206	2.394	0.000	0.001	0.006
HALLMARK_OXIDATIVE_PHOSPHORYLATION	180	0.150	2.310	0.000	0.002	0.015
HALLMARK_UV_RESPONSE_DN	137	0.169	2.281	0.004	0.002	0.020
HALLMARK_WNT_BETA_CATENIN_SIGNALING	41	0.290	2.252	0.000	0.002	0.025
HALLMARK_APICAL_JUNCTION	189	0.136	2.210	0.002	0.003	0.035
HALLMARK_ALLOGRAFT_REJECTION	185	0.133	2.125	0.000	0.005	0.057
HALLMARK_MITOTIC_SPINDLE	197	0.130	2.099	0.002	0.005	0.068
HALLMARK_HYPOXIA	189	0.126	2.064	0.002	0.006	0.088
HALLMARK_P53_PATHWAY	185	0.132	2.049	0.010	0.006	0.093
HALLMARK_TGF_BETA_SIGNALING	54	0.236	2.027	0.004	0.007	0.100
HALLMARK_INTERFERON_ALPHA_RESPONSE	86	0.189	2.013	0.002	0.007	0.108
HALLMARK_ANGIOGENESIS	33	0.268	1.813	0.010	0.023	0.320
HALLMARK_APOPTOSIS	154	0.113	1.615	0.050	0.059	0.669
HALLMARK_COAGULATION	127	0.121	1.587	0.051	0.065	0.715
HALLMARK_IL6_JAK_STAT3_SIGNALING	81	0.129	1.376	0.126	0.152	0.956

Table A-2. Hallmark Gene Sets - DOWN

NAME	SIZE	ES	NES	p-value	FDR	FWER
HALLMARK_INTERFERON_GAMMA_RESPONSE	176	-0.188	-2.946	0.000	0.000	0.000
HALLMARK_MYOGENESIS	185	-0.161	-2.575	0.000	0.000	0.001
HALLMARK_XENOBIOTIC_METABOLISM	179	-0.124	-1.915	0.006	0.056	0.212
HALLMARK_KRAS_SIGNALING_DN	172	-0.123	-1.883	0.008	0.050	0.244
HALLMARK_CHOLESTEROL_HOMEOSTASIS	70	-0.184	-1.795	0.014	0.062	0.360
HALLMARK_PANCREAS_BETA_CELLS	39	-0.242	-1.788	0.016	0.053	0.367
HALLMARK_APICAL_SURFACE	42	-0.215	-1.615	0.036	0.107	0.662
HALLMARK_INFLAMMATORY_RESPONSE	191	-0.099	-1.610	0.055	0.097	0.671
HALLMARK_ADIPOGENESIS	181	-0.098	-1.503	0.069	0.139	0.833
HALLMARK_BILE_ACID_METABOLISM	103	-0.125	-1.499	0.070	0.127	0.841
HALLMARK_FATTY_ACID_METABOLISM	146	-0.097	-1.369	0.102	0.198	0.957
HALLMARK_ESTROGEN_RESPONSE_LATE	183	-0.085	-1.363	0.107	0.186	0.963
HALLMARK_SPERMATOGENESIS	122	-0.102	-1.329	0.148	0.193	0.978
HALLMARK_HEME_METABOLISM	183	-0.082	-1.318	0.129	0.189	0.985
HALLMARK_PEROXISOME	99	-0.098	-1.160	0.259	0.315	1.000
HALLMARK_IL2_STAT5_SIGNALING	191	-0.072	-1.145	0.273	0.311	1.000
HALLMARK_PROTEIN_SECRETION	95	-0.091	-1.028	0.413	0.422	1.000
HALLMARK_ANDROGEN_RESPONSE	92	-0.088	-0.974	0.442	0.469	1.000

Table A-3. C6 Oncogenic Gene Sets - UP

NAME	SIZE	ES	NES	p-value	FDR	FWER
CSR_EARLY_UP.V1_UP	144	0.431	2.142	0.000	0.002	0.002
PDGF_ERK_DN.V1_DN	135	0.388	1.914	0.000	0.007	0.011
CSR_LATE_UP.V1_UP	143	0.364	1.808	0.000	0.011	0.025
MYC_UP.V1_UP	150	0.360	1.792	0.000	0.010	0.030
BMI1_DN.V1_UP	132	0.362	1.772	0.000	0.010	0.036
MEL18_DN.V1_UP	128	0.355	1.712	0.000	0.013	0.059
PDGF_UP.V1_UP	136	0.339	1.665	0.000	0.016	0.086
ESC_V6.5_UP_EARLY.V1_DN	156	0.310	1.562	0.003	0.038	0.218
EGFR_UP.V1_UP	171	0.310	1.560	0.000	0.035	0.223
GLI1_UP.V1_UP	22	0.454	1.553	0.027	0.033	0.237
BMI1_DN_MEL18_DN.V1_UP	131	0.309	1.514	0.003	0.044	0.325
HINATA_NFKB_MATRIX	10	0.565	1.500	0.059	0.046	0.358
IL15_UP.V1_UP	161	0.297	1.489	0.004	0.048	0.394
E2F1_UP.V1_DN	171	0.291	1.486	0.000	0.045	0.399
ESC_J1_UP_LATE.V1_DN	168	0.291	1.486	0.003	0.042	0.399
ESC_J1_UP_EARLY.V1_DN	163	0.292	1.485	0.000	0.040	0.399
P53_DN.V1_UP	167	0.288	1.446	0.011	0.053	0.504
E2F3_UP.V1_DN	111	0.301	1.419	0.006	0.065	0.602
CAMP_UP.V1_UP	175	0.277	1.415	0.007	0.064	0.617
CAHOY_ASTROGLIAL	88	0.302	1.400	0.026	0.069	0.662
CYCLIN_D1_KE_.V1_UP	177	0.272	1.387	0.007	0.073	0.700
RB_DN.V1_DN	108	0.292	1.372	0.027	0.081	0.756
RB_P107_DN.V1_UP	122	0.283	1.362	0.024	0.085	0.787
E2F1_UP.V1_UP	177	0.256	1.300	0.039	0.142	0.920
EIF4E_UP	84	0.283	1.290	0.058	0.153	0.946

Table A-4. C6 Oncogenic Gene Sets - DOWN

NAME	SIZE	ES	NES	p-value	FDR	FWER
KRAS.KIDNEY_UP.V1_UP	130	-0.526	-2.342	0.000	0.000	0.000
CAHOY_NEURONAL	93	-0.518	-2.176	0.000	0.000	0.000
IL15_UP.V1_DN	142	-0.428	-1.937	0.000	0.001	0.002
CTIP_DN.V1_DN	101	-0.424	-1.805	0.000	0.005	0.021
MEL18_DN.V1_DN	131	-0.384	-1.726	0.000	0.012	0.067
STK33_SKM_DN	220	-0.361	-1.711	0.000	0.013	0.085
BRCA1_DN.V1_UP	102	-0.396	-1.709	0.000	0.011	0.085
CTIP_DN.V1_UP	99	-0.395	-1.709	0.000	0.010	0.085
BMI1_DN_MEL18_DN.V1_DN	129	-0.382	-1.703	0.000	0.009	0.087
CAHOY_OLIGODENDROCUTIC	87	-0.402	-1.683	0.002	0.010	0.109
KRAS.LUNG_UP.V1_DN	104	-0.387	-1.677	0.000	0.010	0.115
PRC1_BMI_UP.V1_DN	147	-0.364	-1.675	0.003	0.009	0.117
IL2_UP.V1_DN	149	-0.366	-1.673	0.000	0.009	0.122
BMI1_DN.V1_DN	120	-0.372	-1.660	0.001	0.011	0.152
ALK_DN.V1_DN	109	-0.382	-1.659	0.003	0.010	0.155
KRAS.600.LUNG.BREAST_UP.V1_DN	229	-0.346	-1.655	0.000	0.010	0.169
LTE2_UP.V1_UP	169	-0.353	-1.640	0.001	0.011	0.194
CYCLIN_D1_KE_.V1_DN	169	-0.352	-1.614	0.003	0.015	0.262
CAHOY_ASTROCYTIC	96	-0.375	-1.596	0.003	0.017	0.315
KRAS.600_UP.V1_UP	222	-0.331	-1.592	0.001	0.017	0.330
LEF1_UP.V1_DN	161	-0.343	-1.586	0.000	0.017	0.348
ATF2_S_UP.V1_DN	167	-0.333	-1.546	0.007	0.027	0.501
RPS14_DN.V1_UP	165	-0.332	-1.527	0.001	0.032	0.575
KRAS.BREAST_UP.V1_DN	113	-0.342	-1.498	0.006	0.042	0.682
PTEN_DN.V1_DN	138	-0.327	-1.484	0.004	0.046	0.735

APPENDIX B.R01 – SCG MODELING AND CED

B.1. Specific Aims

Spinal Cord Glioma (**SCG**) accounts for 8-10% of all primary spinal cord tumors, and high-grade lesions result in 5-year survival rates as low as 11-23% [51]. Treatment options are limited due to poor surgical margins, radioresistance, and chemoresistance. There have been numerous translational studies demonstrating surgical efficacy in rodent models of glioma but the anatomy of such models present limitations that are difficult to scale into patients [35, 37, 143-145]. This highlights a critical gap in the field: a well characterized large animal SCG model for surgical testing. **To address this gap, we propose the advancement of a genetic minipig SCG model capable of evaluating neurosurgical strategies.**

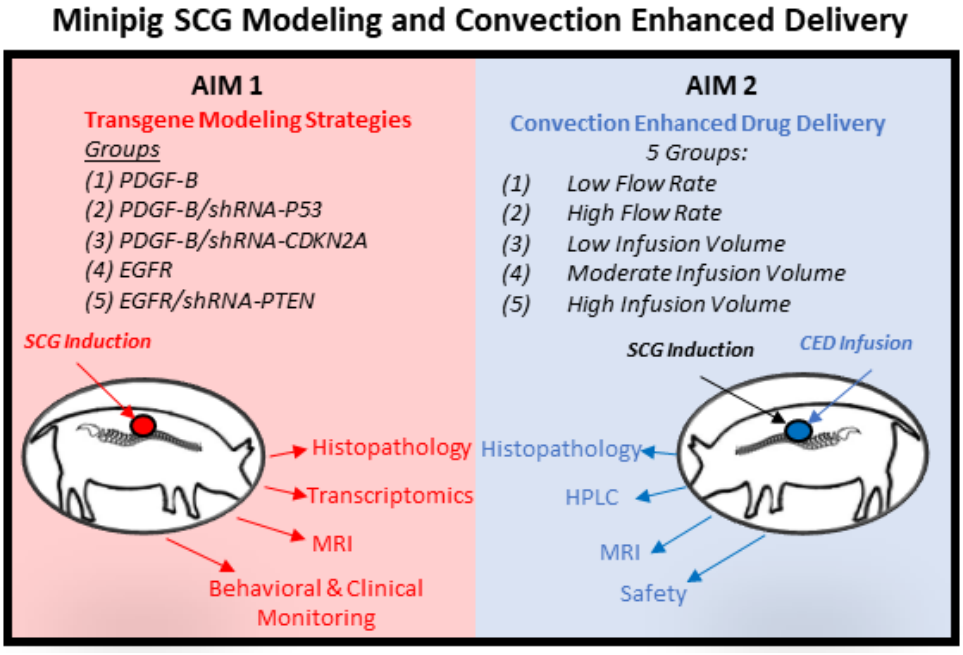

Figure B-1. Experimental Design.

The minipig is the ideal model for surgical translational studies due to anatomic similarity to the human spinal cord. Given the Boulis and Canoll laboratories' longstanding experience in spinal cord drug delivery and glioma modeling, we have combined our expertise to establish the first non-xenograft minipig SCG model. Our data demonstrate *de novo* growth of high-grade SCGs in 100% of pigs [102]. Further study will provide a more versatile model with variable molecular and growth characteristics, improving its utility for use in the development of surgical and therapeutic strategies.

Because resection of SCG is impossible, direct delivery of therapeutics into the tumor remain one of the most promising approaches. However, direct drug delivery can only be rigorously studied and validated in a large animal model. *Unlike spontaneous canine gliomas, our model can be widely distributed to allow for rigorous testing of many approaches*. CED is a well-known paradigm for CNS drug delivery [35-37, 146]. The failure of human glioma CED trials have been attributed to "one-time treatments" and poor drug distribution [147-149]. As such, we will demonstrate the utility of the pig SCG model by studying CED mediated chemotherapeutic delivery.

B.1.1 - AIM 1. Develop the minipig SCG model to include clinically relevant transgenes and modulate phenotype.

Rationale*: The present model induces high-grade SCG in a highly penetrant fashion through lentiviral PDGF-B, HRAS-G12V, and shRNA-P53. We propose the use of common genetic lesions found in human glioma for more faithful genetic recapitulation of the human disease and induction of SCG of varying grade and phenotype. We will evaluate SCG induction by scaling established vector driven modeling approaches.*

Design: Five experimental groups (6/group) will be used to investigate SCG induction, targeting PDGF-B, p53, CDKN2A, EGFR and PTEN through lentiviral transgene delivery. **Evaluation Metrics**: (1) Behavioral and Clinical Monitoring, (2) Magnetic Resonance Imaging (MRI), (3) Histopathology, Immunohistochemical, Immunofluorescent Analyses, and (4) Transcriptomic Analysis. Successful completion will provide the first set of well characterized SCG large animal models of varying phenotype for surgical translational studies.

Hypothesis: *We hypothesize that Groups 1 (PDGF-B) and 4 (EGFR) will induce indolent SCGs and that groups 2 (PDGF-B/shRNA-P53), 3 (PDGF-B/shRNA-CDKN2A), and 5 (EGFR/shRNA-PTEN) will induce more aggressive SCG, with each group presenting concordant individual phenotypes.*

B.1.2 - AIM 2. Use the minipig SCG model to test of local convection enhanced drug delivery.

Rationale: Prior studies of intratumoral CED in the intracranial setting have reported failures, likely due to single treatments or poor drug distribution. Despite an ongoing CED phase I trial on recurrent SCG [146], drug delivery is poorly understood. The utility of our SCG model will be demonstrated by elucidating the effects of CED infusion parameters on tumor drug delivery, with immediate impact on the current and future human trials.

Design: In this aim, we will investigate CED parameters and demonstrate improvement of drug distribution in a minipig model of SCG. 5 groups (6/group) will be conducted with adjusted CED parameters to assess the impact of Infusion Volume (Vi) and Flow Rate (FR) on volume of distribution (Vd). Minipigs with SCG will receive intra-tumoral CED

infusion of a gadolinium-based contrast agent + nimustine hydrochloride (ACNU) over up to 7 days. Animals will be evaluated and compared with the following **Evaluation Metrics**: (1) Safety through behavioral and clinical monitoring, (2) serial MRIs, (3) histopathology, and (4) high-pressure liquid chromatography (HPLC) of serial biopsies.

Hypothesis 1: We hypothesize that increase in both Vi and FR will directly correlate in Vd measured on T1w enhancement and optimal parameters at FR (2.0 ul/min) and Vi (15 mL) with minimal reflux and clinical sequelae.

Hypothesis 2: Surrogate radiologic tracking with gadolinium T1w enhancement will demonstrate statistically significant correlations with parenchymal concentrations of ACNU.

B.2. Significance

Clinical need for therapeutic strategies in SCG: SCGs comprise 8-10% of all primary spinal cord tumors, with up to 10,000 cases occurring annually. Despite significant morbidity and mortality, there is no consensus for the treatment of SCGs [51, 52]. Current options include surgical resection with radiotherapy and/or chemotherapy (**Figure 2**). However, these approaches have shown poor efficacy with 5 year survival rates of 11-23% in high grade lesions. [51] Typically, these patients will receive open-surgical biopsy and cannot undergo surgical resection due to a lack of actionable surgical margins. Importantly, SCG is considered an orphan disease that is overlooked in comparison to its intracranial counterpart. In the absence of effective treatment options, patients with SCG are in a vulnerable patient population with no effective treatment options available. Thus, the significance of this proposal is inherent in its deliverables, whereby advancement of

topical models and understanding of CED parameters will advance translational strategies for SCG.

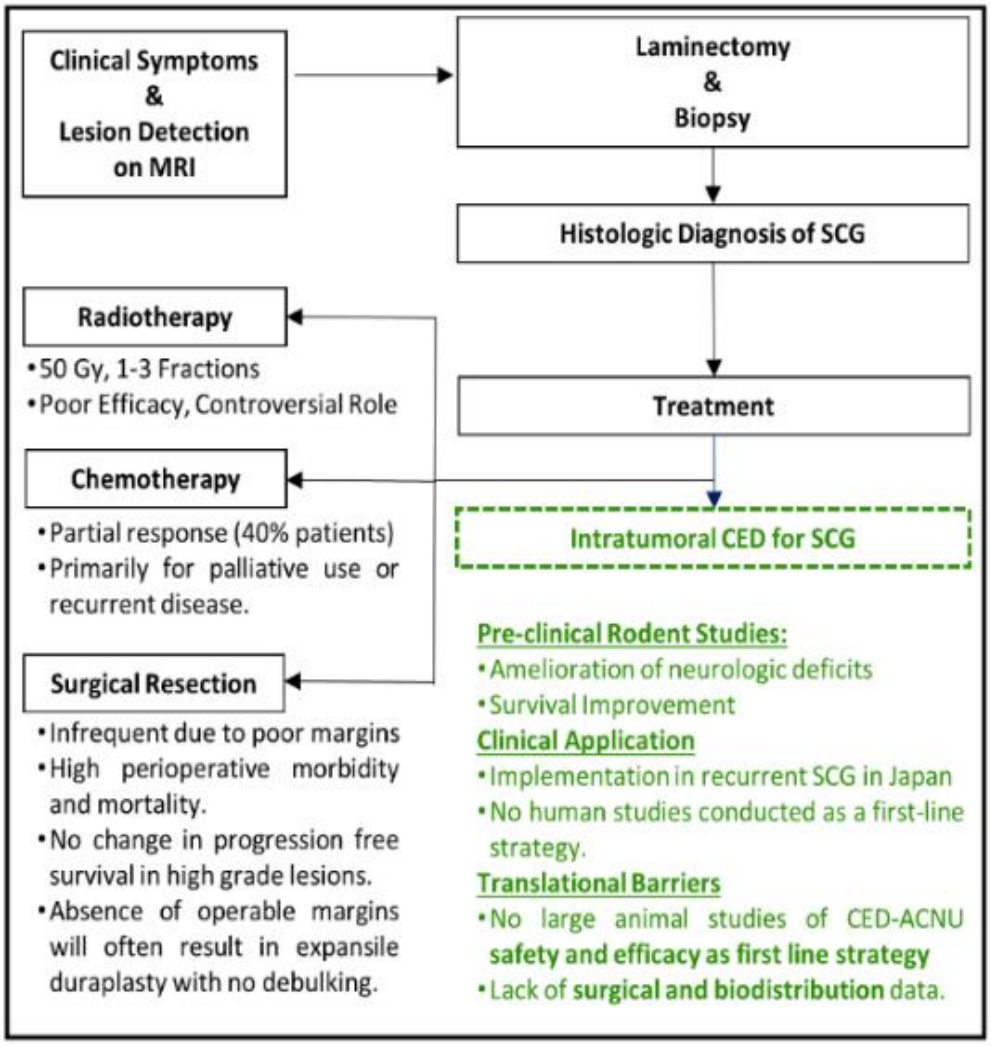

Figure B-2 - Figure 2. Spinal Cord Glioma Treatment Outline. Adapted information, Abd el barr et al. and Tobin et al [51-53]

Scaling glioma modeling strategies to develop well characterized surgical platforms. Despite significant advances in our knowledge of the disease process, there have unfortunately been limited changes to the clinical outcomes in high grade glioma. In part, this represents the malignant nature of a disease that is refractory to the standard of care. On the other hand, this raises the question of the translational value of existing preclinical animal models, especially from a surgical standpoint [71, 72, 102]. Xenograft and syngeneic models have provided a space for proof of concept studies, but are largely confined to rodent systems [104]. This limitation has stifled translation of neurosurgical strategies, device development, and drug delivery [41, 80, 82, 98, 108]. There are numerous such strategies with measured preclinical optimism including CED, oncolytic vectors, laser interstitial thermal therapy (LITT), focused ultrasound (FUS), and intraoperative surgical guidance (e.g. 5-ALA) [34-41]. Recognizing these considerations, groups have utilized U87 xenografts for glioma modeling in pigs, but have continued to face the known limitations of the U87 cell line and the need for immunosuppression [80, 81]. Vector-driven approaches, however, provide a modeling strategy that is readily scaled into large animals such as the minipig [102].

Our minipig SCG model (miniSCG$^{PDGFB/HRAS/shP53}$) is induced through lentiviral targeting of the RTK/RAS/PI3K and P53 axes. The present model has compelling histopathologic, radiologic, and transcriptomic data ([102]) and can be readily employed for evaluating surgical approaches. We believe that the current model can be refined to optimize its application for testing various therapeutic approaches. For example, the capacity to adjust underlying genetic lesions, respective phenotypes, grade, and growth rate will be useful for future therapeutic study. For these reasons, our proposal will investigate

the use of common transgenes implicated in gliomagenesis based on prior literature. This represents an opportunity to produce highly characterized large animal models of SCG that would serve as the foundation for surgical translational strategies and future subsequent testing of therapeutic efficacy. Published data on these models would have immediate application in the preclinical development programs by teams currently designing trials for SCG.

Employment of prolonged CED and elucidation of optimal infusion parameters. The use of localized chemotherapy through CED to treat inoperable CNS tumors is a well-documented and feasible concept in rodents and NHPs [44, 150, 151]. The advantages of intratumoral CED include: circumvention of the blood brain barrier, higher local concentrations, minimization of systemic toxicity, and diffusion along white matter tracts [152]. In addition, the pattern of spread of CED infusion in the spinal cord along white matter tracts mirrors the invasive pathways of glioma cells [153].

Intratumoral CED has indeed been applied in rodent models of SCG and has demonstrated therapeutic efficacy [35, 154]. In a Phase I trial by Endo et al, CED was employed in two patients with recurrent SCG, after longitudinal failure of conventional therapy [146]. The reported marked radiologic regression of the SCG with no notable side effects in these patients. However, the authors of this study were not able to employ CED as a first line strategy, conduct prolonged infusion, or track the infusion radiologically. Taking a lesson from the intracranial disease, one of the main possible causes of failure of the Phase III PRECISE trial was poor drug distribution and single treatments [147, 149, 155]. There are even less data in the SCG setting where the central canal and surrounding cerebrospinal fluid may act as “sinks” and incur leeching of the CED infusate [156].

Consequently, the completion of our proposed research will provide such critical data, which will have significant and immediate impact on ongoing and future trials for CED in SCG. The minipig SCG model will serve the same purpose for a wide array of therapeutic approaches.

B.3. Innovation

The proposed study draws from previous *in vivo* vector-driven rodent modeling approaches and aims to scale this strategy into large animals to generate well-characterized minipig models of SCG. Importantly, this would circumvent the need for generation and maintenance of transgenic breeds, providing a cost-effective translational pathway for rapid induction in widely available pigs. The genetic profile, immune system, and the size and anatomy of the porcine CNS is recognized to better model the human [82, 85-87]. The use of viral vector-driven approaches in murine models, targeting distinct genetic lesions implicated in the human disease, have been widely reported as reliable, highly penetrant, and with striking histopathologic and molecular validity [63, 73, 75, 78]. Our present model, miniSCG$^{PDGFB/HRAS/shP53}$, applied the vector driven concept and has demonstrated the feasibility of scaling such strategies into the minipig. Furthermore, given that this was the first model of its kind, there have not been rigorous studies of CED implementation in SCG in disease models that more closely resemble human surgical anatomy **despite ongoing human trials**. Therefore, the centerpiece of innovation of our proposal comes from the combination of 1) a more anatomically relevant large animal model, 2) scaling vector-driven gliomagenesis into the minipig with known molecular drivers, and 3) the first robust study of CED parameters in a large animal model.

APPENDIX C. R01 - INTRACRANIAL GBM AND CED

C.1. Specific Aims

Glioblastoma (GBM) is the most common and most deadly primary brain tumor in adults. While there have been numerous surgical translational studies demonstrating anti-tumor activity in rodents, the anatomy of such models present limitations that are difficult to scale into humans [37, 82, 102, 143-145]. *This highlights a critical need in the field: the development of a large animal GBM model for surgical testing.* **To address this gap, we propose the development of a minipig GBM model for evaluating neurosurgical strategies.**

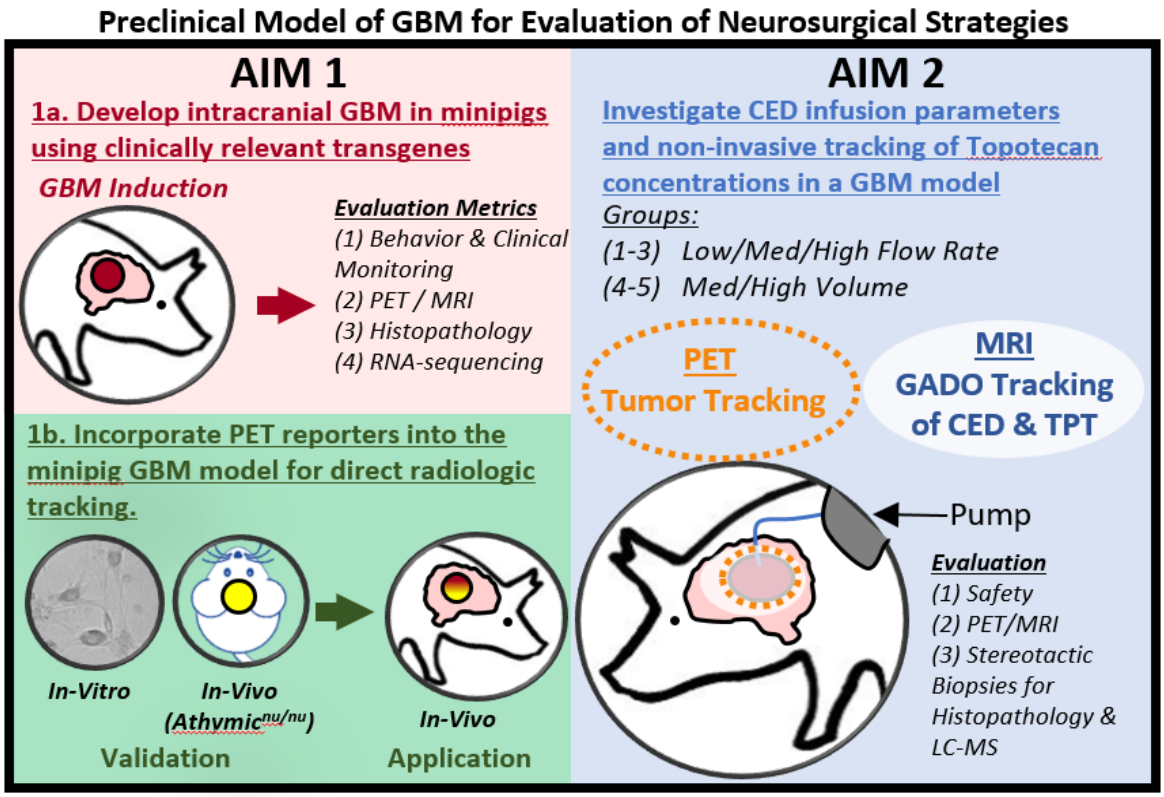

Figure C-1. Proposed experimental design.

The minipig is the ideal model for surgical translational experiments in the CNS. We have combined our expertise in large animal CNS gene delivery (Emory), convection-enhanced delivery (CED), and tumor modeling (Columbia) to establish a minipig GBM model for this purpose. We have previously demonstrated *de novo* growth of GBM in 100% of pigs in the brain (*AIM1)* and spinal cord [102]. The proposed study (**Figure D-1**) will investigate the induction of intracranial GBM using further neuropathologically relevant transgenes to establish an enhanced minipig model for use in translational studies (**AIM1a**). Furthermore, positron emission tomography (PET) and contrast-enhanced magnetic resonance imaging (MRI) provide distinct but incomplete representations of tumor burden. To address this, we will employ transgenic PET reporters (**AIM 1b**) to delineate a greater degree of true tumor burden compared to conventional imaging and allow direct, non-invasive, *in-vivo* tumor tracking in the minipig.

Our model will streamline the development of neurosurgical approaches to GBM. CED is one approach that has shown promising results in our prior rodent and human studies (*AIM2) [98, 157, 158].* However, the limited success of other past human glioma CED trials can be attributed to "short-duration one-time treatments", unknown drug distribution, and CED parameters that cannot be studied well in patients [147-149]. We will investigate these critical CED parameters and demonstrate the utility of the minipig GBM model (**AIM2**).

C.1.1 AIM 1. Development of neuropathologically-relevant / PET visible neurosurgical minipig models of GBM.

AIM 1a. Develop Intracranial GBM In Gottingen minipigs using clinically relevant transgenes. Rationale: *Our prior data demonstrate GBM induction through lentiviral transgene delivery. Here we propose using well-vetted methodologies integrating transgenes relevant to human GBM to induce novel and highly-characterized GBM models for use as neurosurgical translational platforms.* Design: We will model GBM through the delivery of: Group 1 (PDGF-B+shRNA-P53) or Group 2 (EGFR+shRNA-PTEN). Animals will undergo behavioral & clinical-monitoring, PET/MRI for tracking tumor growth, histopathology, and RNA-sequencing.

Hypothesis: *Both groups will induce GBM with recapitulation of neuropathologic, radiologic, and molecular features.*

AIM 1b. Incorporate PET reporters into the minipig GBM model for direct radiologic tracking. Rationale: *Existing PET tracers for GBM show only certain portions of the tumor bulk. Transgenic PET reporters will allow direct and enhanced radiologic tracking of the lesion, thereby providing a more complete system of tracking tumor burden. As such clinically-available imaging methods can be combined, correlated, and studied in the minipig GBM model.* Design: Three PET transgenic reporters and tracers will be screened in cell-culture and *athymic*$^{nu/nu}$ mice with PET and IHC evaluation. The optimal tracer/reporter combination will be employed in the minipig GBM model and evaluated with PET/MRI, histopathology, and stereotactic biopsies to determine tumor burden compared to imaging.

Hypothesis: *The D2 receptor mutant (D2R80A) + F-18 Fallypride will yield PET signal beyond conventional imaging to track the minipig GBM model with histopathologic confirmation.*

C.1.2. AIM 2. Investigate CED infusion parameters and non-invasive tracking of Topotecan concentrations in a GBM model.

Rationale: *Our prior experience with CED has highlighted the need for 1) validating non-invasive tracking of topotecan (TPT) using T1W MRI gadolinium signal in a disease model and 2) elucidating optimal intratumoral CED variables.* Design: We will investigate CED parameters and TPT distribution in the minipig GBM model. 5 groups will utilize modified CED parameters to assess the impact of Infusion Volume (Vi) and Flow Rate (FR) on the volume of distribution (Vd). Minipigs with GBM will receive prolonged CED infusion (gadolinium+TPT) and be evaluated as in AIM 1a, with additional liquid chromatography-mass spectrometry (LC-MS) of stereotactic biopsies.

Hypothesis 1*: The increase in both Vi and FR will directly correlate with Vd measured on T1w gadolinium enhancement, with optimal parameters at FR (2.0 ul/min) and Vi (90 mL).*

Hypothesis 2: *Surrogate radiologic tracking with gadolinium will demonstrate statistically significant correlations with LC-MS concentrations of TPT in the minipig GBM model in both tumor and surrounding parenchyma.*

C.2. Significance

Successful completion of the aims in this proposal will have a significant impact on 1) the development of future surgical approaches to GBM by providing a consistent,

immunocompetent, and more neuropathologically relevant large animal model that can be created quickly, 2) the capacity for enhanced PET mediated tumor tracking as a platform for PET/MRI research and therapeutic read-out for the model, and 3) a rigorous understanding of CED parameters and TPT tracking, directly impacting planned clinical trials.

The development of a large mammalian model of GBM fills a translational gap in the field for the study pre-clinical neurosurgical strategies. Despite significant advances in our knowledge of GBM, there have been limited improvements in outcomes. In part, this represents the recalcitrance of GBM. On the other hand, this highlights the limitations of surgical translation based on existing rodent models [71, 72, 102, 104], which has stifled the translation of neurosurgical strategies [41, 80, 82, 98, 108]. The development of numerous technologies including CED, oncolytic vectors, laser interstitial thermal therapy (LITT), focused ultrasound (FUS), intraoperative surgical guidance (e.g. 5-ALA), intra-arterial delivery, and robotic resection [34-44] would benefit from a readily available highly characterized immunocompetent large animal model of GBM. ***Published data on this model would have immediate application in neurosurgical-related investigations and especially surgical and drug delivery innovations in the brain benefitting from the dimension provided by a large animal model.*** The limitations of animal modeling are well appreciated, and the responsiveness to various therapeutics can be easily assessed in future studies.

The utilization of vector-driven gliomagenesis provides a well-vetted method for the minipig GBM model. The cost of large animal studies has, for good reason, focused molecular biology of genetically engineered GBM models to rodents. Recognizing these

considerations and the need for large mammalian models, groups have utilized U87 xenografts in pigs, but have continued to face the known limitations of U87 and the need for immunosuppression [80, 81]. Vector-driven approaches, however, provide a strategy that may be applied to phenotypically normal large animals for wide implementation [102]. Our prior studies demonstrate induction of GBM in both the brain and spinal cord through lentiviral targeting of the RTK/RAS/PI3K and P53 axes. Our present model demonstrates compelling histopathologic, radiologic, and transcriptomic data ([102], see *preliminary* data AIM1a). ***Given our prior success of GBM modeling using our proposed transgenes in small animals, we believe our strategy presents a high likelihood of success to develop the first set of advanced minipig GBM models.***

The use of the clinical PET tracer F-18 Fluciclovine (AIM1a) to validate PET/MRI tracking of the minipig GBM model will allow for radiologic coregistration for tracking of tumor borders. The feasibility of CED is well established [36]. However, a major issue is the capacity to delineate tumor dimensions during CED or other intratumoral drug delivery strategies that use MR-based contrast agents. We will achieve this through the use of a clinical PET tracer, F-18 Fluciclovine, in the pig model (AIM1a) [159, 160]. ***This will be applied for drug delivery studies (AIM 2), to track tumor borders and/or response to therapy in future pig studies. Furthermore, the radiotracer of choice, F-18 Fluciclovine, is FDA approved so may be adapted for use in our planned human CED trials to mimic preclinical study.*** [161, 162] We will also employ this F-18 Fluciclovine signal as a comparative readout for validation of multiparametric (PET/MRI) imaging in the AIM1b model.

The use of PET genetic reporters (AIM1b) in a minipig GBM model overcomes a limitation of existing imaging techniques for more complete resolution of tumor extent in a non-invasive fashion. The existing gold standard for monitoring GBM includes MRI (e.g T1w post-gadolinium) and less commonly the use of PET tracers (e.g. Fluciclovine, FET, FDG). While these are highly effective tools, they fail to image the complete extent of the tumor and its spread. For example, GADO-based MRI imaging primarily captures the breakdown of the blood-brain-barrier (BBB), while F-18 Fluciclovine as one of the most promising tracers for GBM captures a somewhat overlapping but distinct region on PET imaging [159, 160]. By screening several PET reporters for transgenic expression in cells cultured from our GBM model, we can use respective tracers with minimal or no background and image a more complete representation of the tumor in-vivo. ***This will create an optimal setting for non-invasive tracking of the tumor while evaluating tumor resection, novel clinical pet tracers, MR imaging techniques, and a variety of other neurosurgical applications in the minipig GBM model. If successful, this model can be directly applied in AIM2.***

Lentiviral delivery of transgenic PET reporters in large mammalian models will provide impact outside of the GBM field for other strategies requiring non-invasive monitoring of gene expression. Using lentiviral delivery of a PET reporter will not only allow for tracking of our tumor but has the capacity for monitoring long-term gene expression in a non-invasive fashion. Large animal disease models, gene delivery, and cell transplantation strategies would benefit from validation and characterization of non-invasive PET transgenic reporters in the CNS. This strategy may similarly be applied outside the CNS in a wealth of existing porcine tumor models.

A practical method to monitor drug distribution overcomes a current limitation in the clinical application of CED and demonstrates our minipig GBM model's utility as a neurosurgical platform. Optimization of CED strategies in patients is limited by the lack of methodology for monitoring drug distribution in real-time. While methods such as radiolabeling may provide a means of direct monitoring, these methods may prove cost in-effective or may impact the diffusion, function, or bioavailability of the pharmacologic agent. Rather than modify the drug, we propose a non-invasive imaging methodology using gadolinium as a surrogate marker to approximate drug distribution (AIM2). While some of our past work utilized microdialysis implants, here we instead will use gadolinium T1w voxel intensity as an ideal surrogate non-invasive marker – because of its widespread clinical availability, low cost, and safety. ***Importantly, we have not been able to examine this tracking method in GBM tissue in a reproducible large animal disease model until now (large animal GBM model, combinatorial PET tracking).*** We will test and validate the use of T1w gadolinium signal as a surrogate marker for Topotecan (TPT) with varying infusion parameters to understand and optimize Vd in tumor parenchyma. ***After we have completed AIM2, other CED infusion variables can be easily tested in our model including: Alternate drugs, drug combinations, dose-escalation, catheter design changes, improvements in pump design, and number/positioning of implanted catheters.***

The ability to understand infusion parameters for optimal drug delivery overcomes one of the main limitations in prior phase III trials of chemotherapeutic CED. Because of the aggressive nature of GBM and post-resection recurrence, direct delivery of therapeutics remains one of the most promising translational approaches. The advantages of intratumoral CED include bypassing the blood-brain barrier, higher local concentrations,

minimization of systemic toxicity, and diffusion along white matter tracts [44, 152, 155, 163]. In the past, one of the main contributors to the failure of the Phase III PRECISE study was poor drug distribution and single treatments [147, 149, 155]. Our own more recent Phase I trials examining CED of TPT in humans have shown promising results with radiographic response (AIM2, preliminary data). However, we are unable to study drug delivery parameters in patients. ***As a result, we set out to model GBM in a large animal to provide a space for understanding not only CED parameters but other CED variables and neurosurgical strategies in the future.***

C.3. Innovation

Our proposal challenges the notion of pre-clinical translational reliance on phenotypically normal mammalian models used by investigators and regulatory bodies in the pathway for developing neurosurgical strategies. **This is a major limitation.** In our prior work (Columbia) to bring topotecan CED to a phase I trial, we have been **unable** to rigorously study drug delivery variables or drug tracking in a large animal disease model. Although vector-driven gliomagenesis, clinical and experimental PET reporters, and CED are not entirely new concepts, the confluence of their application forms the key innovative points in our proposal.

<u>Innovation 1: Application of lentiviral transgene mediated gliomagenesis to produce highly characterized, neuropathologically and molecularly relevant minipig GBM models for neurosurgical strategies.</u> The use of vector-driven approaches in murine models, targeting distinct genetic lesions implicated in the human GBM, has been widely reported as reliable, highly penetrant, and with striking histopathologic and molecular validity [63, 73, 75, 78]. Our study draws from these well-vetted approaches providing a

high chance of success in the minipig. The genetic profile, immune system, and the size and anatomy of the porcine CNS are recognized to better model the human *(see Vertebrate Animals section)* [82, 85-87, 164, 165]. Our prior data in exploring GBM modeling in both the brain and spinal cord (PDGF-B, shRNA-P53, HRAS-G12V) has demonstrated the feasibility of this strategy in the minipig. Importantly, the success of our proposal would circumvent the need for the generation and maintenance of transgenic pigs, providing a more cost-effective translational pathway for GBM induction. Furthermore, this approach allows us to test additional clinically relevant genetic alterations that have already been shown to induce glioma in murine models [73-75, 78, 131, 139, 166, 167], including alterations in EGFR, PTEN, and IDH1. ***Innovation is thus inherent in this deliverable, whereby novel minipig GBM models will allow direct application in studying key variables of a promising translational strategy.***

Innovation 2: Novel incorporation of PET reporters into the GBM model permitting enhanced tumor tracking. The use of viral vector delivered PET reporters has been validated in murine and feline models in the CNS [168, 169]. This has not been employed in minipigs, or using lentiviral strategies, nor has it been utilized in vector-driven models of cancer for de-novo lesion growth. By developing a PET trackable lesion, our model can be used to monitor glioma growth and response to treatment in drug delivery studies, and can be combined with clinically-available imaging methods (MRI/MRS/PET) to advance the translation of these studies and facilitate the development of new PET tracers for clinical use, or a variety of other applications. ***Overall, the genetically engineered PET system will provide direct visualization of tumor growth and treatment response, analogous to how luciferase has been used in***

rodent models, thereby providing a 'ground truth' to tumor burden that can be combined and correlated with clinically available imaging methods.

Innovation 3: Optimization of CED infusion parameters in a large animal intracranial GBM model and validation of non-invasive TPT tracking in tumor tissue. There have not been rigorous studies of CED in large animal GBM disease models. While we have studied CED feasibility in minipigs without tumors [36, 98], our recent phase I human trial highlighted the effects of tumor on local tissue properties and the importance of accounting for these effects when optimizing CED parameters. By combining the development of a well-characterized GBM model, PET imaging, and the first rigorous study of CED parameters we believe that this ***provides an innovative and novel pathway to both demonstrate the utility of the model and directly impact clinical use of CED.***

REFERENCES

1. Nizamutdinov, D., et al., *Prognostication of Survival Outcomes in Patients Diagnosed with Glioblastoma.* World Neurosurg, 2018. **109**: p. e67-e74.
2. Oronsky, B., et al., *A Review of Newly Diagnosed Glioblastoma.* Front Oncol, 2020. **10**: p. 574012.
3. Stupp, R., et al., *High-grade glioma: ESMO Clinical Practice Guidelines for diagnosis, treatment and follow-up.* Ann Oncol, 2014. **25 Suppl 3**: p. iii93-101.
4. Tamimi, A.F. and M. Juweid, *Epidemiology and Outcome of Glioblastoma*, in *Glioblastoma*, S. De Vleeschouwer, Editor. 2017: Brisbane (AU).
5. Tora, M.S. and D.C.J.T.C.R. Adamson, *Discernable differences in the genetic and molecular profile of cerebellar glioblastoma.* 2019. **8**(Suppl 6): p. S553-S558.
6. Engelhard, H.H., et al., *Clinical presentation, histology, and treatment in 430 patients with primary tumors of the spinal cord, spinal meninges, or cauda equina.* J Neurosurg Spine, 2010. **13**(1): p. 67-77.
7. Louis, D.N., et al., *The 2016 World Health Organization Classification of Tumors of the Central Nervous System: a summary.* Acta Neuropathol, 2016. **131**(6): p. 803-20.
8. Yan, H., et al., *IDH1 and IDH2 mutations in gliomas.* N Engl J Med, 2009. **360**(8): p. 765-73.
9. Chang, S.M., et al., *Patterns of care for adults with newly diagnosed malignant glioma.* JAMA, 2005. **293**(5): p. 557-64.

10. Dietrich, J., *Clinical presentation, diagnosis, and initial surgical management of high-grade gliomas*, in *UptoDate*, P.Y.W. Jay S Loeffler, April F Eichler, , Editor. 2021.

11. Wagner, S., et al., *Secondary dissemination in children with high-grade malignant gliomas and diffuse intrinsic pontine gliomas.* Br J Cancer, 2006. **95**(8): p. 991-7.

12. Narin, O., et al., *Cerebrospinal fluid spread of anaplastic glioma.* J Clin Oncol, 2007. **25**(5): p. 596-7.

13. Ostrom, Q.T., et al., *Risk factors for childhood and adult primary brain tumors.* Neuro Oncol, 2019. **21**(11): p. 1357-1375.

14. Shete, S., et al., *Genome-wide association study identifies five susceptibility loci for glioma.* Nat Genet, 2009. **41**(8): p. 899-904.

15. Wrensch, M., et al., *Variants in the CDKN2B and RTEL1 regions are associated with high-grade glioma susceptibility.* Nat Genet, 2009. **41**(8): p. 905-8.

16. Sanson, M., et al., *Chromosome 7p11.2 (EGFR) variation influences glioma risk.* Hum Mol Genet, 2011. **20**(14): p. 2897-904.

17. Stupp, R., et al., *Radiotherapy plus concomitant and adjuvant temozolomide for glioblastoma.* N Engl J Med, 2005. **352**(10): p. 987-96.

18. Krishnan, R., et al., *Functional magnetic resonance imaging-integrated neuronavigation: correlation between lesion-to-motor cortex distance and outcome.* Neurosurgery, 2004. **55**(4): p. 904-14; discusssion 914-5.

19. Pirotte, B., et al., *Integrated positron emission tomography and magnetic resonance imaging-guided resection of brain tumors: a report of 103 consecutive procedures.* J Neurosurg, 2006. **104**(2): p. 238-53.

20. Ganslandt, O., et al., *Magnetic source imaging supports clinical decision making in glioma patients.* Clin Neurol Neurosurg, 2004. **107**(1): p. 20-6.

21. Nickel, K., et al., *The patients' view: impact of the extent of resection, intraoperative imaging, and awake surgery on health-related quality of life in high-grade glioma patients-results of a multicenter cross-sectional study.* Neurosurg Rev, 2018. **41**(1): p. 207-219.

22. Hervey-Jumper, S.L., et al., *Awake craniotomy to maximize glioma resection: methods and technical nuances over a 27-year period.* J Neurosurg, 2015. **123**(2): p. 325-39.

23. Sanai, N., Z. Mirzadeh, and M.S. Berger, *Functional outcome after language mapping for glioma resection.* N Engl J Med, 2008. **358**(1): p. 18-27.

24. Brown, T.J., et al., *Association of the Extent of Resection With Survival in Glioblastoma: A Systematic Review and Meta-analysis.* JAMA Oncol, 2016. **2**(11): p. 1460-1469.

25. Stummer, W., et al., *Fluorescence-guided surgery with 5-aminolevulinic acid for resection of malignant glioma: a randomised controlled multicentre phase III trial.* Lancet Oncol, 2006. **7**(5): p. 392-401.

26. Quigley, M.R. and J.C. Maroon, *The relationship between survival and the extent of the resection in patients with supratentorial malignant gliomas.* Neurosurgery, 1991. **29**(3): p. 385-8; discussion 388-9.

27. Lacroix, M., et al., *A multivariate analysis of 416 patients with glioblastoma multiforme: prognosis, extent of resection, and survival.* J Neurosurg, 2001. **95**(2): p. 190-8.

28. Kreth, F.W., et al., *Gross total but not incomplete resection of glioblastoma prolongs survival in the era of radiochemotherapy.* Ann Oncol, 2013. **24**(12): p. 3117-23.

29. Dixit, S., et al., *Retrospective comparison of chemoradiotherapy followed by adjuvant chemotherapy, with or without previous gliadel implantation (carmustine) after initial surgery in patients with newly diagnosed high-grade gliomas: in regard to Noel et al. (Int J Radiat Oncol Biol Phys 2011; DOI: 10.1016/j.ijrobp.2010.11.073).* Int J Radiat Oncol Biol Phys, 2011. **81**(5): p. 1593.

30. Pallud, J., et al., *Long-term results of carmustine wafer implantation for newly diagnosed glioblastomas: a controlled propensity-matched analysis of a French multicenter cohort.* Neuro Oncol, 2015. **17**(12): p. 1609-19.

31. Duntze, J., et al., *Implanted carmustine wafers followed by concomitant radiochemotherapy to treat newly diagnosed malignant gliomas: prospective, observational, multicenter study on 92 cases.* Ann Surg Oncol, 2013. **20**(6): p. 2065-72.

32. Xiao, Z.Z., et al., *Carmustine as a Supplementary Therapeutic Option for Glioblastoma: A Systematic Review and Meta-Analysis.* Front Neurol, 2020. **11**: p. 1036.

33. *GLIADEL® Wafer (carmustine implant) for intracranial use [Prescribing Information]. Atlanta, GA: Arbor Pharmacauticals, LLC; 2013.*

34. Jahan, N., et al., *Triple combination immunotherapy with GVAX, anti-PD-1 monoclonal antibody, and agonist anti-OX40 monoclonal antibody is highly effective against murine intracranial glioma.* Oncoimmunology, 2019. **8**(5): p. e1577108.

35. Ogita, S., et al., *Convection-enhanced delivery of a hydrophilic nitrosourea ameliorates deficits and suppresses tumor growth in experimental spinal cord glioma models.* Acta Neurochir (Wien), 2017. **159**(5): p. 939-946.

36. D'Amico, R.S., et al., *Validation of an effective implantable pump-infusion system for chronic convection-enhanced delivery of intracerebral topotecan in a large animal model.* J Neurosurg, 2019: p. 1-10.

37. Sonabend, A.M., et al., *Convection-enhanced delivery of etoposide is effective against murine proneural glioblastoma.* Neuro Oncol, 2014. **16**(9): p. 1210-9.

38. Passaro, C., et al., *Arming an Oncolytic Herpes Simplex Virus Type 1 with a Single-chain Fragment Variable Antibody against PD-1 for Experimental Glioblastoma Therapy.* Clin Cancer Res, 2019. **25**(1): p. 290-299.

39. Chin, C., et al., *Immunotherapy and Epigenetic Pathway Modulation in Glioblastoma Multiforme.* Front Oncol, 2018. **8**: p. 521.

40. Millesi, M., et al., *Analysis of 5-aminolevulinic acid-induced fluorescence in 55 different spinal tumors.* Neurosurg Focus, 2014. **36**(2): p. E11.

41. Bunevicius, A., N.J. McDannold, and A.J. Golby, *Focused Ultrasound Strategies for Brain Tumor Therapy.* Oper Neurosurg (Hagerstown), 2020. **19**(1): p. 9-18.

42. Ellis, J.A., et al., *Reassessing the Role of Intra-Arterial Drug Delivery for Glioblastoma Multiforme Treatment.* J Drug Deliv, 2015. **2015**: p. 405735.

43. Sutherland, G.R., et al., *Robotics in the neurosurgical treatment of glioma.* Surg Neurol Int, 2015. **6**(Suppl 1): p. S1-8.

44. Ung, T.H., et al., *Convection-enhanced delivery for glioblastoma: targeted delivery of antitumor therapeutics.* CNS Oncol, 2015. **4**(4): p. 225-34.

45. Zhao, H., et al., *The prognostic value of MGMT promoter status by pyrosequencing assay for glioblastoma patients' survival: a meta-analysis.* World J Surg Oncol, 2016. **14**(1): p. 261.

46. Weller, M., et al., *Molecular predictors of progression-free and overall survival in patients with newly diagnosed glioblastoma: a prospective translational study of the German Glioma Network.* J Clin Oncol, 2009. **27**(34): p. 5743-50.

47. Sanson, M., et al., *Isocitrate dehydrogenase 1 codon 132 mutation is an important prognostic biomarker in gliomas.* J Clin Oncol, 2009. **27**(25): p. 4150-4.

48. Hartmann, C., et al., *Long-term survival in primary glioblastoma with versus without isocitrate dehydrogenase mutations.* Clin Cancer Res, 2013. **19**(18): p. 5146-57.

49. Reifenberger, G., et al., *Molecular characterization of long-term survivors of glioblastoma using genome- and transcriptome-wide profiling.* Int J Cancer, 2014. **135**(8): p. 1822-31.

50. Poon, M.T.C., et al., *Longer-term (>/= 2 years) survival in patients with glioblastoma in population-based studies pre- and post-2005: a systematic review and meta-analysis.* Sci Rep, 2020. **10**(1): p. 11622.

51. Abd-El-Barr, M.M., K.T. Huang, and J.H. Chi, *Infiltrating spinal cord astrocytomas: Epidemiology, diagnosis, treatments and future directions.* J Clin Neurosci, 2016. **29**: p. 15-20.

52. Tobin, M.K., et al., *Intramedullary spinal cord tumors: a review of current and future treatment strategies.* Neurosurg Focus, 2015. **39**(2): p. E14.

53. Abd-El-Barr, M.M., et al., *Recent advances in intradural spinal tumors.* Neuro Oncol, 2018. **20**(6): p. 729-742.

54. Hernandez-Duran, S., et al., *Primary spinal cord glioblastoma multiforme treated with temozolomide.* J Clin Neurosci, 2015. **22**(12): p. 1877-82.

55. Lowis, S.P., et al., *Chemotherapy for spinal cord astrocytoma: can natural history be modified?* Childs Nerv Syst, 1998. **14**(7): p. 317-21.

56. Mora, J., et al., *Successful treatment of childhood intramedullary spinal cord astrocytomas with irinotecan and cisplatin.* Neuro Oncol, 2007. **9**(1): p. 39-46.

57. Lombardi, M.Y. and M. Assem, *Glioblastoma Genomics: A Very Complicated Story*, in *Glioblastoma*, S. De Vleeschouwer, Editor. 2017: Brisbane (AU).

58. Gonzalez-Tablas, M., et al., *Heterogeneous EGFR, CDK4, MDM4, and PDGFRA Gene Expression Profiles in Primary GBM: No Association with Patient Survival.* Cancers (Basel), 2020. **12**(1).

59. Rao, S.K., et al., *A survey of glioblastoma genomic amplifications and deletions.* J Neurooncol, 2010. **96**(2): p. 169-79.

60. Xu, X., et al., *MicroRNA518b functions as a tumor suppressor in glioblastoma by targeting PDGFRB.* Mol Med Rep, 2017. **16**(4): p. 5326-5332.

61. Chandrashekar, D.S., et al., *UALCAN: A Portal for Facilitating Tumor Subgroup Gene Expression and Survival Analyses.* Neoplasia, 2017. **19**(8): p. 649-658.

62. Dunn, G.P., et al., *Emerging insights into the molecular and cellular basis of glioblastoma.* Genes Dev, 2012. **26**(8): p. 756-84.

63. Lynes, J., et al., *Lentiviral-induced high-grade gliomas in rats: the effects of PDGFB, HRAS-G12V, AKT, and IDH1-R132H.* Neurotherapeutics, 2014. **11**(3): p. 623-35.

64. Knobbe, C.B., J. Reifenberger, and G. Reifenberger, *Mutation analysis of the Ras pathway genes NRAS, HRAS, KRAS and BRAF in glioblastomas.* Acta Neuropathol, 2004. **108**(6): p. 467-70.

65. Lo, H.W., *Targeting Ras-RAF-ERK and its interactive pathways as a novel therapy for malignant gliomas.* Curr Cancer Drug Targets, 2010. **10**(8): p. 840-8.

66. Cancer Genome Atlas Research, N., *Comprehensive genomic characterization defines human glioblastoma genes and core pathways.* Nature, 2008. **455**(7216): p. 1061-8.

67. Zhang, M., et al., *Genomic Landscape of Intramedullary Spinal Cord Gliomas.* Sci Rep, 2019. **9**(1): p. 18722.

68. Aldape, K., et al., *Challenges to curing primary brain tumours.* Nat Rev Clin Oncol, 2019. **16**(8): p. 509-520.

69. da Hora, C.C., et al., *Patient-Derived Glioma Models: From Patients to Dish to Animals.* Cells, 2019. **8**(10).

70. Hubert, C.G., et al., *A Three-Dimensional Organoid Culture System Derived from Human Glioblastomas Recapitulates the Hypoxic Gradients and Cancer Stem*

Cell Heterogeneity of Tumors Found In Vivo. Cancer Res, 2016. **76**(8): p. 2465-77.

71. Lenting, K., et al., *Glioma: experimental models and reality.* Acta Neuropathol, 2017. **133**(2): p. 263-282.
72. Chen, L., et al., *Vertebrate animal models of glioma: understanding the mechanisms and developing new therapies.* Biochim Biophys Acta, 2013. **1836**(1): p. 158-65.
73. Massey, S.C., et al., *Simulating PDGF-Driven Glioma Growth and Invasion in an Anatomically Accurate Brain Domain.* Bull Math Biol, 2018. **80**(5): p. 1292-1309.
74. Ellis, J.A., et al., *Retroviral delivery of platelet-derived growth factor to spinal cord progenitor cells drives the formation of intramedullary gliomas.* Neurosurgery, 2012. **70**(1): p. 198-204; discussion 204.
75. Assanah, M., et al., *Glial progenitors in adult white matter are driven to form malignant gliomas by platelet-derived growth factor-expressing retroviruses.* J Neurosci, 2006. **26**(25): p. 6781-90.
76. Hede, S.M., et al., *GFAP promoter driven transgenic expression of PDGFB in the mouse brain leads to glioblastoma in a Trp53 null background.* Glia, 2009. **57**(11): p. 1143-53.
77. Dai, C., et al., *PDGF autocrine stimulation dedifferentiates cultured astrocytes and induces oligodendrogliomas and oligoastrocytomas from neural progenitors and astrocytes in vivo.* Genes Dev, 2001. **15**(15): p. 1913-25.

78. Rahme, G.J., et al., *A recombinant lentiviral PDGF-driven mouse model of proneural glioblastoma.* Neuro Oncol, 2018. **20**(3): p. 332-342.

79. Hesselager, G., et al., *Complementary effects of platelet-derived growth factor autocrine stimulation and p53 or Ink4a-Arf deletion in a mouse glioma model.* Cancer Res, 2003. **63**(15): p. 4305-9.

80. Khoshnevis, M., et al., *Development of induced glioblastoma by implantation of a human xenograft in Yucatan minipig as a large animal model.* J Neurosci Methods, 2017. **282**: p. 61-68.

81. Selek, L., et al., *Imaging and histological characterization of a human brain xenograft in pig: the first induced glioma model in a large animal.* J Neurosci Methods, 2014. **221**: p. 159-65.

82. Flisikowska, T., A. Kind, and A. Schnieke, *The new pig on the block: modelling cancer in pigs.* Transgenic Res, 2013. **22**(4): p. 673-80.

83. Snyder, J.M., et al., *20 - Nervous System*, in *Comparative Anatomy and Histology (Second Edition)*, P.M. Treuting, S.M. Dintzis, and K.S. Montine, Editors. 2018, Academic Press: San Diego. p. 403-444.

84. Ong, H.H. and F.W. Wehrli, *Quantifying axon diameter and intra-cellular volume fraction in excised mouse spinal cord with q-space imaging.* Neuroimage, 2010. **51**(4): p. 1360-6.

85. Schomberg, D.T., et al., *Translational Relevance of Swine Models of Spinal Cord Injury.* J Neurotrauma, 2017. **34**(3): p. 541-551.

86. Sauleau, P., et al., *The pig model in brain imaging and neurosurgery.* Animal, 2009. **3**(8): p. 1138-51.

87. Leonard, A.V., et al., *Localization of the corticospinal tract within the porcine spinal cord: Implications for experimental modeling of traumatic spinal cord injury.* Neurosci Lett, 2017. **648**: p. 1-7.

88. Texakalidis, P., et al., *Thoracoscopic delivery of therapeutics in the swine sympathetic chain: Implications for future neuromodulation.* J Clin Neurosci, 2020. **77**: p. 199-202.

89. Swindle, M.M. and A.C. Smith, *Swine in the laboratory: surgery, anesthesia, imaging, and experimental techniques*. 2015: CRC press.

90. Yang, Y., et al., *Quantitative Iron Neuroimaging Can Be Used to Assess the Effects of Minocycline in an Intracerebral Hemorrhage Minipig Model.* Transl Stroke Res, 2020. **11**(3): p. 503-516.

91. Bech, J., et al., *Ex vivo diffusion-weighted MRI tractography of the Gottingen minipig limbic system.* Brain Struct Funct, 2020. **225**(3): p. 1055-1071.

92. Zaer, H., et al., *An Intracortical Implantable Brain-Computer Interface for Telemetric Real-Time Recording and Manipulation of Neuronal Circuits for Closed-Loop Intervention.* Front Hum Neurosci, 2021. **15**: p. 618626.

93. Keung, M.S., et al., *Characterization of Lower Urinary Tract Dysfunction after Thoracic Spinal Cord Injury in Yucatan Minipigs.* J Neurotrauma, 2021.

94. Saadoun, S. and N.D. Jeffery, *Acute Traumatic Spinal Cord Injury in Humans, Dogs, and Other Mammals: The Under-appreciated Role of the Dura.* Front Neurol, 2021. **12**: p. 629445.

95. Dai, J.X., et al., *Large animal models of traumatic brain injury.* Int J Neurosci, 2018. **128**(3): p. 243-254.

96. Kuluz, J., et al., *Pediatric spinal cord injury in infant piglets: description of a new large animal model and review of the literature.* J Spinal Cord Med, 2010. **33**(1): p. 43-57.

97. Mamelak, A.N., et al., *A high-definition exoscope system for neurosurgery and other microsurgical disciplines: preliminary report.* Surg Innov, 2008. **15**(1): p. 38-46.

98. Sonabend, A.M., et al., *Prolonged intracerebral convection-enhanced delivery of topotecan with a subcutaneously implantable infusion pump.* Neuro Oncol, 2011. **13**(8): p. 886-93.

99. Mihara, K., et al., *Intraoperative laparoscopic detection of sentinel lymph nodes with indocyanine green and superparamagnetic iron oxide in a swine gallbladder cancer model.* PLoS One, 2021. **16**(3): p. e0248531.

100. Niu, G., et al., *Porcine model elucidates function of p53 isoform in carcinogenesis and reveals novel circTP53 RNA.* Oncogene, 2021. **40**(10): p. 1896-1908.

101. Watson, A.L., et al., *Engineered Swine Models of Cancer.* Front Genet, 2016. **7**: p. 78.

102. Tora, M.S., et al., *Lentiviral Vector Induced Modeling of High-Grade Spinal Cord Glioma in Minipigs.* Sci Rep, 2020. **10**(1): p. 5291.

103. Villa, C., et al., *The 2016 World Health Organization classification of tumours of the central nervous system.* Presse Med, 2018. **47**(11-12 Pt 2): p. e187-e200.

104. Jacobs, V.L., et al., *Current review of in vivo GBM rodent models: emphasis on the CNS-1 tumour model.* ASN Neuro, 2011. **3**(3): p. e00063.

105. Maes, W. and S.W. Van Gool, *Experimental immunotherapy for malignant glioma: lessons from two decades of research in the GL261 model.* Cancer Immunol Immunother, 2011. **60**(2): p. 153-60.

106. Lei, L., et al., *Glioblastoma models reveal the connection between adult glial progenitors and the proneural phenotype.* PLoS One, 2011. **6**(5): p. e20041.

107. Sonabend, A.M., et al., *The transcriptional regulatory network of proneural glioma determines the genetic alterations selected during tumor progression.* Cancer Res, 2014. **74**(5): p. 1440-1451.

108. Schook, L.B., et al., *A Genetic Porcine Model of Cancer.* PLoS One, 2015. **10**(7): p. e0128864.

109. Semple, B.D., et al., *Brain development in rodents and humans: Identifying benchmarks of maturation and vulnerability to injury across species.* Prog Neurobiol, 2013. **106-107**: p. 1-16.

110. Buonerba, C., et al., *A comprehensive outlook on intracerebral therapy of malignant gliomas.* Crit Rev Oncol Hematol, 2011. **80**(1): p. 54-68.

111. Squires, A., et al., *SpinoBot: An MRI-Guided Needle Positioning System for Spinal Cellular Therapeutics.* Ann Biomed Eng, 2018. **46**(3): p. 475-487.

112. Gutierrez, J., et al., *Preclinical Validation of Multilevel Intraparenchymal Stem Cell Therapy in the Porcine Spinal Cord.* Neurosurgery, 2015. **77**(4): p. 604-12; discussion 612.

113. Medin, P.M., et al., *Spinal cord tolerance to reirradiation with single-fraction radiosurgery: a swine model.* Int J Radiat Oncol Biol Phys, 2012. **83**(3): p. 1031-7.

114. Pleticha, J., et al., *Pig lumbar spine anatomy and imaging-guided lateral lumbar puncture: a new large animal model for intrathecal drug delivery.* J Neurosci Methods, 2013. **216**(1): p. 10-5.

115. Malysz-Cymborska, I., et al., *MRI-guided intrathecal transplantation of hydrogel-embedded glial progenitors in large animals.* Sci Rep, 2018. **8**(1): p. 16490.

116. Kantor, B., et al., *Methods for gene transfer to the central nervous system.* Adv Genet, 2014. **87**: p. 125-97.

117. Merkl, C., et al., *RNA interference in pigs: comparison of RNAi test systems and expression vectors.* Mol Biotechnol, 2011. **48**(1): p. 38-48.

118. Federici, T., et al., *Surgical technique for spinal cord delivery of therapies: demonstration of procedure in gottingen minipigs.* J Vis Exp, 2012(70): p. e4371.

119. Mazzini, L., et al., *Results from Phase I Clinical Trial with Intraspinal Injection of Neural Stem Cells in Amyotrophic Lateral Sclerosis: A Long-Term Outcome.* Stem Cells Transl Med, 2019. **8**(9): p. 887-897.

120. Zoli, S., et al., *Experimental two-stage simulated repair of extensive thoracoabdominal aneurysms reduces paraplegia risk.* Ann Thorac Surg, 2010. **90**(3): p. 722-9.

121. Hu, L.S., et al., *Reevaluating the imaging definition of tumor progression: perfusion MRI quantifies recurrent glioblastoma tumor fraction, pseudoprogression, and radiation necrosis to predict survival.* Neuro Oncol, 2012. **14**(7): p. 919-30.

122. Rueden, C.T., et al., *ImageJ2: ImageJ for the next generation of scientific image data.* BMC Bioinformatics, 2017. **18**(1): p. 529.

123. Dobin, A., et al., *STAR: ultrafast universal RNA-seq aligner*. Bioinformatics, 2013. **29**(1): p. 15-21.

124. Anders, S., P.T. Pyl, and W. Huber, *HTSeq--a Python framework to work with high-throughput sequencing data.* Bioinformatics, 2015. **31**(2): p. 166-9.

125. Love, M.I., W. Huber, and S. Anders, *Moderated estimation of fold change and dispersion for RNA-seq data with DESeq2.* Genome Biol, 2014. **15**(12): p. 550.

126. Subramanian, A., et al., *Gene set enrichment analysis: a knowledge-based approach for interpreting genome-wide expression profiles.* Proc Natl Acad Sci U S A, 2005. **102**(43): p. 15545-50.

127. Wang, Q., et al., *Tumor Evolution of Glioma-Intrinsic Gene Expression Subtypes Associates with Immunological Changes in the Microenvironment.* Cancer Cell, 2017. **32**(1): p. 42-56 e6.

128. Neftel, C., et al., *An Integrative Model of Cellular States, Plasticity, and Genetics for Glioblastoma.* Cell, 2019. **178**(4): p. 835-849 e21.

129. Verhaak, R.G., et al., *Integrated genomic analysis identifies clinically relevant subtypes of glioblastoma characterized by abnormalities in PDGFRA, IDH1, EGFR, and NF1.* Cancer Cell, 2010. **17**(1): p. 98-110.

130. Brennan, C.W., et al., *The somatic genomic landscape of glioblastoma.* Cell, 2013. **155**(2): p. 462-77.

131. Alessandrini, F., et al., *Glioblastoma models driven by different mutations converge to the proneural subtype.* Cancer Lett, 2020. **469**: p. 447-455.

132. Singh, S.K., et al., *Post-translational Modifications of OLIG2 Regulate Glioma Invasion through the TGF-beta Pathway.* Cell Rep, 2016. **16**(4): p. 950-966.

133. Hwang, S.U., et al., *Production of transgenic pigs using a pGFAP-CreER(T2)/EGFP (LoxP) inducible system for central nervous system disease models.* J Vet Sci, 2018. **19**(3): p. 434-445.

134. Glud, A.N., et al., *Direct MRI-guided stereotaxic viral mediated gene transfer of alpha-synuclein in the Gottingen minipig CNS.* Acta Neurobiol Exp (Wars), 2011. **71**(4): p. 508-18.

135. Westermark, B., *Platelet-derived growth factor in glioblastoma-driver or biomarker?* Ups J Med Sci, 2014. **119**(4): p. 298-305.

136. Patel, A.P., et al., *Single-cell RNA-seq highlights intratumoral heterogeneity in primary glioblastoma.* Science, 2014. **344**(6190): p. 1396-401.

137. Bedard, P.L., et al., *Tumour heterogeneity in the clinic.* Nature, 2013. **501**(7467): p. 355-64.

138. Hambardzumyan, D., et al., *Modeling Adult Gliomas Using RCAS/t-va Technology.* Transl Oncol, 2009. **2**(2): p. 89-95.

139. Muller, S., et al., *Single-cell sequencing maps gene expression to mutational phylogenies in PDGF- and EGF-driven gliomas.* Mol Syst Biol, 2016. **12**(11): p. 889.

140. Pearson, J.R.D. and T. Regad, *Targeting cellular pathways in glioblastoma multiforme.* Signal Transduct Target Ther, 2017. **2**: p. 17040.

141. Nunez, F.M., et al., *Genetically Engineered Mouse Model of Brainstem High-Grade Glioma.* STAR Protoc, 2020. **1**(3): p. 100165.

142. Bastola, S., et al., *Glioma-initiating cells at tumor edge gain signals from tumor core cells to promote their malignancy.* Nat Commun, 2020. **11**(1): p. 4660.

143. Enriquez Perez, J., et al., *Convection-enhanced delivery of temozolomide and whole cell tumor immunizations in GL261 and KR158 experimental mouse gliomas.* BMC Cancer, 2020. **20**(1): p. 7.

144. Haryu, S., et al., *Convection-enhanced delivery of sulfasalazine prolongs survival in a glioma stem cell brain tumor model.* J Neurooncol, 2018. **136**(1): p. 23-31.

145. Lin, C.Y., et al., *Controlled release of liposome-encapsulated temozolomide for brain tumour treatment by convection-enhanced delivery.* J Drug Target, 2018. **26**(4): p. 325-332.

146. Endo, T., et al., *Regression of Recurrent Spinal Cord High-Grade Glioma After Convection-Enhanced Delivery of Nimustine Hydrochloride: Case Reports and Literature Review.* Oper Neurosurg (Hagerstown), 2019.

147. Jahangiri, A., et al., *Convection-enhanced delivery in glioblastoma: a review of preclinical and clinical studies.* J Neurosurg, 2017. **126**(1): p. 191-200.

148. Kunwar, S., et al., *Phase III randomized trial of CED of IL13-PE38QQR vs Gliadel wafers for recurrent glioblastoma.* Neuro Oncol, 2010. **12**(8): p. 871-81.

149. Sampson, J.H., et al., *Poor drug distribution as a possible explanation for the results of the PRECISE trial.* J Neurosurg, 2010. **113**(2): p. 301-9.

150. Goodwin, C.R., et al., *Local delivery methods of therapeutic agents in the treatment of diffuse intrinsic brainstem gliomas.* Clin Neurol Neurosurg, 2016. **142**: p. 120-127.

151. Sugiyama, S., et al., *Safety and feasibility of convection-enhanced delivery of nimustine hydrochloride co-infused with free gadolinium for real-time monitoring in the primate brain.* Neurol Res, 2012. **34**(6): p. 581-7.

152. Endo, T., et al., *Properties of convective delivery in spinal cord gray matter: laboratory investigation and computational simulations.* J Neurosurg Spine, 2016. **24**(2): p. 359-366.

153. Wang, J., et al., *Invasion of white matter tracts by glioma stem cells is regulated by a NOTCH1-SOX2 positive-feedback loop.* Nat Neurosci, 2019. **22**(1): p. 91-105.

154. Tyler, B.M., et al., *Delayed onset of paresis in rats with experimental intramedullary spinal cord gliosarcoma following intratumoral administration of the paclitaxel delivery system OncoGel.* J Neurosurg Spine, 2012. **16**(1): p. 93-101.

155. Healy, A.T. and M.A. Vogelbaum, *Convection-enhanced drug delivery for gliomas.* Surg Neurol Int, 2015. **6**(Suppl 1): p. S59-67.

156. Lonser, R.R., et al., *Convection-enhanced delivery to the central nervous system.* J Neurosurg, 2015. **122**(3): p. 697-706.

157. Bruce, J.N., et al., *Regression of Recurrent Malignant Gliomas with Convection-Enhanced Delivery of Topotecan.* Neurosurgery, 2011.

158. Lopez, K.A., et al., *Convection-Enhanced Delivery of Topotecan into a PDGF-Driven Model of Glioblastoma Prolongs Survival and Ablates Both Tumor-Initiating Cells and Recruited Glial Progenitors.* Cancer Res, 2011. **71**(11): p. 3963-71.

159. Kondo, A., et al., *Phase IIa clinical study of [(18)F]fluciclovine: efficacy and safety of a new PET tracer for brain tumors.* Ann Nucl Med, 2016. **30**(9): p. 608-618.

160. Parent, E.E., et al., *[(18)F]Fluciclovine PET discrimination between high- and low-grade gliomas.* EJNMMI Res, 2018. **8**(1): p. 67.

161. Sasajima, T., et al., *Trans-1-amino-3-18F-fluorocyclobutanecarboxylic acid (anti-18F-FACBC) is a feasible alternative to 11C-methyl-L-methionine and magnetic resonance imaging for monitoring treatment response in gliomas.* Nucl Med Biol, 2013. **40**(6): p. 808-15.

162. Parent, E.E., et al., *[(18)F]-Fluciclovine PET discrimination of recurrent intracranial metastatic disease from radiation necrosis.* EJNMMI Res, 2020. **10**(1): p. 148.

163. Kim, J.H., T.H. Mareci, and M. Sarntinoranont, *A voxelized model of direct infusion into the corpus callosum and hippocampus of the rat brain: model development and parameter analysis.* Med Biol Eng Comput, 2010. **48**(3): p. 203-14.

164. Christensen, A.B., et al., *Pirouetting pigs: A large non-primate animal model based on unilateral 6-hydroxydopamine lesioning of the nigrostriatal pathway.* Brain Res Bull, 2018. **139**: p. 167-173.

165. Bogdanski, R., et al., *Cerebral histopathology following portal venous infusion of bacteria in a chronic porcine model.* Anesthesiology, 2000. **93**(3): p. 793-804.

166. Holland, E.C., et al., *A constitutively active epidermal growth factor receptor cooperates with disruption of G1 cell-cycle arrest pathways to induce glioma-like lesions in mice.* Genes Dev, 1998. **12**(23): p. 3675-85.

167. Weiss, W.A., et al., *Genetic determinants of malignancy in a mouse model for oligodendroglioma.* Cancer Res, 2003. **63**(7): p. 1589-95.

168. Yoon, S.Y., et al., *Quantitative, noninvasive, in vivo longitudinal monitoring of gene expression in the brain by co-AAV transduction with a PET reporter gene.* Mol Ther Methods Clin Dev, 2014. **1**: p. 14016.

169. Haywood, T., et al., *Positron emission tomography reporter gene strategy for use in the central nervous system.* Proc Natl Acad Sci U S A, 2019. **116**(23): p. 11402-11407.